BURNING RATE COMPARISON OF A MATHEMATICAL MODEL WITH EXPERIMENTAL RESULTS FOR AP/HTPB/IRON OXIDE BASED COMPOSITE PROPELLANTS

A THESIS SUBMITTED TO
THE GRADUATE SCHOOL OF NATURAL AND APPLIED SCIENCES
OF
MIDDLE EAST TECHNICAL UNIVERSITY

BY

SERHAT CEM ÖZCAN

IN PARTIAL FULFILLMENT OF THE REQUIREMENTS
FOR
THE DEGREE OF MASTER OF SCIENCE
IN
MECHANICAL ENGINEERING

AUGUST 2019

Approval of the thesis:

BURNING RATE COMPARISON OF A MATHEMATICAL MODEL WITH EXPERIMENTAL RESULTS FOR AP/HTPB/IRON OXIDE BASED COMPOSITE PROPELLANTS

submitted by **SERHAT CEM ÖZCAN** in partial fulfillment of the requirements for the degree of **Master of Science in Mechanical Engineering Department, Middle East Technical University** by,

Prof. Dr. Halil Kalıpçılar
Dean, Graduate School of **Natural and Applied Sciences** _____

Prof. Dr. M. A. Sahir Arıkan
Head of Department, **Mechanical Engineering** _____

Prof. Dr. Abdullah Ulaş
Supervisor, **Mechanical Engineering, METU** _____

Examining Committee Members:

Assist. Prof. Dr. Feyza Kazanç Özerinç
Mechanical Engineering, METU _____

Prof. Dr. Abdullah Ulaş
Mechanical Engineering, METU _____

Prof. Dr. Hüseyin Vural
Mechanical Engineering, METU _____

Prof. Dr. Murat Köksal
Mechanical Engineering, Hacettepe University _____

Assist. Prof. Dr. Sıtkı Uslu
Mechanical Engineering, TOBB ETU _____

Date:

I hereby declare that all information in this document has been obtained and presented in accordance with academic rules and ethical conduct. I also declare that, as required by these rules and conduct, I have fully cited and referenced all material and results that are not original to this work.

Name, Surname: Serhat Cem Özcan

Signature :

ABSTRACT

BURNING RATE COMPARISON OF A MATHEMATICAL MODEL WITH EXPERIMENTAL RESULTS FOR AP/HTPB/IRON OXIDE BASED COMPOSITE PROPELLANTS

Özcan, Serhat Cem
M.S., Department of Mechanical Engineering
Supervisor: Prof. Dr. Abdullah Ulaş

August 2019, 108 pages

Ballistic properties play a crucial role for designing solid propellant rocket motors. Among those properties, burning rate is one of the most critical properties that must be known in order to predict the performance of the motor accurately.

While various experimental methods such as Ballistic Evaluation Motor tests, strand burner experiments and full scale motor testing are used to obtain burning rate, these methods may lead to time and money consumption problems [1]. In order to save time and reduce the cost, theoretical models for predicting the burning rate have been developed from 1960's.

In this study, Cohen and Strand model [2] and Beckstead, Derr and Price [3] model have been combined and numerically coded to predict the burning rates of Ammonium Perchlorate/Hydroxyl Terminated Polybutadiene (AP/HTPB) based composite propellants. Additionally, to incorporate the catalyst effect, the code was expanded based on the Krishnan and Jeenu model [4]. To compare the predictions of the model, strand burner experiments have been conducted for various propellants having AP di-

ameters of 10μm, 40μm, 90μm, and 200μm and having solid loading of 70, 73, 77, and 80 percent. The matrix was expanded with the Fe_2O_3 addition to the AP/HTPB propellants and a total of 390 strand burner experiments have been conducted for those propellants to compare the results with the numerical scheme predictions.

For the results, it is observed that burning rates increase with lowering AP particle size, increasing AP percent and adding catalyst to the propellants. For mid-size AP (40μm and 90μm) based propellants, numerical predictions give better results but approaching towards either 10μm or 200μm AP based propellants, discrepancies between predictions and results become larger. All in all, promising predictions are observed as a general conclusion for this study.

Keywords: Composite Propellants, Iron Oxide Addition, Burning Rate, Strand Burner, Numerical Modeling

ÖZ

AP/HTPB/DEMİR OKSİT BAZLI YAKITLARIN MATEMATİKSEL MODEL VE DENEY SONUÇLARIYLA YANMA HIZI KARŞILAŞTIRMASI

Özcan, Serhat Cem
Yüksek Lisans, Makina Mühendisliği Bölümü
Tez Yöneticisi: Prof. Dr. Abdullah Ulaş

Ağustos 2019 , 108 sayfa

Katı yakıtlı roket motoru tasarımında balistik özellikler çok önemli bir rol oynamaktadır. Bu özellikler arasında bilinmesi gereken en kritik özelliklerden biri yanma hızı olup, motor performansını hassas olarak tahmin etmek için gereklidir.

Yanma hızını elde edebilmek için Balistik Araştırma Motoru testleri, çubuk yakıcı testleri ve motor ateşlemeleri gibi yöntemler kullanılmakta olup, bu metodlar zaman ve para açısından kayba yol açmaktadır [1]. Zaman kazanmak ve maliyeti azaltmak amacıyla 1960'lardan itibaren yanma hızını tahmin edebilmek için teorik modeller geliştirilmektedir.

Bu çalışmada, AP/HTPB bazlı kompozit yakıtların yanma hızını öngörmek amacıyla Cohen-Strand [2] ve Beckstead-Derr-Price [3] modelleri kombine edilmiş ve bu modeller numerik olarak kodlanmıştır. Buna ek olarak, katalizör etkilerini görmek için Krishnan-Jeenu modeli [4] de yazılan koda eklenmiştir. Modelin öngörüleriyle karşılaştırma yapabilmek amacıyla çubuk yakıcı test düzeneğinde bir test matrisi oluşturulmuştur ve bu matriste 10μm, 40μm, 90μm, and 200μm AP çapına ve 70%,

73%, 77%, and 80% AP yükleme oranına sahip AP/HTPB bazlı yakıtlar incelenmiştir. Katalizör eklenmiş model öngörülerini karşılaştırabilmek amacıyla Fe_2O_3, AP/HTPB bazlı yakıtlara eklenerek test matrisi genişletilmiştir. Toplam 390 çubuk yakıcı deneyi numerik şema öngörüleriyle karşılaştırma yapabilmek amacıyla yapılmıştır.

Sonuç olarak, yanma hızının AP çapının düşürülmesiyle, AP yüzdesinin arttırılmasıyla ve yakıtlara katalizör eklenmesiyle arttığı gözlenmiştir. Orta boyutlu AP (40μm ve 90μm) bazlı yakıtlar için numerik yanma hızı öngörüleri 10μm ve 200μm AP bazlı yakıtların yanma hızı öngörülerine göre daha iyi sonuçlar vermiştir. Genel olarak, ümit vaat eden öngörülerin bu çalışmada elde edildiği gözlenmiştir.

Anahtar Kelimeler: Kompozit Yakıtlar, Demir Oksit Eklemesi, Yanma Hızı, Çubuk Yakıcı, Numerik Modelleme

To My Family

ACKNOWLEDGMENTS

I would like to express my deepest thanks and appreciations to my supervisor, Prof. Dr. Abdullah ULAŞ, for his supervision and continuous guidance throughout this study.

My special thanks go to my colleagues at TÜBİTAK SAGE, especially Caner Ekin KİPER for his effort at every stage of the work, Burak SÖĞÜTCÜ, Mehmet Fatih BOZYİĞİT, Anıl TATLIDİLLİ and Dr. Pelin Edinç CÜRDANELİ for their support at conducting experiments, Chief of the Propellants and Explosives Division Dr. Değer ŞEN ÇETİN for her effort providing the propellants. I would like to give my special appreciations to the Chief of the Propulsion Systems Division in TÜBİTAK-SAGE, Dr. Bülent SÜMER, for helping me out throughout the study.

TÜBİTAK-SAGE, Ankara who supported this work is also gratefully acknowledged.

I would like to express my sincere appreciations to Sertaç CÜRDANELİ for being there whenever I need and for his crucial advices at every stage of the work.

I am forever grateful for my fiancée Irmak ÖZGÜN's patience, unfailing support and encouragement. It is such a blessing to have her during this difficult period.

Lastly, the greatest thanks go to my mother Zuhal ÖZCAN, my father Ali ÖZCAN and my entire family for their patience and continuous support throughout my whole life.

TABLE OF CONTENTS

ABSTRACT v

ÖZ vii

ACKNOWLEDGMENTS x

TABLE OF CONTENTS xi

LIST OF TABLES xiv

LIST OF FIGURES xv

LIST OF ABBREVIATIONS xxi

CHAPTERS

1 INTRODUCTION 1

1.1 Rocket Motors and Propellants 1

1.1.1 Solid Rocket Motors 3

1.1.1.1 Motor Case 4

1.1.1.2 Igniter 5

1.1.1.3 Insulation 5

1.1.1.4 Nozzle 5

1.1.1.5 Solid Propellant Grain 6

1.1.2 Solid Propellants 6

1.1.2.1 Homogeneous Propellants 6

1.1.2.2 Heterogeneous Propellants 8
1.2 Burning Rate of Solid Propellants 9
1.2.1 Factors That Affect the Burning Rate 10
1.2.2 Methods to Measure Burning Rate 11
1.2.2.1 Test Firings 11
1.2.2.2 Strand Burner Method 12
1.2.2.3 Closed Vessel Method 13
1.2.2.4 X-Ray Method 13
1.2.2.5 Other methods 13
1.3 Motivation 14
1.4 Scope of the Thesis 15
1.5 Content of the Thesis 16
2 LITERATURE SURVEY 17
3 METHODOLOGY 27
3.1 Numerical Methodology 27
3.1.1 AP Monopropellant Model 27
3.1.2 AP/HTPB Composite Propellants Model 33
3.1.3 Catalyzed AP/HTPB Model 47
3.2 Experimental Methodology 50
3.2.1 Test Setup 51
3.2.1.1 Control Panel 52
3.2.1.2 CO_2 Laser Source 53
3.2.1.3 Nitrogen Tube and Regulator 56

3.2.1.4 Optical Lens 57
3.2.1.5 Shutter 59
3.2.1.6 Directive Lens 60
3.2.1.7 Combustion Chamber 61
3.2.1.8 Voltage Supplier 63
3.2.1.9 Data Acquisition System 63
3.2.1.10 Heating and Cooling System 64
3.2.2 Test Matrix and Test Plan 65
3.2.2.1 Test Matrix 65
3.2.2.2 Test Plan 67
4 RESULTS AND DISCUSSION 71
4.1 Experimental Results 71
4.2 Numerical Scheme Predictions and Comparison with the Experimental Results 84
5 CONCLUSION 99
REFERENCES 103

LIST OF TABLES

TABLES

Table 1.1 Homogeneous Propellant Ingredients [5]. 7

Table 1.2 Composite Propellant Ingredients [5]. 9

Table 3.1 Calculated Results by Cohen and Strand [2] for AP Monopropellant Combustion. 31

Table 3.2 AP Monopropellant Parameters found by Current Work. 33

Table 3.3 Calculated Internal Quantities by Cohen and Strand [2] for King's [6] 73% AP/HTPB Propellants. 38

Table 3.4 Test Matrix for only AP/HTPB based Composite Propellants. 66

Table 3.5 Test Matrix for AP/HTPB based Composite Propellants with Fe_2O_3 Additives. 67

LIST OF FIGURES

FIGURES

Figure 1.1 Typical Solid Rocket Motor [7]. 2

Figure 1.2 Typical Liquid Rocket Motor [7]. 2

Figure 1.3 Typical Hybrid Rocket Engine[7]. 3

Figure 1.4 Components of a Solid Rocket Motor [8]. 4

Figure 1.5 Typical Nozzle for Solid Propellant Rocket Engine [9]. 5

Figure 1.6 Homogeneous Propellant Sample [10]. 7

Figure 1.7 Composite Propellant Sample. 8

Figure 1.8 Linear Regression of Solid Propellants [11]. 10

Figure 1.9 Typical Test Firing [12]. 12

Figure 1.10 Example of Burning Rate Graph [13]. 14

Figure 2.1 Combustion Process Proposed by Hermance [14]. 17

Figure 2.2 Comparison of Experimental Data with Theoretical Model of Hermance [14]. 18

Figure 2.3 Flame Structure Proposed by BDP [3]. 19

Figure 2.4 Comparison of Experimental Data with Theoretical Model of BDP [3]. 19

Figure 2.5 Comparison of Experimental Data with Theoretical Model of King [15]. 20

Figure 2.6 Comparison of Experimental Data with Theoretical Model by Cohen and Strand [2]. 21

Figure 2.7 Phases of Solid Propellant Combustion Proposed by Jeppson et al [16]. 22

Figure 2.8 Comparison of Experimental Data by King [6] with Theoretical Work of Jeppson et al [16]. 23

Figure 2.9 Calculated and Experimental Burning Rate by Vigor Yang et al [17], AP/HTPB(70/30) Propellants on the Right - AP/HTPB(73/27) Propellants on the Left. 23

Figure 2.10 Comparison of Experimental Data with Theoretical Model of Rasmussen et al [18], Oxidizer/Fuel Ratio 80/20 on the Left - 75/25 on the Right. 24

Figure 2.11 Comparison of Experimental Data with Theoretical Model for Catalyzed Composite Propellants by Krishnan et al [4]. 25

Figure 3.1 Flame Temperature of Oxidizer with respect to Pressure. 29

Figure 3.2 AP/HTPB Propellant Flame Structure. 34

Figure 3.3 AP Particles Protruding and Recessing at Surface. 37

Figure 3.4 β_{ox} Values Comparison of Cohen and Strand model [2] with the Current Work Predictions. 43

Figure 3.5 Oxidizer Surface Temperature Comparison of Cohen et al [2] with the Current Work Predictions for 73 AP% - 20μ Propellants. 44

Figure 3.6 Binder Surface Temperature Comparison of Cohen et al [2] with the Current Work Predictions for 73 AP% - 20μ Propellants. 44

Figure 3.7 Burning Rate Comparison of Cohen and Strand Model [2] with the Current Work Predictions for 73 AP% - 20μ Propellants. 45

Figure 3.8 Burning Rate Comparison of Cohen and Strand Model [2] with the Current Work Predictions for 73 AP% - 5μ Propellants. 46

Figure 3.9 Burning Rate Comparison of Cohen and Strand Model [2] with the Current Work Predictions for 73 AP% - 200μ Propellants. 47

Figure 3.10 Comparison of Experimental Work with Theoretical Studies by Krishnan and Jeenu [4] for Catalyzed Composite Propellants. 50

Figure 3.11 Schematic of the Test Setup. 51

Figure 3.12 General View of the Test Setup. 52

Figure 3.13 Strand Burner Control Panel. 53

Figure 3.14 CO_2 Laser Source Controller. 54

Figure 3.15 CO_2 Laser Details. 55

Figure 3.16 Exit Port of the Laser. 55

Figure 3.17 Nitrogen Tube and Regulator. 56

Figure 3.18 Nitrogen Tube Details. 56

Figure 3.19 Regulator on the Nitrogen Tube. 57

Figure 3.20 Optical Lens. 58

Figure 3.21 Power-meter that Reads Data from Reflected Part. 58

Figure 3.22 Optical Lens and Shutter. 59

Figure 3.23 Shutter Blades Closed on the Left and Opened on the Right. . . . 59

Figure 3.24 Uniblitz Shutter Actuator. 60

Figure 3.25 Optical Lens, Shutter and Directive Lens. 60

Figure 3.26 Combustion Chamber. 61

Figure 3.27 General Test Setup from Side View. 62

Figure 3.28 Voltage Supplier. 63

Figure 3.29 Data Acquisition System. 64

Figure 3.30 Temperature Adjustment System. 64

Figure 3.31 Propellant Sample Holder Details. 68

Figure 3.32 A Sample for all Propellants Experimented. 69

Figure 4.1 An Example of Experimental Data Obtained - 77% AP 200 μm data of 50 bars pressure. 72

Figure 4.2 An Example of a Strand Burner Test (77% AP - 40μm Composite Propellant, 50 bar). 73

Figure 4.3 Experimental Results for Propellants Having 10 μm AP. 74

Figure 4.4 Experimental Results for Propellants Having 40 μm AP. 76

Figure 4.5 Experimental Results for Propellants Having 90 μm AP. 76

Figure 4.6 Experimental Results for Propellants Having 200 μm AP. 77

Figure 4.7 Experimental Results for 73% AP Based Propellants with Having %1 Fe_2O_3. 78

Figure 4.8 Experimental Results for 73% AP Based Propellants with Having %2 Fe_2O_3. 79

Figure 4.9 Experimental Results for 80% AP Based Propellants with Having %1 Fe_2O_3. 80

Figure 4.10 Comparison of Catalyzed vs. Uncatalyzed 10μm AP Based Propellants Burning Rate. 81

Figure 4.11 Comparison of Catalyzed vs. Uncatalyzed 40μm AP Based Propellants Burning Rate. 82

Figure 4.12 Comparison of Catalyzed vs. Uncatalyzed 90μm AP Based Propellants Burning Rate. 83

Figure 4.13 Comparison of Catalyzed vs. Uncatalyzed 200μm AP Based Propellants Burning Rate. 84

Figure 4.14 Burning Rate Comparison of AP/HTPB based Propellants with AP size of 10 μm. 85

Figure 4.15 Literature Data for AP/HTPB based Propellants with 10 μm or close AP sizes. 86

Figure 4.16 Burning Rate Comparison of AP/HTPB based Propellants with AP size of 40 μm. 88

Figure 4.17 Sensitivity Analysis of Q_f on Burning Rate of 77% AP Based Propellants (40 micron AP). 89

Figure 4.18 Sensitivity Analysis of Q_{PF} on Burning Rate of 77% AP Based Propellants (40 micron AP). 90

Figure 4.19 Burning Rate Comparison of AP/HTPB based Propellants with AP size of 90 μm. 91

Figure 4.20 Literature Data for AP/HTPB based Propellants with 90 μm AP sizes. 92

Figure 4.21 Burning Rate Comparison of AP/HTPB based Propellants with AP size of 200 μm. 93

Figure 4.22 Literature Data for AP/HTPB based Propellants with 200 μm AP sizes. 94

Figure 4.23 Burning Rate Comparison of 73% AP + 1% Fe_20_3 based Propellants (Experimental Data from Krishnan [4]). 95

Figure 4.24 Burning Rate Comparison of 73% AP + 2% Fe_20_3 based Propellants (Experimental Data from Krishnan [4]). 96

Figure 4.25 Burning Rate Comparison of 80% AP + 1% Fe_20_3 based Propellants (Experimental Data from Gaurav [19]). 97

LIST OF ABBREVIATIONS

ABBREVIATIONS

a	Burning Rate Constant
a_2	Kinetics constant for the oxidizer monopropellant flame
A_{AP}	Kinetics prefactor for the oxidizer monopropellant flame reaction
A_f	Arrhenius frequency factor for binder
A_{fc}	Oxidizer particle area fraction of the enhanced condensed phase exothermic decomposition
A_{fh}	Average flame height factor with respect to the oxidizer
Al	Aluminum
AN	Ammonium Nitrate
AP	Ammonium Perchlorate
$APCP$	Ammonium Perchlorate Composite Propellants
A_{ox}	Kinetics Prefactor for Oxidizer Surface Decomposition
A_S	Kinetics Prefactor for Subsurface Condensed Phase Reactions
BEM	Ballistic Evaluation Motor
B_{fh}	Average flame height factor with respect to the binder
c^*	Characteristic Velocity
CEA	Chemical Equilibrium with Applications
C_f	Specific heat of binder
C_F	Thrust Coefficient
C_g	Specific heat of oxidizer combustion product gases
C_S	Specific heat of the oxidizer
$CTPB$	Carboxyl Terminated Polybutadiene

$CuSt$	Copper Stearate
$DEGDN$	Diethylene Glycol Dinitrate
DOA	Dioctyl Adipate
DOP	Dioctyl Phthalate
E_{AP}	Activation energy for the oxidizer monopropellant flame reaction
EC	Ethyl Centralite
E_f	Activation Energy for binder
$EPDM$	Ethylene Propylene Diene Monomer
E_{ox}	Activation Energy for Oxidizer Surface Decomposition
E_S	Activation Energy for Subsurface Condensed Phase Reactions
Fe_2O_3	Ferric Oxide
h/D	Height of protrusion or depression relative to positive, negative intersecting binder surface plane
HMX	Cyclotetramethylene Tetranitramine
$HTPB$	Hydroxyl Terminated Polybutadiene
IDP	Isodecyl Pelargonete
$IPDI$	Isophorone Diisocyanate
I_{SP}	Specific Impulse
K	constant dependent on type of catalyst and surface/subsurface reaction
K_0	Oxidizer ignition delay parameter, constant
KNO_3	Potassium Nitrate
LiF	Lithium Fluoride
m	Diameter exponent in particle ignition term
$\dot{m}_f$	Binder Mass Burning Rate
$\dot{m}_{ox}$	Oxidizer Mass Burning Rate
$\dot{m}_t$	Propellant Mass Burning Rate

$\dot{m}_f''$	Binder Mass Flux Rate
$\dot{m}_{ox}''$	Oxidizer Mass Flux Rate
$\dot{m}_{ox}''$	Propellant Mass Flux Rate
Mg	Magnesium
n	Pressure Exponent
NC	Nitrocellulose
NG	Nitroglycerine
P_{bar}	Pressure in bar values
$PbSa$	Lead Salicylate
P_C	Chamber Pressure
PS	Polysulfide
Q_{binder}	Energy required to heat the binder to its surface temperature
$\mathrm{Q}_{binder,source}$	Source of the energy that heats the binder to its surface temperature
Q_F	Heat content of adiabatic oxidizer monopropellant flame
Q_{FF}	Heat release associated with final flame
Q_L	Net heat release at the oxidizer surface
Q_{ox}	Heat release in the oxidizer monopropellant flame
$Q_{oxidizer}$	Energy required to heat the oxidizer to its surface temperature
$\mathrm{Q}_{oxidizer,source,PF}$	Source of the primary flame energy that heats the oxidizer
$\mathrm{Q}_{oxidizer,source,ox}$	Source of the monopropellant flame energy that heats the oxidizer
Q_{PF}	Heat release in the primary diffusion flame
R	Universal Gas Constant
$\dot{r}_b$	Burning Rate
$\dot{r}_f$	Binder Burning Rate
$\dot{r}_{ox}$	Oxidizer Burning Rate
RDX	Cyclotrimethylene Trinitramine

S_0	Total Surface Area
S_f	Binder Surface Area
S_{ox}	Oxidizer Surface Area
S_P	Planar Surface Area
T_0	Propellant Conditioning Temperature
TDI	Toluene-2, 4-Diisocyanate
TEA	Triethanolamine
T_i	Initial Temperature
t_{ign}	Ignition Delay Time
$TMETN$	Trimehylolethane Trinitrate
T_{ox}	Oxidizer monopropellant flame temperature
T_S	Oxidizer Surface Temperature
$T_{s,f}$	Binder Surface Temperature
X_D^*	Mixing length for diffusion flame
X_{PDF}^*	Flame standoff distance at which Q_{PF} is released over the oxidizer
$X_{PDF,f}^*$	Flame standoff distance at which Q_{PF} is released over the binder
X_{ox}^*	Flame standoff distance at which Q_{ox} is released
X_{PF}^*	Reaction length for diffusion flame
α	Oxidizer Weight Fraction in Propellant
β_f	Fraction of oxidizer that enters into the diffusion flame reaction to heat the oxidizer
β_{ox}	Fraction of oxidizer that is used to heat the oxidizer
β_P	Fraction of oxidizer involved in gas phase reactions
Γ	catalyst specific surface dependent constant
Φ	stoichiometric oxidizer/fuel ratio
λ_g	Gas thermal conductivity

ρ_b	Density of Composite Propellant
ρ_f	Density of Binder
ρ_{ox}	Density of Oxidizer
σ_{AP}	Reaction order, oxidizer monopropellant flame reaction
σ_P	Temperature Sensitivity
ϵ^*_{FF}	Dimensionless flame height associated with final flame
ϵ_{ox}	Dimensionless flame height, oxidizer flame
ϵ_{PF}	Dimensionless flame height, primary flame situated over the oxidizer
$\epsilon_{PF,f}$	Dimensionless flame height, primary flame situated over the binder
ΔH_{ev}	Oxidizer heat of vaporization
ΔH_g	Latent heat of oxidizer decomposition products
ΔH_s	Latent heat of the solid oxidizer
ζ	Volume Faction of Oxidizer in Propellant
Ω	Diminishing return coefficient

CHAPTER 1

INTRODUCTION

This chapter will discuss general information about solid rocket motors and solid propellants. Brief definition of burning rate is included, motivation for this work is explained, and scope of the thesis is presented. Finally, content of the thesis is given.

1.1 Rocket Motors and Propellants

A rocket motor is an energy transfer system in which a pressurized high temperature gas is generated in the combustion chamber and by expanding the gas, a thrust is obtained. As a result, energy generated inside the chamber is converted into kinetic energy [5].

Although there are nuclear rocket engines and electrical rocket propulsion systems, chemical rocket motors are the most preferred types since there are plenty of advancements needed in nuclear rocketry to use them efficiently and source of the electrical propulsion is not very feasible yet [20]. Chemical rocket engines can be classified into 3 subsystems as solid, liquid, and hybrid propellant rocket engines depending on the state of fuel and oxidizer [7].

For the solid propellant rocket motors, fuel and oxidizer have a state of solid, and they are already mixed together inside the combustion chamber [21]. A typical sample of solid rocket motor is provided in Figure 1.1 below.

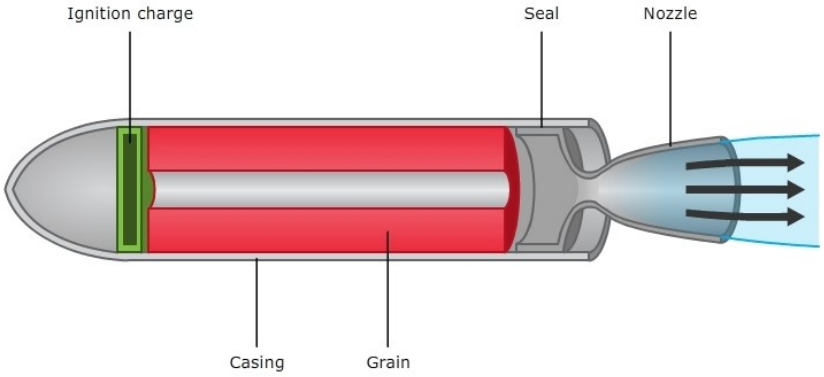

Figure 1.1: Typical Solid Rocket Motor [7].

For the liquid propellant engine, as the name suggests, fuel and oxidizer are in liquid state and they are stored in separate tanks. Before combustion process begins, they are pumped into the combustion chamber by injection and then they react to start the process. An example of this type of motor is given in Figure 1.2.

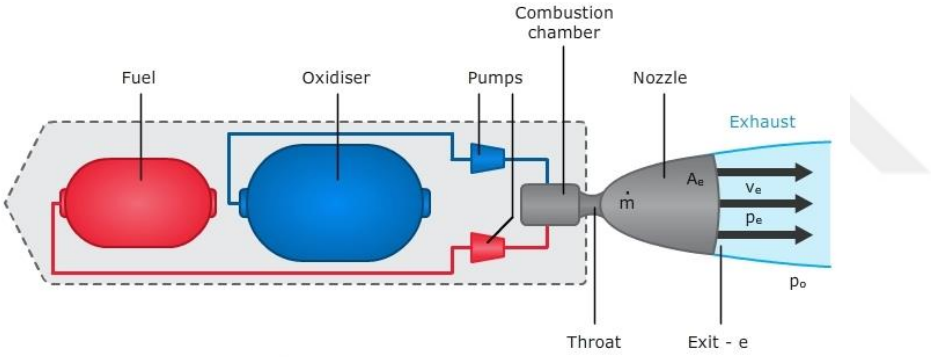

Figure 1.2: Typical Liquid Rocket Motor [7].

Finally for the hybrid propellant engine, fuel is stored in solid state while oxidizer is in liquid phase in a separate tank [22]. To start the combustion process, oxidizer is released through a valve, and reaction of it with the fuel triggers the combustion. In Figure 1.3, a typical hybrid rocket motor is presented.

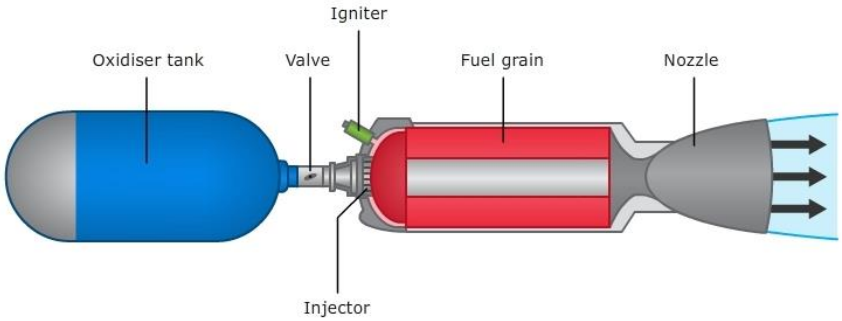

Figure 1.3: Typical Hybrid Rocket Engine[7].

All given rocket motors have different applications of use, but starting from the below part, solid propellant rocket motors are investigated within the scope of this work.

1.1.1 Solid Rocket Motors

Compared to the other chemical rocket propulsion systems, solid rocket motors are less complicated [23] and easier to manufacture. They are used for single operation and their thrust level has a broad range from a few Newtons produced by a small thruster to a few million Newtons produced by a large booster used for a space launch vehicle. Moreover, concerning economic issues, they are relatively cheaper to produce [24].

On the other hand, considering disadvantages, it can be said that there is the lack of controllability and non-reusability [25]. In a liquid propellant engine, the amount of thrust can be controllable and engine itself can be re-usable [26]. In addition to that, solid propellant rocket motors have lower performances considering specific impulses they have [27].

All in all, since they are the most common used propulsion systems, solid propellant rocket motors are investigated within the scope of this thesis. Components of a solid propellant rocket motor is provided in Figure 1.4.

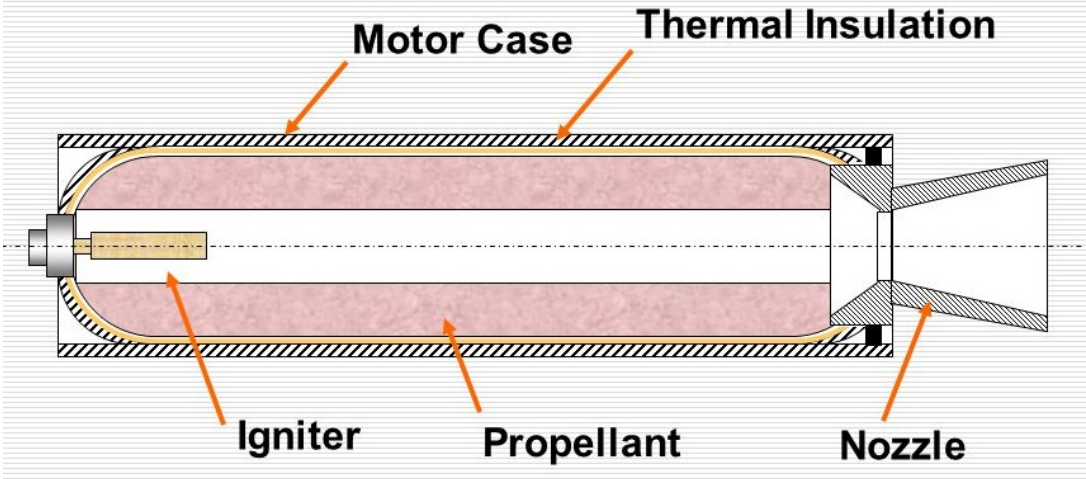

Figure 1.4: Components of a Solid Rocket Motor [8].

Considering the main parts, a solid propellant rocket motor consists of following components [28]:

- Motor Case
- Igniter
- Insulation
- Nozzle
- Solid Propellant Grain

1.1.1.1 Motor Case

Motor case is the outer part of the rocket motor and components of the motor such as igniter, insulation and propellant grain are coated by the case. As a result of combustion phenomena, there is a high pressure generated inside the combustion chamber, and the motor case must be designed to withstand that pressure. Metals such as aluminum or steel and composite materials can be the raw material for the motor case. The material choice and physical characteristics like length and diameter depend on the requirements and can be different for each motor.

1.1.1.2 Igniter

To start the combustion process, there is an energiser needed and igniters are used for this operation. Depending on the types, there can be counted 2 different igniters, first one is pyrogen and the other is pyrotechnic. Pyrogen igniters are small boosters [20] and pyrotechnic igniters consist of pyrotechnic charges to ignite the solid propellant grain.

1.1.1.3 Insulation

During the combustion process, the temperature of the combustion chamber can become thousands of Kelvins, so an insulation material is needed to secure the motor components. Insulations are also used to ease the stresses generated inside the chamber [29]. EPDM and silica materials are commonly used as insulators in solid propellant rocket motors.

1.1.1.4 Nozzle

To accelerate and expand hot gases generated inside the chamber, nozzles are used. They are the ones that determine the motor performance and thrust level, and it is crucial designing the nozzle to expect better performance from rocket motors [30]. Typical convergent-divergent nozzle is given in Figure 1.5.

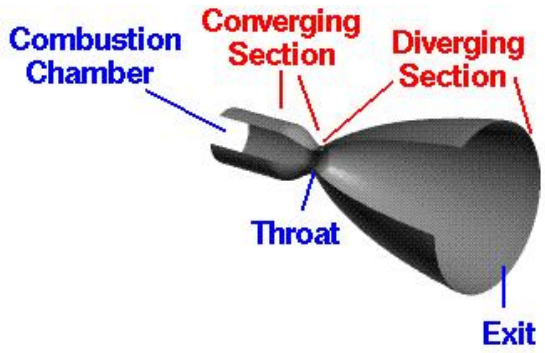

Figure 1.5: Typical Nozzle for Solid Propellant Rocket Engine [9].

1.1.1.5 Solid Propellant Grain

The energetic part of the motor that is ignited by igniters is called the grain. Total impulse of the motor is dependent on the grain, and grain geometries are designed to meet the requirements. There are 2 types of grains; free standing grains are the ones that are produced independently from the case and some support elements such as wedges and springs are used for this type of grain [31]. Case bonded grains are manufactured by casting the propellant ingredients into the motor case and curing them together.

1.1.2 Solid Propellants

Solid propellants are used in rocketry and some gun applications. From a small booster to space launch vehicles, solid propellants can be used to obtain broad range of thrust. To procure the chemical reaction, a solid propellant itself has all the ingredients. Those ingredients can be varied depending on the requirements for each motor, and each composition results in having different rocket motor performances. Solid propellants can be divided into 2 sub-categories as homogeneous (known as double-base propellants) and heterogeneous (composite) propellants. Below, explanation of those propellants can be found.

1.1.2.1 Homogeneous Propellants

Homogeneous propellants are the types of propellants that are famously known as double-base propellants. Their name is coming from the physical structure they have which enables homogeneous distribution. Nitrocellulose (NC) and Nitroglycerine (NG) can be counted as the main ingredients for this type of propellants [29]. An example of this type of propellant is provided below in Figure 1.6.

Figure 1.6: Homogeneous Propellant Sample [10].

In Table 1.1, the ingredient types and some examples for each ingredient can be found for homogeneous propellants:

Table 1.1: Homogeneous Propellant Ingredients [5].

Ingredient Type	**Example of the Ingredient**
Plasticizer(fuel and oxidizer)	NG: Nitroglycerine TMETN:Trimehylolethane Trinitrate DEGDN: Diethylene Glycol Dinitrate
Binder (fuel and oxidizer)	NC: Nitrocellulose
Stabilizer	EC: Ethyl Centralite
Catalyst	PbSa:Lead Salicylate CuSt:Copper Stearate LiF:Lithium Fluoride
High Energy Additive	RDX:Cyclotrimethylene Trinitramine HMX: Cyclotetramethylene Tetranitramine
Metal Fuel	Al: Aluminum
Flame Suppressant	KNO_3: Potassium Nitrate

Although homogeneous propellants have good aging and mechanical properties, it is difficult to obtain complicated grain geometries with them and their performance is

low compared to composite propellants [32].

1.1.2.2 Heterogeneous Propellants

Composite propellant is the name that is known in rocketry area when heterogeneous propellant is discussed and their basic ingredients are oxidizer, binder and metallic fuel. Samples of heterogeneous propellants are given in Figure 1.7.

Figure 1.7: Composite Propellant Sample.

In Table 1.2, the ingredient types and some examples for each ingredient can be found for composite propellants:

Table 1.2: Composite Propellant Ingredients [5].

Ingredient Type	**Example of the Ingredient**
Oxidizer	AP:Ammonium Perchlorate AN:Ammonium Nitrate RDX:Cyclotrimethylene Trinitramine HMX: Cyclotetramethylene Tetranitramine
Binder	HTPB:Hydroxyl Terminated Polybutadiene CTPB:Carboxyl Terminated Polybutadiene PS: Polysulfide
Curing agents	IPDI:Isophorone Diisocyanate TDI: Toluene-2,4-Diisocyanate
Bonding agent	TEA: Triethanolamine
Plasticizer	DOA:Dioctyl Adipate IDP:Isodecyl Pelargonete DOP: Dioctyl Phthalate
Catalyst	Fe_2O_3:Ferric Oxide LiF: Lithium Floride
Metal Fuel	Al:Aluminum Mg: Magnesium

Composite propellants may have smoky exhaust, but on the other hand, it is possible to obtain complex propellant grain geometries with them and their performance is better compared to double-base propellants [33]. Having these advantages over homogeneous propellants makes them widely used in rocket field therefore, they are specifically investigated within the scope of this work.

1.2 Burning Rate of Solid Propellants

In order to understand the phenomena inside the solid propellant rocket motor, internal ballistics are examined. From the beginning of the ignition process till the burn-out of the motor, internal ballistic studies allow the designer to route the attitude

of the rocket motor [34]. Thrust, specific impulse (I_{SP}), characteristic velocity (c^*), thrust coefficient (C_F), chamber pressure, and burning rate can be counted as important ballistic parameters to evaluate the rocket motor performance [35]. Among those parameters, burning rate of solid propellants is the center of interest for this study.

Burning rate can be stated in 2 different ways. First one is the mass burning rate, which has a unit of kg/s and it identifies the mass burnt within a unit of time. Second one, which is used more often, is the linear burning rate of the propellant that gives the regression rate normal to the propellant burning surface and it has a unit of mm/s [36]. In Figure 1.8, direction of surface regression is exemplified for solid propellants at different time periods.

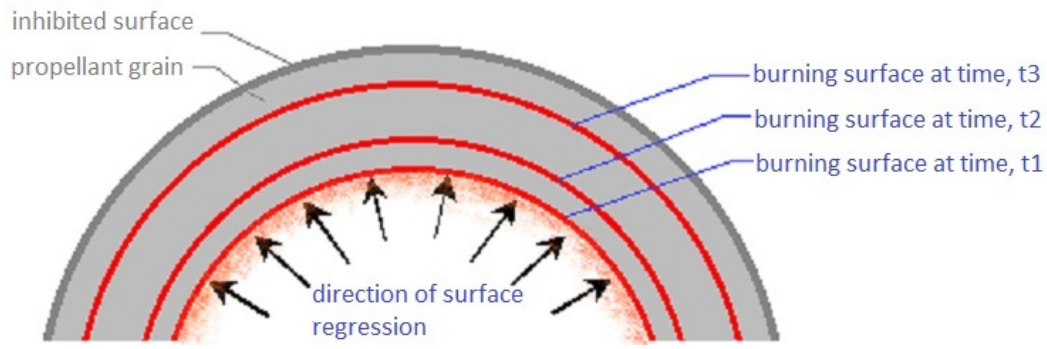

Figure 1.8: Linear Regression of Solid Propellants [11].

Designing the rocket motor, if requirements have to be sorted from the most important one, knowing the burning rate of the propellant at every condition can be easily said to be superior to other parameters. Beginning from the following sections, factors that affect the burning rate and methods to measure burning rate are provided.

1.2.1 Factors That Affect the Burning Rate

There are a lot of factors that affect the burning rate of solid propellants. In terms of physical and chemical point of view, some of them are presented below:

- Composition of the propellant [37]

- Reducing the oxidizer particle size increases the burning rate.
- Burning rate increases with increasing oxidizer percent.
- Catalyst percentage increases the burning rate.
- Adding metal powder to the propellant increases the burning rate.

- Chamber pressure
  - For a solid propellant combustion, burning rate is expressed by Saint Robert's Law as follows [38]:

$$\dot{r}_b = aP_c^n \tag{1.1}$$

    where, a is the burning rate constant and n is the pressure exponent.

- Propellant initial temperature
  - Solid propellants are precisely affected by initial grain temperature, and this reflects their temperature sensitivity. Following relation is given to describe the burning rate variation with temperature [29]:

$$\sigma_P = \frac{dln(\dot{r}_b)}{dT_i} \tag{1.2}$$

    where, σ_P is the temperature sensitivity and T_i is the initial temperature of the propellant. This relation gives the change of burning rate with respect to propellant initial temperature while taking pressure constant.

1.2.2 Methods to Measure Burning Rate

To evaluate the burning rate of the solid propellants, there are several experimental methods performed. The ones preferred for industrial purposes are presented in this section.

1.2.2.1 Test Firings

To begin with the first method, test motor firing is the most efficient way used to obtain burning rate. Depending on the opportunities, sub-scaled motors or full-scaled

motors can be used for this operation. Usually, that sub-scaled motors are called Ballistic Evaluation Motors (BEM) in industry, and they are preferably used to reduce the cost compared to the full-scaled motors. For the practical concerns, they are also more favorable since they are the reduced size of full-scaled motors. Typical test motor firing is presented below in Figure 1.9.

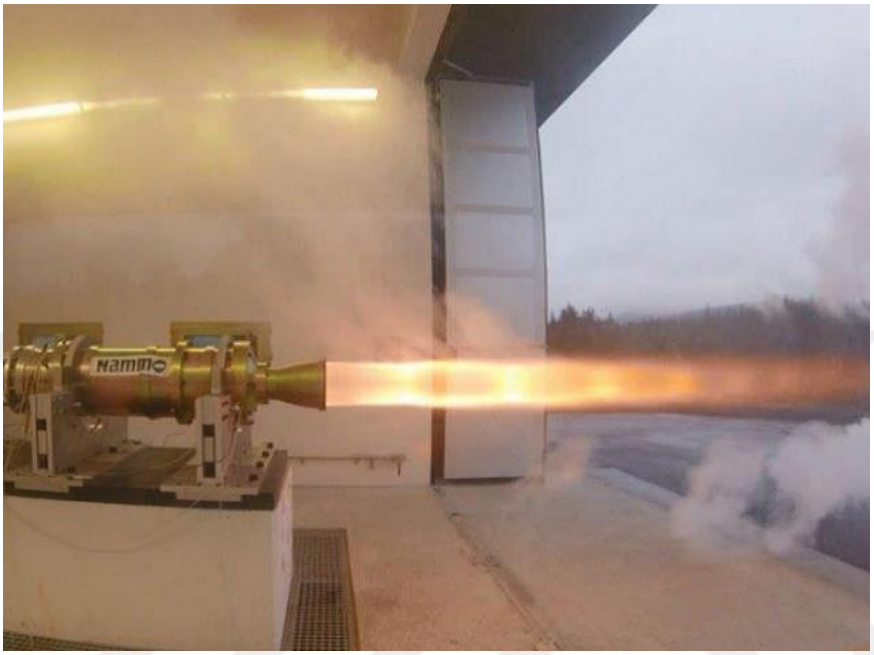

Figure 1.9: Typical Test Firing [12].

Applicable to both sub-scaled and full-scaled motors, burning rate is obtained with knowing the motor burning time and propellant web thickness. Dividing web thickness to burning time makes it possible to obtain burning rate of the propellant using these methods. Although they are the most efficient way to get the burning rate, time and money consumption becomes an issue for this method compared to the other experimental methods.

1.2.2.2 Strand Burner Method

With the invention by B.L. Jr. Crawford [39], strand burner has been used mostly for industrial applications. It is a method to obtain linear burning rate of solid propellants. In this method, end-burning mechanism is utilized and the propellant is burnt from the top cross sectional surface. There are wires embedded into the propellant and

their voltages are measured through data acquisition system.

When the propellant burns, wires start to break away by the flame passing through them. Knowing the time that each wire breaks away, propellant linear burning rate can be calculated since the distance between two wires is known. There can be a lot of advantages counted to use the strand burner method. First of all, conditions can be settled before the firing such as pressure of the burner can be adjusted to a desired value or the temperature inside the chamber can be arranged. In addition to that, a lot of propellant samples can be tested within a desired time. Also, experimental costs are lower and the process is simple. Accurate test results can also be obtained using this method [40].

1.2.2.3 Closed Vessel Method

In this method, there is a closed vessel as the name suggests, and there are pressure sensors and relief valves used in the system. Some igniter materials such as black powder is used to ignite the propellant, and pressure with respect to time graphs are obtained at the end of this experiment. By knowing the geometric information about the propellant such as mass, diameter, length; the burning rate can be obtained with this method.

1.2.2.4 X-Ray Method

Using a radiation source, burning rate of the propellants can be obtained with knowing grain length and total burning time. This method is much more expensive compared to the other burning rate methods [41].

1.2.2.5 Other methods

There are several other methods to obtain burning rate:

- Microwave method [42]
- Ultrasonic Pulse-Echo method [41]

- Plasma Capacitance Gages [43]

Each method has its own advantages and disadvantages, but experimentally obtained burning rate is usually interpreted in Saint Robert's Law as described before.

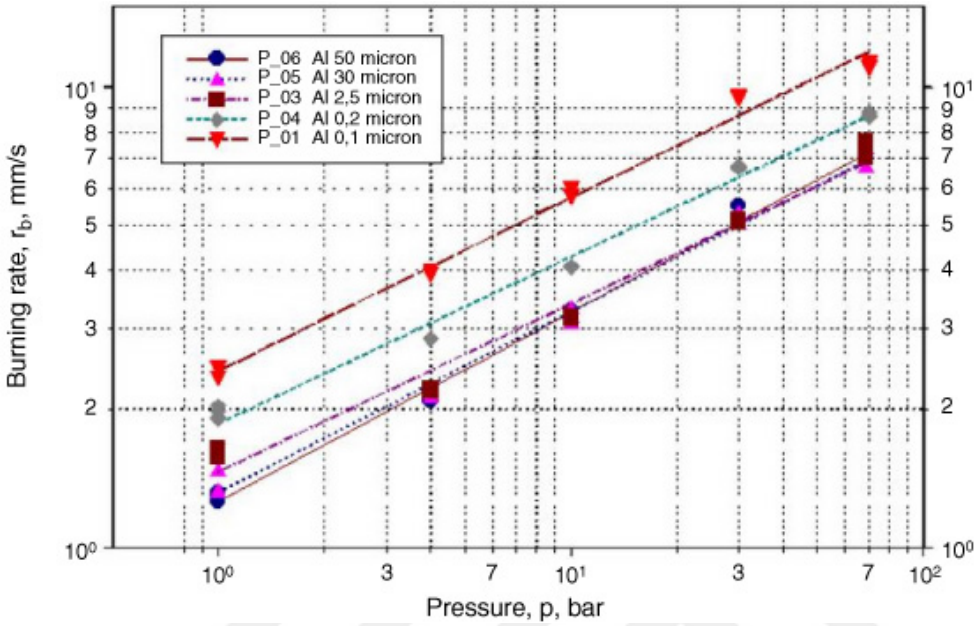

Figure 1.10: Example of Burning Rate Graph [13].

By getting the logarithmic graph of chamber pressure vs. burning rate, there is the typical burning rate graph shown in Figure 1.10. Constants of Saint Robert's Law, a and n are obtained from the graph. As it is stated, each method can be sorted depending on the accuracy of the results, economic concerns, time spent, and repeatability etc. but strand burner method is utilized to serve the purpose of this thesis.

1.3 Motivation

Designers of solid rocket motors choose the optimum propellants based on the design criteria that includes ballistic and mechanical properties. The process of choosing the optimum propellant may require many prototype propellant tests. Although these tests give the most accurate results, they may become costly and usually take much time. Both to decrease the cost and speed up the process, burning rate of solid propellants have been studied to obtain mathematical models from past [14] to recent times

[17].

Motivation behind this study includes combining accurate models in literature and if possible developing them for predicting burning rate more accurately. For industrial concerns, basic aim of this work is to predict burning rates of the propellants developed at Tübitak SAGE. For the propellants selection, ingredients with most usage rate are chosen to serve the purpose of this thesis. Among the oxidizer/binder pairs given in above sections, AP/HTPB pair is the most preferable one in industries, so the first aim of this thesis is obtaining an accurate model for predicting burning rates of that oxidizer and binder pair. After succeeding this model, catalyst additives such as Fe_2O_3 added AP/HTPB composite propellants are investigated. Having an opportunity to compare burning rate data of in-house developed propellants with the numerical scheme predictions is another motivation for this work.

1.4 Scope of the Thesis

While developing new propellants such as changing the ingredients to satisfy requirements, methods like ballistic evaluation motor tests, closed vessel or motor firings are still the first choices in industries. The problem is that these methods consume too much time and money and the purpose of this study is to predict burning rates of most widely used solid propellants in industries by theoretical models. This way, not only time consumption would be minimized, but also burning rates would be obtained without spending money.

First of all, composite propellants are mainly preferred in solid rocket motors, therefore first choice of this study is to predict burning rates of composite propellants. Second choice is made about oxidizer and binder types used in composite propellants. For the oxidizer, AP is the most preferable because of its proven characteristics and accessibility, and for the binder HTPB is very commonly used in general [1]. Therefore, Ammonium Perchlorate composite propellants (APCP) were selected with the binder material of HTPB for this study. Test matrix is constituted for different AP loaded composite propellants with having different particle sizes. Those propellants are burnt using a strand burner setup, on the other hand for the numerical section,

the models in the literature such as Cohen and Strand [2], BDP [3], Krishnan and Jeenu [4] were combined in a mathematical code to predict burning rates of those propellants. Comparing numerical predictions with experimental results is one of the most important goals of this study, after being able to succeed for that model, catalyst added composite propellants are investigated. For the catalyst addition, Fe_2O_3 was chosen because of it's highly usage rate in rocketry. Additional test matrix is composed to investigate the burning rates of catalyst added composite propellants. Again, different AP loadings and different particle sizes are used in that matrix to see the effect of each. By creating the matrix, it is also considered to have similar propellants that were studied in the literature before to compare the results with own results. Comparison of them with the numerical scheme predictions is also provided.

1.5 Content of the Thesis

In Chapter 2, details of the literature survey is given. The survey includes theoretical models to predict burning rates of AP/HTPB and Fe_2O_3 based composite propellants.

Chapter 3 contains methodology of the study. That part is separated into two as numerical and experimental methods. Numerical part includes flow charts of the theoretical models and experimental part consists of detailed test setup and generated test matrices.

Results of the experimental work and comparison of the data with numerical scheme predictions are provided in Chapter 4. Data from the literature and discussion of the results are also presented in that part of the study.

In the final chapter, general conclusion is provided, and what can be done in future is discussed.

CHAPTER 2

LITERATURE SURVEY

As it is stated before, theoretical studies to predict the burning rate have begun from 1960's. To begin with the very basic model, the one that Hermance [14] offered is presented first. It is known as the first model that incorporates heterogeneity on the propellant surface coming from the oxidizer and binder. The combustion process is pictured as the sum of fuel pyrolysis, oxidizer decomposition, heterogeneous chemical reaction between the fuel and decomposed oxidizer, and gas phase combustion of all products. From solid to gas phase, the pictured model is given in Figure 2.1.

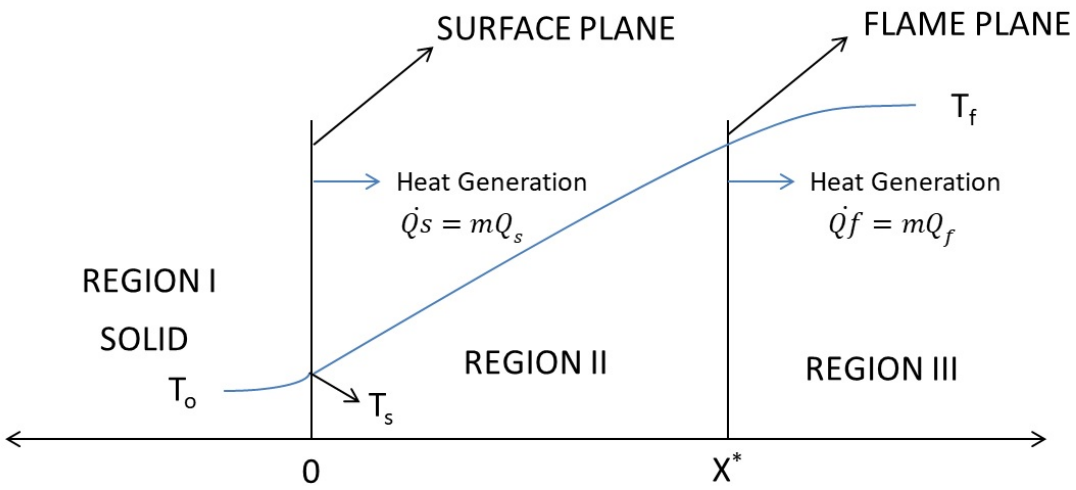

Figure 2.1: Combustion Process Proposed by Hermance [14].

The zones used in this model are separated into 3, and energy equations are used to describe the temperature profile in each zone [14]. With the help of heat releases at the surface of the propellants and mass flux area ratios, final expressions for burning rate are obtained.

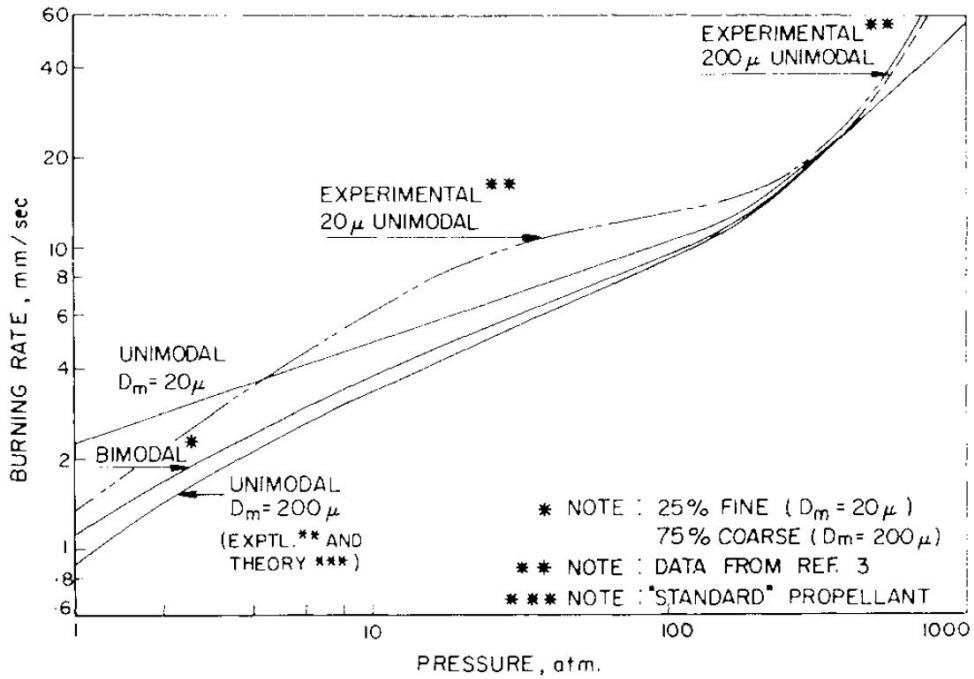

Figure 2.2: Comparison of Experimental Data with Theoretical Model of Hermance [14].

Comparing theoretical model with experimental results, Hermance [14] seems to catch the effect of oxidizer particle size, and good agreement between data and the model can be seen from Figure 2.2. Not only for good results it has, but also this model is important since it makes a basis for theoretical modeling of composite propellants.

Continuing with the Beckstead, Derr and Price model [3], which is famously known as BDP model, it is based on a flame structure surrounding individual oxidizer crystals. In their work, it is believed that assumption of Hermance [14] for the propellant surface was unrealistic, and a model to predict the combustion of AP based composite propellants was developed. Three separate flame zones are considered in corresponding work: a primary flame, a premixed oxidizer flame, and a final diffusion flame which is presented in Figure 2.3.

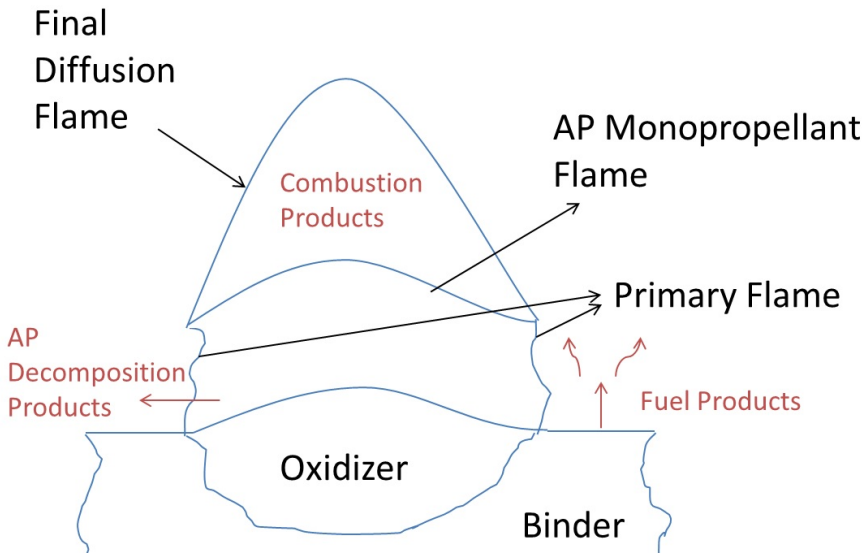

Figure 2.3: Flame Structure Proposed by BDP [3].

Conservation of mass and energy equations are used and also propellant surface geometry is utilized. Flame standoff distances and gas phase heat releases are final equations to obtain the burning rate for this model. Comparison of BDP model [3] with the experimental results is provided in Figure 2.4.

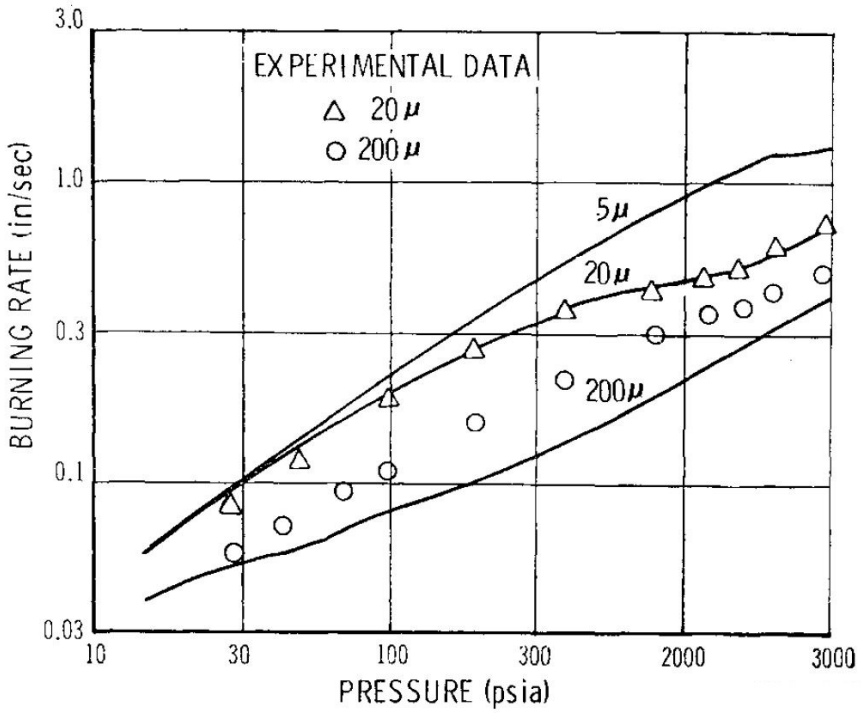

Figure 2.4: Comparison of Experimental Data with Theoretical Model of BDP [3].

The model predicts the results accurately especially for propellants that have lower diameter of AP's. As the particle size increases, there seems to be differences between predictions and experimental results.

After giving the BDP model [3], numerical scheme developed by King [15] is given below. It is a model for non-metalized composite propellants containing unimodal oxidizer. Many concepts used in the BDP model [3] are also used in the King model [15], but there are some modifications:

- Variable oxidizer/binder surface area ratio is used.
- By defining areas used in the BDP model [3], some corrections are made.
- Instead of three separate flame zones, two-flame (diffusion flame and AP mono-propellant flame) zones are considered.

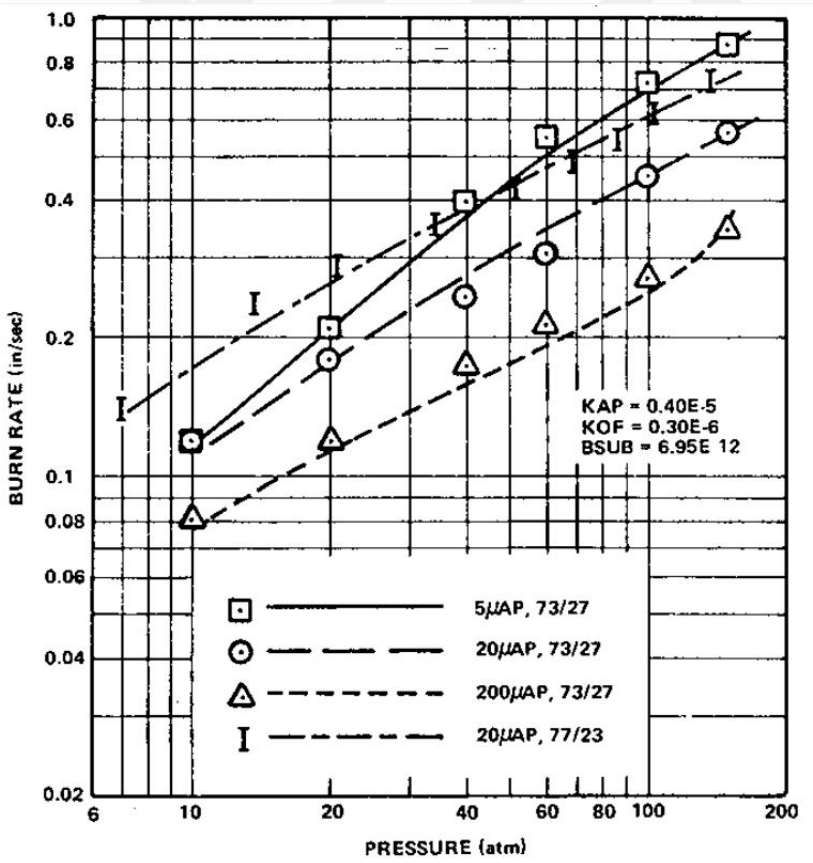

Figure 2.5: Comparison of Experimental Data with Theoretical Model of King [15].

As far as it is seen from Figure 2.5, King [15] was able to develop a more accurate model compared to BDP [3], and for all comparisons given, there seems to be good agreement between theoretical predictions and experimental results.

Another model, which shows up as an improved model to the BDP [3], is presented below. The name of the authors were Cohen and Strand. They suggest some corrections [2] to the BDP model [3]:

- At high pressure values, BDP model [3] doesn't accurately predict the burning rate.
- Binder regression rate is not properly obtained.
- In BDP model [3] single average surface temperature is offered, but they offer a new methodology that includes separate surface temperatures for oxidizer and binder.

Cohen and Strand model [2] has several improvements to the BDP model [3] and basically separate energy equation is written for the oxidizer and binder.

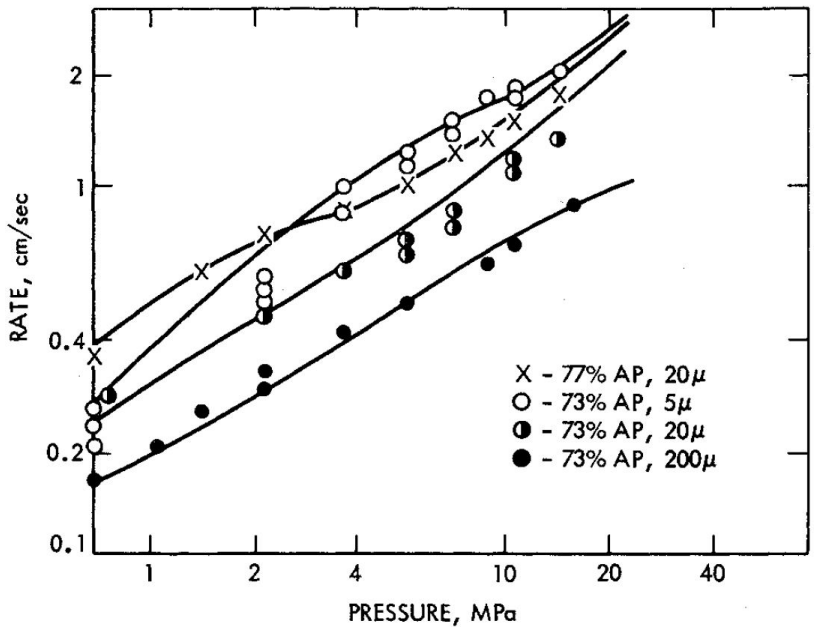

Figure 2.6: Comparison of Experimental Data with Theoretical Model by Cohen and Strand [2].

Evaluating what Cohen and Strand [2] has obtained, it is seen from Figure 2.6 that for all different propellant types, their theoretical model is in very good agreement with the experimental results.

Having seen the Cohen and Strand model [2], Jeppson, Beckstead and Jing model [16] is presented next. This model accounts for the combustion of composite propellants in 3 phases: Solid phase, condensed phase region of mixed liquid and gas, and premixed gas flame which is shown in Figure 2.7.

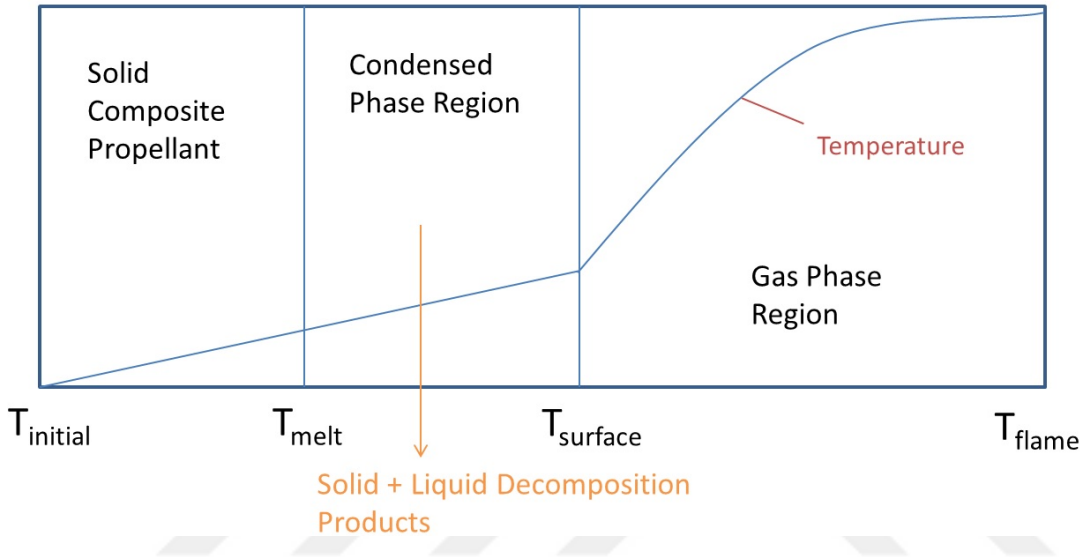

Figure 2.7: Phases of Solid Propellant Combustion Proposed by Jeppson et al [16].

Their model was able to predict the experimental data of King [6] very well as can be seen from the Figure 2.8.

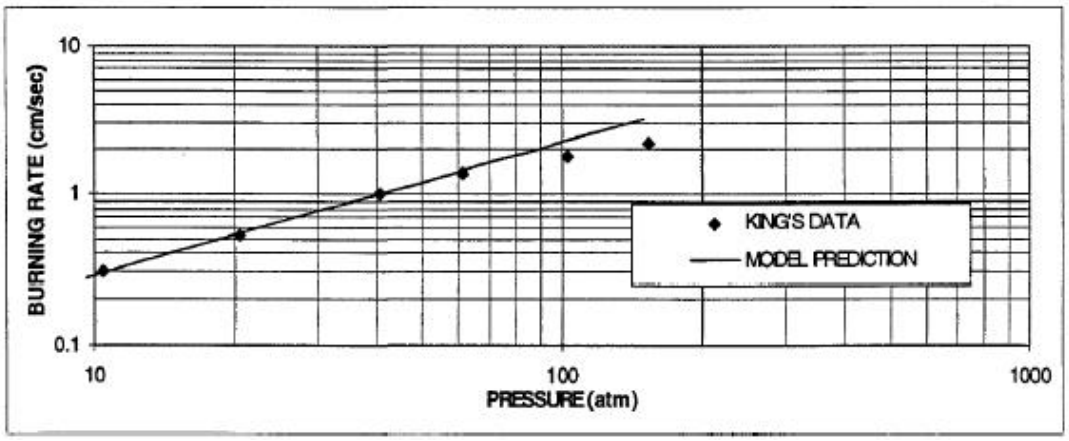

Figure 2.8: Comparison of Experimental Data by King [6] with Theoretical Work of Jeppson et al [16].

Coming through recent models, Vigor Yang and Weidong Cai [17] developed one to predict burning rates. It is based on AP/HTPB composite propellants and conservation equations considering chemical kinetics with unsteady thermophysical properties solved using finite-volume technique.

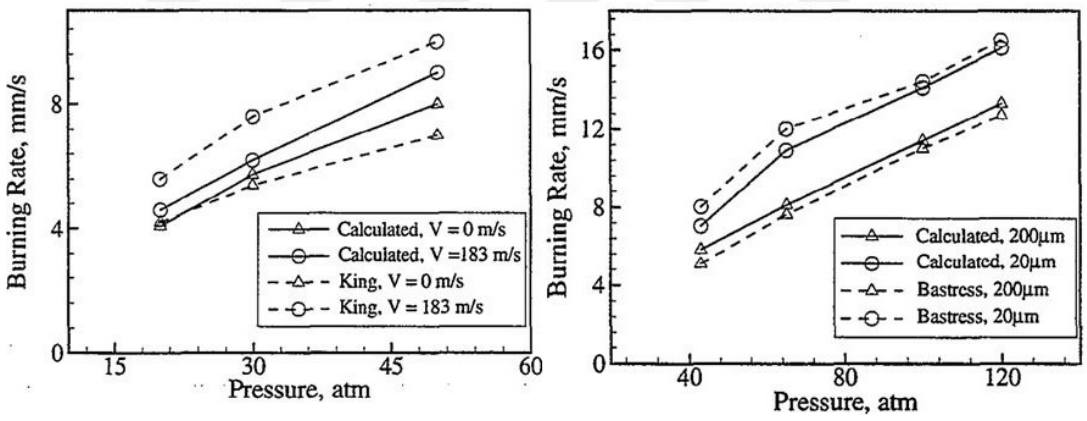

Figure 2.9: Calculated and Experimental Burning Rate by Vigor Yang et al [17], AP/HTPB(70/30) Propellants on the Right - AP/HTPB(73/27) Propellants on the Left.

Their numerical scheme predictions are in good agreement with the experimental results for AP/HTPB (70/30) propellants as can be seen from Figure 2.9. For 73/27 AP/HTPB propellants, they also have good predictions at zero crossflow condition.

Rasmussen and Frederick model [18] is evaluated next. Multilevel flame form sim-

ilar to the BDP model [3] is developed and unsteady conduction equations are used separately for oxidizer and binder in the model. Conservation of mass and energy equations are utilized and characteristic flame temperature with flame heights are used to obtain the burning rate.

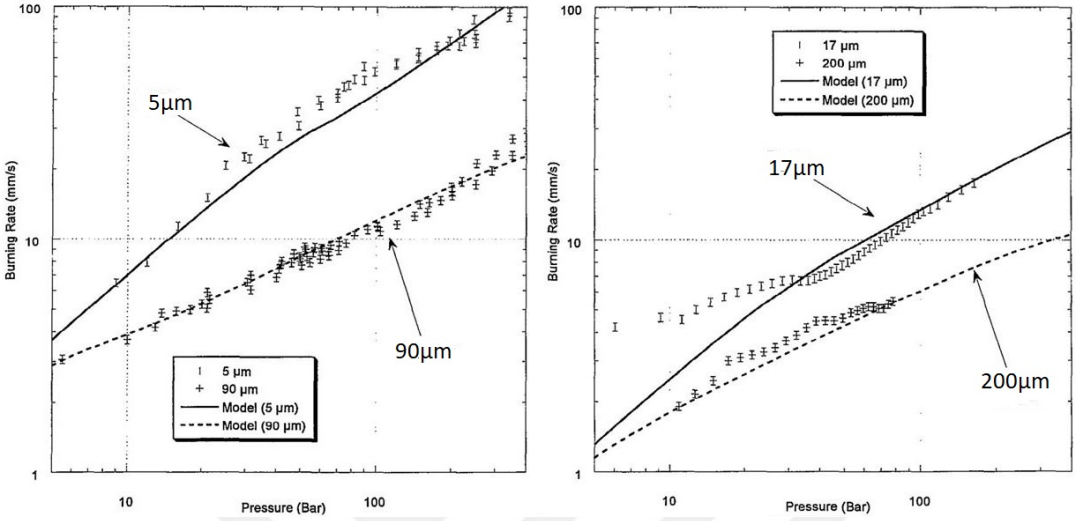

Figure 2.10: Comparison of Experimental Data with Theoretical Model of Rasmussen et al [18], Oxidizer/Fuel Ratio 80/20 on the Left - 75/25 on the Right.

According to their results, all model predictions seem to fit well with experimental results as given in Figure 2.10. These results cover variety of particle sizes of AP with a range from 5μm to 200μm.

Lastly for a catalyzed model, surface reaction model developed by Krishnan and Jeenu [4] is mentioned. Specifically, effect of Fe_2O_3 to the AP/HTPB based composite propellants was investigated, and a numerical scheme had been developed within their study.

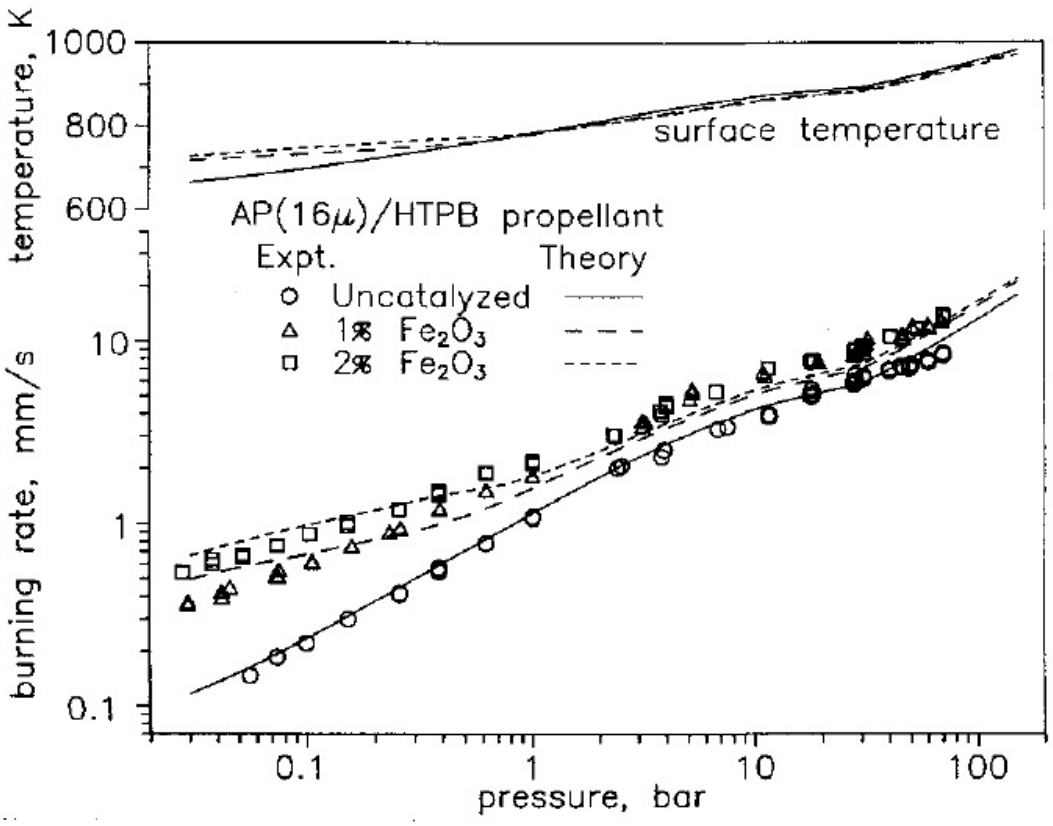

Figure 2.11: Comparison of Experimental Data with Theoretical Model for Catalyzed Composite Propellants by Krishnan et al [4].

For the uncatalyzed, 1% and 2% catalyzed AP/HTPB propellants, this model was able to predict burning rate with being consistent with the experimental results as can be seen from Figure 2.11. Uncatalyzed propellants have a lower burning rate especially at lower pressures compared to the same propellants with being catalyzed.

CHAPTER 3

METHODOLOGY

Providing basic information about burning rates of composite propellants and investigating theoretical models to obtain burning rate, this chapter is going to discuss methods utilized in this study to obtain burning rates. First subsection of this chapter is about numerical methods to predict burning rates and the second subsection is the experimental methods to obtain real time data.

3.1 Numerical Methodology

This part of the study includes theoretical studies to obtain mathematical models for predicting burning rates. As it is stated before, models that include basic solid propellant combustion theories were studied. Beginning from the next section, AP Monopropellant model is provided first. Then AP/HTPB composite propellants is presented, and finally catalyzed AP/HTPB propellants is examined.

3.1.1 AP Monopropellant Model

To begin with the AP monopropellant model, the one that is proposed by Cohen and Strand [2] is taken as a basis which also takes Price, Boggs and Derr model [44] as a reference. Conservation of mass and energy equations are solved in this numerical scheme for propellants that consist of only AP. Flow chart of this method begins with an initial guess for surface temperature of AP. Using Arrhenius equation for mass fluxes and utilizing conservation of energy equations with flame heights, final burning rate of the propellant is obtained which is then used in heat balance at the

surface to find another surface temperature. Both initial guess and final finding of this temperature are compared and iterated until convergence is obtained. Details of this scheme are provided below.

- First of all, an initial guess of oxidizer surface temperature T_S is assumed.
- Using Arrhenius type of equation, mass flux is obtained.

$$\dot{m}''_{ox} = \rho_{ox}\dot{r}_{ox} = A_{ox}exp(-E_{ox}/RT_s) \tag{3.1}$$

- Oxidizer reacts in the condensed phase and gas phase when combustion process begins. Fraction of the AP that reacted in gas phase is found next:

$$\beta_p = 1 - \frac{A_s exp(-E_s/RT_s)}{\dot{m}''_{ox}} \tag{3.2}$$

- Conservation of energy equations are used to find the heat content of AP.

$$Q_F = C_g(T_{ox} - 298) - C_s(T_0 - 298) + \Delta H_g \tag{3.3}$$

  where, first term on the right hand side represents the heat capacity for oxidizer to reach monopropellant flame temperature, second term is the heat needed to decompose the solid oxidizer and last term on the right hand side ΔH_g is the latent heat of oxidizer decomposition products.

$$Q_L = \beta_p(\Delta H_{ev} - \Delta H_g) - (1 - \beta_p)Q_F \tag{3.4}$$

$$Q_{ox} = Q_F + Q_L \tag{3.5}$$

- For the flame heights and dimensionless flame heights, following equations are solved.

$$X_{ox} = \frac{\dot{m}''_{ox}}{a_2 + A_{AP}exp(-E_{AP}/(RT_{ox}))P^{\delta_{AP}}} \tag{3.6}$$

$$\varepsilon_{ox} = \frac{C_g}{\lambda_g}\dot{m}''_{ox}X_{ox} \tag{3.7}$$

- Finally, using conservation of energy at the surface, a surface temperature of oxidizer is obtained. This temperature is compared to the initial guess until convergence is achieved.

$$T_s = T_0 - (Q_L + \Delta H_s)/C_s + (Q_{ox}/C_s)exp(-\varepsilon_{ox}) \tag{3.8}$$

There are parameters aforesaid that must be known(e.g. ρ_{ox}, A_{ox}, E_{ox}, A_s, E_s, Q_F, C_g, T_{ox}, C_s, Q_{ox}, λ_g, X_{ox}, a_2, A_{AP}, E_{AP}) in order to apply the given numerical procedure. To predict burning rates, all these parameters must be well defined. Some of them are provided (A_{ox}, E_{ox}, Q_F, Q_{ox}, X_{ox}), but the ones that cannot be reached are deducted from given data (a_2, A_{AP}, E_{AP}, A_s, E_s), other literature data (C_s), from NASA CEA outputs (C_g, T_{ox}, λ_g) or measured (ρ_{ox}) in Tübitak SAGE facilities. The details of the parametric work are presented below. First of all, using NASA CEA program which takes reactants and operating conditions as inputs to give chemical product concentrations and thermodynamic properties, C_g and T_{ox} values are obtained for pure AP combustion. This is done by running the program from 10 to 200 bars of pressure values with an increment of 10 bars at each step. Moreover to the variable pressure values, initial temperature of the AP is also changed since the parameters are strictly dependent on both temperature and pressure. In Figure 3.1, flame temperature of oxidizer with respect to pressure is provided at variable temperature values.

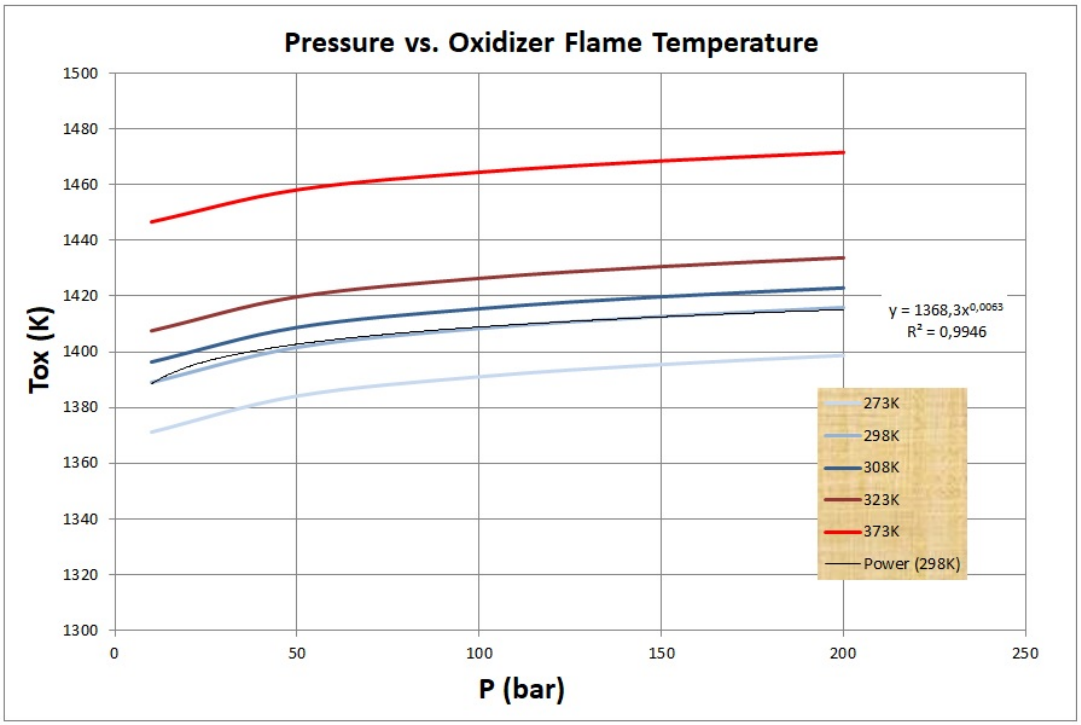

Figure 3.1: Flame Temperature of Oxidizer with respect to Pressure.

From Figure 3.1, it is seen that flame temperature alters drastically with changes in initial temperature of the oxidizer. Since propellants at room temperatures are

investigated within the scope of this study, corresponding room temperature values for flame temperature are used in the numerical scheme. Similar evaluation can also be said for the specific heat of oxidizer combustion product gases and again room temperature values are used for it in the method. Obtained pressure dependent values from NASA CEA outputs for C_g and T_{ox} are provided below.

$$T_{ox} = 1368.3(P_{bar}^{0.0063}) \tag{3.9}$$

$$C_g = 1.4029(P_{bar}^{0.0012}) \tag{3.10}$$

For the thermophysical property, specific heat of AP, Yang et al [45] proposed that C_s = 1460 J/kg.K and converting it's unit to cal/gK, following relation is obtained.

$$C_s = 1460/1000 * 0.2390057361 = 0.3489 cal/gK \tag{3.11}$$

The parameters A_{ox} and E_{ox} are taken as given in Cohen and Strand model [2]:

$$A_{ox} = 1.409 * (10^{42}) g/cm^2 sec \tag{3.12}$$

$$E_{ox} = 167.901 kcal/mol \tag{3.13}$$

For the condensed phase reactions, Arrhenius form of equation is utilized and to find the parameters A_s and E_s mentioned in Eq.(3.2), there is the parametric table (Table 3.1) utilized which is provided in Cohen and Strand paper [2].

Table 3.1: Calculated Results by Cohen and Strand [2] for AP Monopropellant Combustion.

Pressure, MPa	Burning rate, cm/s	Surface Temperature, K	β_p	Flame Height, μm	Q_L, cal/g	Q_{ox}, cal/g
2.15	0.287	865.6	0.761	8.72	185.8	637.9
3.83	0.471	869.9	0.783	5.24	203.1	658.2
6.8	0.811	874.8	0.806	2.93	221.0	6791.1
12.11	1.451	880.1	0.828	1.59	237.7	699.0
21.50	2.605	885.5	0.848	0.86	252.7	717.1

From Table 3.1, it is seen that 5 different parameters T_s, β_p,X_{ox},Q_L and Q_{ox} are provided for AP monopropellant at 5 different pressure values. Using the values given; β_p, A_s and E_s are deducted. This is done by assigning an initial value to E_s, and in return 5 different A_s values are obtained using Eq.(3.2) for 5 different pressures. These 5 A_s values are taken into an array and by using Matlab, iteration for E_s is performed until the difference between maximum and minimum of the array becomes smaller than 1% percent. As a result, following values are obtained.

$$A_s = 4.14216 * (10^{32}) g/cm^2 sec \tag{3.14}$$

$$E_s = 132.6 kcal/mol \tag{3.15}$$

Similar method is used to find the heat content of adiabatic oxidizer monopropellant flame. Using the 5 values provided for Q_L and Q_{ox} from Table 3.1, 5 different Q_F values are obtained by using Eq.(3.5). From those Q_F values, 5 ΔH_g values are obtained by using Eq.(3.3). Curve-fitting 5 ΔH_g values with dependent to pressure, equation to find ΔH_g is obtained for this numerical scheme.

$$\Delta H_g = 77.11 * (P_{bar}^{0.02313}) cal/g \tag{3.16}$$

The values taken from the Table 3.1 and the deducted ΔH_g equation above, 5 ΔH_{ev} values are obtained using Eq.(3.4). Taking the average of those 5 values, final value of ΔH_{ev} is procured.

$$\Delta H_{ev} = 469.14 cal/g \tag{3.17}$$

The method to find A_s and E_s values is also used to find a_2, A_{AP} and E_{AP} values from the Eq.(3.6). This time, unknown parameters are three therefore, iteration is made for those parameters.

$$a_2 = 500 \tag{3.18}$$

$$A_{AP} = 450000 g/(cm^3 secatm^{\delta}) \tag{3.19}$$

$$E_{AP} = 33 kcal/mol \tag{3.20}$$

For the gas thermal conductivity, λ_g, NASA CEA program is utilized again. For the 10 and 200 bars of boundary conditions, with the increment of 10 bars at each step, λ_g values are obtained correspondingly. Pressure dependent equation of λ_g is then constituted.

$$\lambda_g = 0.0002511 * (P_{bar}^{0.00834}) cal/cm.s.K \tag{3.21}$$

For the latent heat of the oxidizer, it is used as stated in BDP model [3].

$$\Delta H_s = 75 cal/g \tag{3.22}$$

With the help of provided numerical scheme and parametric study given above, burning rate of AP monopropellant is obtained. Comparison of the numerical scheme predictions with the Cohen and Strand model [2] is presented below. Alongside the burning rate, other parameters given in Cohen and Strand paper [2] are also compared with the predictions of numerical method.

Table 3.2: AP Monopropellant Parameters found by Current Work.

Pressure, MPa	Burning Rate, cm/s	Surface Temperature, K	β_P	Q_L, cal/g	Q_{ox}, cal/g
2.15	0.29329	865.59	0.7595	184.63	636.69
3.83	0.47506	869.89	0.7827	202.55	657.65
6.8	0.8179	874.78	0.8062	220.78	678.95
12.11	1.459	880.1	0.8285	238.09	699.35
21.5	2.599	885.5	0.8484	253.40	717.78

As far as it is seen from Table 3.1 and Table 3.2, parameters that affect the burning rate of the oxidizer such as Q_{ox}, Q_L, β_P and T_s are in very good agreement with the values provided in Cohen and Strand paper [2]. With the numerical scheme aforementioned, parameters differ at most 1% from what is given in Cohen model [2]. Among them, surface temperature of the oxidizer is believed to be most effective one from Arrhenius form of Eq.(3.1). Obtaining almost the same surface temperatures results in having almost the same burning rate data as expected as can be seen from Table 3.2. Considering the burning rates, it is seen that at most 2.2% difference is seen between two predictions which is at lowest pressures. Other than that, more than 99% agreement is obtained.

3.1.2 AP/HTPB Composite Propellants Model

Giving AP Monopropellant model, composite propellants that consist of AP/HTPB are evaluated next. For this model, Cohen et al [2], BDP [3] and Hermance [14] models are utilized. Uniform surface temperature is assumed in BDP [3] model for composite propellants while predicting burning rates. But it is believed that binders should have higher surface temperatures compared to oxidizers [2], which is supported by the fact that an unrealistic surface structure should have occurred on the propellant burning surface since the binder has a lower burning rate than the oxidizer unless the binder has a higher surface temperature. Considering Arrhenius mass equations, higher surface temperature of the binder makes its burning rate closer to

the oxidizer which results in an evenly burning surface structure as observed in experiments.

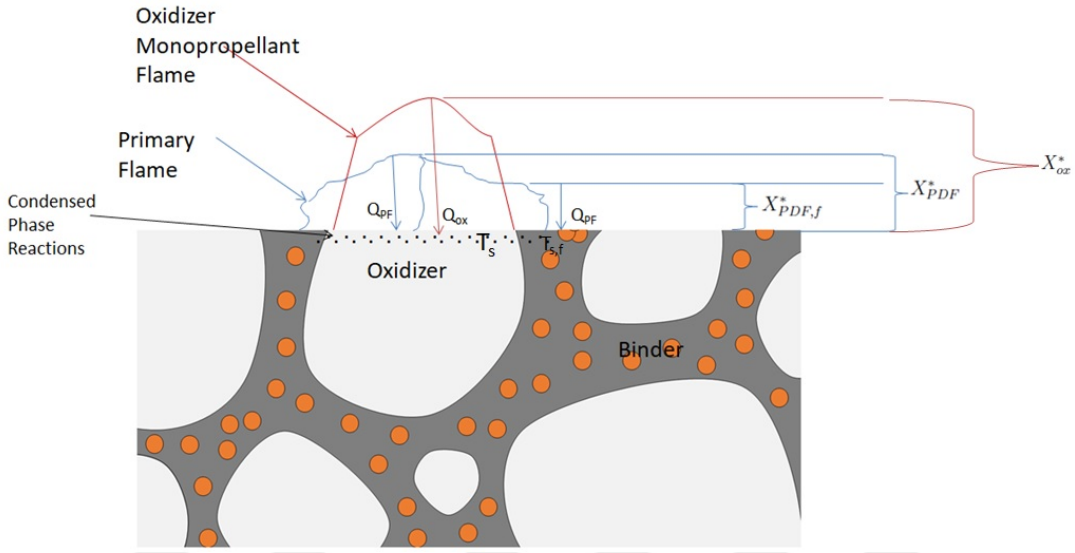

Figure 3.2: AP/HTPB Propellant Flame Structure.

Brief composite propellant model is pictured in Figure 3.2. Details of the model are provided below in this chapter but basically following features are considered:

- Unlike the BDP model [3], two different flame structure is considered with final diffusion flame being ignored since it is believed to have a negligible effect on burning rate.
- Fraction of the primary flame is allowed to be over the binder. Flame height of that fraction which belongs over the binder is required to be smaller than the corresponding height over the oxidizer to make sure that binder will have a higher surface temperature.
- Separate energy balances are required to have different surface temperatures. For the oxidizer, energy required to raise the temperature is supplied from oxidizer monopropellant flame and primary flame. On the other hand, only primary flame controls the temperature of the binder.
- To satisfy the conservation of energy, corresponding heat fluxes multiplied with dimensionless flame heights which is presented in the model details and this represents the fraction of heat conducted to the surface.

Modeling process begins with Arrhenius form of equations and conservation of mass principles. With those, mass flux rates are obtained for oxidizer and binder. To see the effect of different surface temperatures, separate energy equations are used for oxidizer and binder. Then similarly to the AP monopropellant model, initial surface temperature for oxidizer is assumed and iterated through equations until convergence is achieved.

Flow chart of the model is provided below. Burning rate of solid propellant can be related to mass flux as follows:

$$\dot{m}_T'' = \rho_b \dot{r}_b \tag{3.23}$$

Mass flow rate of the propellant is equal to the sum of oxidizer and binder rates.

$$\dot{m}_T = \dot{m}_f + \dot{m}_{ox} \tag{3.24}$$

In terms of area, Eq. (3.24) becomes:

$$\dot{m}_T'' S_0 = \dot{m}_f'' S_f + \dot{m}_{ox}'' S_{ox} \tag{3.25}$$

Dividing both sides to S_0:

$$\dot{m}_T'' = \dot{m}_f'' \frac{S_f}{S_0} + \dot{m}_{ox}'' \frac{S_{ox}}{S_0} \tag{3.26}$$

The amount of oxidizer in the propellant is defined by α:

$$\alpha = \frac{\dot{m}_{ox}}{\dot{m}_T} \tag{3.27}$$

Similarly, the amount of binder for a propellant that consists of only oxidizer and binder is obtained by subtracting α from 1.

$$1 - \alpha = \frac{\dot{m}_f}{\dot{m}_T} \tag{3.28}$$

Combining Eq.(3.27), Eq.(3.28) and Eq.(3.26), total mass flux rate is obtained in terms of oxidizer and binder mass flux rates separately:

$$\dot{m}_T^{''} = \frac{\dot{m}_{ox}^{''}}{\alpha}\frac{S_{ox}}{S_0} \tag{3.29}$$

$$\dot{m}_T^{''} = \frac{\dot{m}_f^{''}}{1-\alpha}\frac{S_f}{S_0} \tag{3.30}$$

And combining Eq.(3.30) and Eq.(3.23), burning rate of the propellant is written in terms of mass flux rates:

$$\rho_b \dot{r}_b = \frac{\dot{m}_f^{''}}{1-\alpha}\frac{S_f}{S_0} \tag{3.31}$$

In order to obtain burning rate, propellant surface geometry is required as can be seen from Eq.(3.31). Ratio of oxidizer surface area to total surface area is used as proposed in BDP model [3].

$$\frac{S_{ox}}{S_0} = \frac{\zeta[6(\frac{h^2}{D_0})+1]}{[6\zeta(\frac{h^2}{D_0})+1]} \tag{3.32}$$

where, ζ is defined as total volume fraction of oxidizer crystals. This is unknown for a given propellant and can be obtained as follows. For a given mass fraction of oxidizer to binder:

$$\frac{\alpha}{1-\alpha} = \frac{\zeta\rho_{ox}}{(1-\zeta)\rho_f} \tag{3.33}$$

Simplifying Eq.(3.35),

$$\zeta = \frac{\alpha\rho_f}{\alpha\rho_f + (1-\alpha)\rho_{ox}} \tag{3.34}$$

Volume fraction of oxidizer in a given propellant is obtained by knowing densities and mass fraction of each component.

In the BDP model [3], it is suggested that AP particles to protrude at low pressure values while they recess at high pressure values.

Figure 3.3: AP Particles Protruding and Recessing at Surface.

According to this assumption, h/D_0 term given in Eq.(3.32) is explained as follows:

$$\frac{h}{D_0} = \frac{1}{2}(1\frac{1}{\sqrt{3}})(1 - \frac{\dot{r}_{ox}}{\dot{r}_f}) + \dot{r}_{ox}\frac{t_{ign}}{D_0} \tag{3.35}$$

In Eq.(3.35) ignition delay time (t_{ign}) is needed. For this term, what Hermance [14] proposed is used in this numerical scheme.

$$t_{ign} = \frac{K_0 D_i^{n+1}}{P^m} \tag{3.36}$$

where K_0 is defined as AP ignition delay constant. In the Hermance model [14] unknown parameters in Eq.(3.36) are provided as $K_0 = 200sec - atm^m cm^{-n}$, m=0.75 and n=0.8 [14].

For the binder, mass flux rate is described as follows:

$$\dot{m}_f^{''} = \rho_f \dot{r}_f \tag{3.37}$$

Considering Arrhenius form of mass flux rate:

$$\dot{m}_f'' = A_f exp(\frac{-E_f}{R_u T_{s,f}}) \tag{3.38}$$

As given for AP monopropellant model, some data for 73% AP/HTPB propellant are also provided by Cohen and Strand model [2] that can be seen in Table 3.3.

Table 3.3: Calculated Internal Quantities by Cohen and Strand [2] for King's [6] 73% AP/HTPB Propellants.

Pressure, MPa	Surface Temperature, K(20μ AP)		Surface structure, h/D (20μ AP)	β_{ox}, (20 μ AP)
	AP	HTPB		
0.68	862.4	1048	-0.168	0.616
1.21	865.7	1098	-0.170	0.627
2.15	868.2	1140	-0.177	0.642
3.83	871.6	1201	-0.179	0.695
6.8	875.6	1280	-0.178	0.744
12.11	879.9	1359	-0.175	0.785

There are unknown parameters in Eq.(3.38) such as E_f and A_f. To obtain mathematical values for them, similar method to obtain A_s and E_s for AP monopropellant is used. Using the values from Table 3.3, arrays are constituted for E_f and A_f. Using Matlab, iteration procedure is followed until the difference between minimum and maximum of an each array becomes less than 1% percent. As a result, following values are obtained.

$$A_f = 672.745 g/cm^2 sec \tag{3.39}$$

$$E_f = 16.8795 kcal/mol \tag{3.40}$$

Combining Eq.(3.29) and Eq.(3.30), following relation is obtained for binder and oxidizer flux rates:

$$\dot{m}_f'' = \frac{1-\alpha}{\alpha}\dot{m}_{ox}'' \frac{S_{ox}}{S_f} \tag{3.41}$$

For the areas given in Eq.(3.41), assuming planar fuel surface, Hermance [14] proposed following relation:

$$S_f = (1-\zeta)S_0 \tag{3.42}$$

Giving all the conservation of mass relations and surface geometry parameters, burning rate of the AP oxidizer is obtained using Arrhenius form of equation.

$$\dot{r}_{ox} = \frac{A_{ox} exp(-E_{ox}/RT_s)}{\rho_{ox}} \tag{3.43}$$

In Eq.(3.43), oxidizer surface temperature T_s is not known. In order to obtain that, Cohen and Strand [2] proposed separate energy balances for the oxidizer and binder. Steps of how the energy balances are obtained are presented below. To begin with the binder, first of all energy needed to heat the binder to surface temperature is defined as the sum of heat capacity required from initial to surface temperature and the heat of decomposition:

$$Q_{binder} = \dot{m}_f'' S_f C_f (T_{s,f} - T_0) + \dot{m}_f'' S_f Q_f \tag{3.44}$$

The source of heating the binder is the primary flame as stated in Figure 3.2. Energy of this source is the fraction that subtracts the energy used to heat the oxidizer from the total primary flame energy.

$$Q_{binder,source} = (1-\beta_{ox})\dot{m}_T Q_{PF} exp(-\xi_{PF,f}) \tag{3.45}$$

The term $\dot{m}_T$ in Eq.(3.45) can be written in terms of oxidizer and binder mass fluxes as stated in Eq.(3.25). Combining Eq.(3.25), Eq.(3.44) and Eq.(3.45), final energy balance is obtained for the binder.

$$\dot{m}_f'' S_f [C_f (T_{s,f} - T_0) + Q_f] = (1-\beta_{ox})(\dot{m}_{ox}'' S_{ox} + \dot{m}_f'' S_f) Q_{PF} exp(-\xi_{PF,f}) \tag{3.46}$$

In Eq.(3.46), there are unknown terms such as Q_f, Q_{PF} and $\xi_{PF,f}$. First two terms Q_f and Q_{PF} stands for the heat of binder decomposition and the heat release in the primary diffusion flame respectively. The other term $\xi_{PF,f}$ is the dimensionless flame height of primary flame that takes place over the binder. That flame height is investigated in this chapter with the other provided flame heights. For the first two terms, it is provided in BDP [3] model that Q_f is on the order of 0-200 cal/g, also it is taken as 50 cal/g in that paper and it is mentioned that Hermance [14] took this term as 175 cal/g. Since the term is open to debate, it is taken as 100 cal/g in this numerical scheme and sensitivity analysis of it is given in Chapter 4 to see its effect on burning rate. Similarly for the Q_{PF} parameter, it is provided in BDP model [3] that it should be on the order of 650 cal/g and is defined in the same model as follows:

$$Q_{PF} = C_g(T_{ox} - T_0) + \alpha\Delta H_s + (1-\alpha)Q_f \tag{3.47}$$

Since C_g, T_{ox}, T_0 and ΔH_s are constants for the propellant types, it is deduced from Eq.(3.47) that Q_{PF} varies with Q_f and α for a given propellant. It is taken as 650 cal/g in this study but sensitivity analysis of this parameter is also provided in Chapter 4. Boundaries of it can be deduced to α being 0.7 at minimum and 0.8 at maximum for this study since from 70% to 80% AP loaded propellants are investigated. For the Q_f, boundaries are taken as 10-200 cal/g and applying these values to Eq.(3.47), boundary of sensitivity analysis made for Q_{PF} is determined to be in between 500 and 800 cal/g.

After obtaining energy equations for the binder, similar conservation of energy principle is applied to the oxidizer by taking a control volume on AP particle. The energy required to heat the oxidizer to its surface temperature is defined as the sum of heat capacity from initial to surface temperature and the heat of decomposition.

$$Q_{oxidizer} = \dot{m}''_{ox} S_{ox} C_s (T_s - T_0) + \dot{m}''_{ox} S_{ox} \Delta H_s + \dot{m}''_{ox} S_{ox} Q_L \tag{3.48}$$

Source of the energy that heats the oxidizer is provided from the primary flame and oxidizer monopropellant flame as stated in Figure 3.2. Fraction of the primary flame energy that is utilized to heat the oxidizer is defined as follows:

$$Q_{oxidizer,source,PF} = \beta_{ox}\beta_f \dot{m}_T Q_{PF} exp(-\xi_{PF}) \tag{3.49}$$

The energy supplied from the monopropellant flame is similarly defined, but this time

the source term requires the mass flow rate of only oxidizer not the total flow rate.

$$Q_{oxidizer,source,ox} = \beta_{ox}(1-\beta_f)\dot{m}_{ox}Q_{ox}exp(-\xi_{ox}) \tag{3.50}$$

Writing down the mass flow rates in terms of fluxes as given in Eq.(3.25) and combining Eq.(3.48), Eq.(3.49) and Eq.(3.50), following energy balance is obtained for the oxidizer.

$$\dot{m}_{ox}^{''}S_{ox}[C_s(T_s-T_0)+\Delta H_s+Q_L] = \beta_f\beta_{ox}(\dot{m}_{ox}^{''}S_{ox}+\dot{m}_f^{''}S_f)Q_{PF}exp(-\xi_{PF})+ \\ \beta_{ox}(1-\beta_f)\dot{m}_{ox}^{''}S_{ox}Q_{ox}exp(-\xi_{ox}) \tag{3.51}$$

In Eq.(3.51) and Eq.(3.46) there are unknown terms such as ξ_{ox}, ξ_{PF}, $\xi_{PF,f}$ which are called dimensionless flame heights. Those are taken as proposed in Cohen et al [2] and BDP [3] model. For the oxidizer flame height, following equation is given by them:

$$X_{ox}^{*} = \frac{\dot{m}_{ox}^{''}}{\alpha + A_{AP}exp(\frac{-E_{AP}}{R_U T_S})P^{\delta_{AP}}} \tag{3.52}$$

Getting flame height of the oxidizer, dimensionless height is calculated as below:

$$\varepsilon_{ox}^{*} = \frac{C_g\dot{m}_{ox}^{''}X_{ox}^{*}}{\lambda_g} \tag{3.53}$$

In this equation, C_g and λ_g are described as specific heat of AP combustion product gases and gas thermal conductivity respectively. After evaluating the oxidizer flame height, the primary diffusion flame height is investigated. This height is separated into two as the one over oxidizer and the other one over binder. To begin with the dimensionless flame height of primary diffusion flame over the oxidizer, Eq.(3.54) is obtained:

$$\varepsilon_{PF}^{*} = \frac{C_g\dot{m}_{T}^{''}X_{PDF}^{*}}{\lambda_g} \tag{3.54}$$

The dimensional height of it is given as follows:

$$X^*_{PDF} = X^*_{PF} + A_{fh} X^*_D \tag{3.55}$$

where A_{fh} is defined in BDP [3] model as average flame height factor, and is in between 0-1. It is proposed in the BDP model [3] that it is equal to 0.3.

Coming to the flame height created by primary diffusion flame on the binder, dimensionless height is defined similarly to that over the oxidizer.

$$\varepsilon^*_{PF,f} = \frac{C_g \dot{m}''_T X^*_{PDF,f}}{\lambda_g} \tag{3.56}$$

Similarly for the dimensional flame height:

$$X^*_{PDF,f} = X^*_{PF} + B_{fh} X^*_D \tag{3.57}$$

where B_{fh} is similar to the A_{fh}, and is assumed in Cohen and Strand model [2] that it is 1/8 of the A_{fh}. The reason for this is that flame should be closer to the binder, and as a result, it is possible for the binder to be heated more compared to the oxidizer which also promotes higher surface temperatures for binder as mentioned before.

$$B_{fh} = \frac{A_{fh}}{8} \tag{3.58}$$

Lastly for the thermophysical properties of AP and HTPB, densities of them were measured in Tübitak SAGE facilities and for the specific heat of the binder what Vigor Yang et al [45] proposed in their paper was used in this study.

$$\rho_{AP} = 1952.7 \frac{kg}{m^3} \tag{3.59}$$

$$\rho_{HTPB} = 950.76 \frac{kg}{m^3} \tag{3.60}$$

$$C_f = 2860 \frac{J}{kgK} \tag{3.61}$$

With the help of the abovementioned equation set, the numerical scheme is completed. The solution starts with initial guesses for S_{ox} and T_s. Then S_f, $\dot{m}_f''$ and $\dot{r}_f$ are calculated and using Eq.(3.32), S_{ox} is obtained. Iteration is done until initial and final S_{ox} are converged. $T_{s,f}$ and β_{ox} are obtained next, and finally using Eq.(3.51) another T_s is obtained. The iteration stops when the difference between initially assumed and finally calculated T_s value is less than 1%. To compare the Cohen and Strand model [2] with the current work assisted by the parametric study provided, some given values in the model are evaluated first, and then final burning rates are compared. For that, data provided for 73%AP - 20μ in the Cohen and Strand model [2] are used, and for the burning rates, data for 73%AP - 5μ, 73%AP - 20μ and 73%AP - 200μ are utilized.

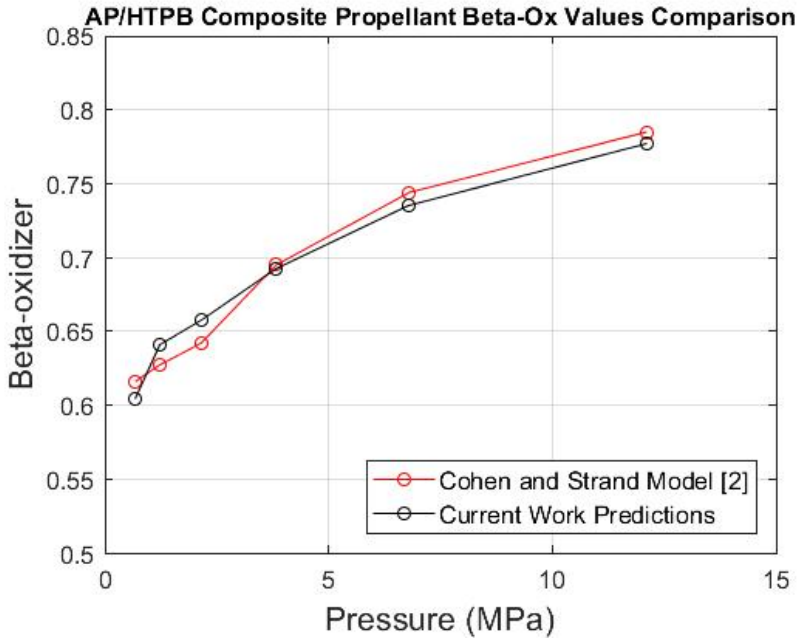

Figure 3.4: β_{ox} Values Comparison of Cohen and Strand model [2] with the Current Work Predictions.

To begin with, β_{ox} comparison of what is obtained in current work and the values given in Cohen and Strand model [2] is given in Figure 3.4. β_{ox} is defined as the fraction of AP that is used to heat itself, and regarding the values, good approxima-

tion can be found between two predictions. The discrepancies may come from having used different parameters. Giving this comparison, another is made for surface temperatures of both AP and HTPB individually.

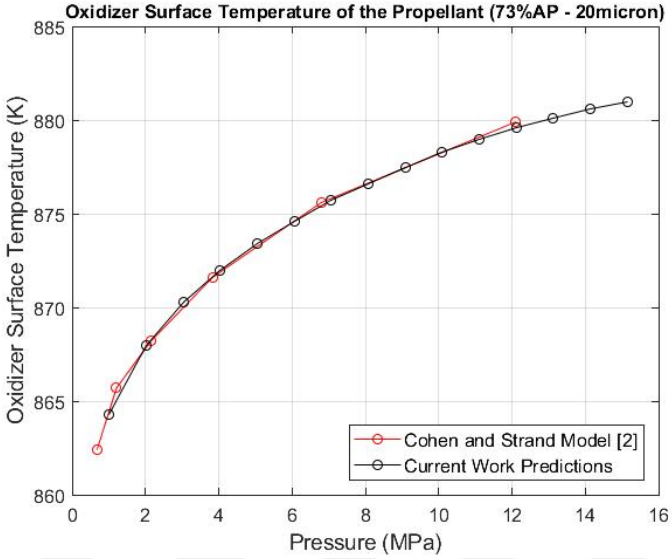

Figure 3.5: Oxidizer Surface Temperature Comparison of Cohen et al [2] with the Current Work Predictions for 73 AP% - 20μ Propellants.

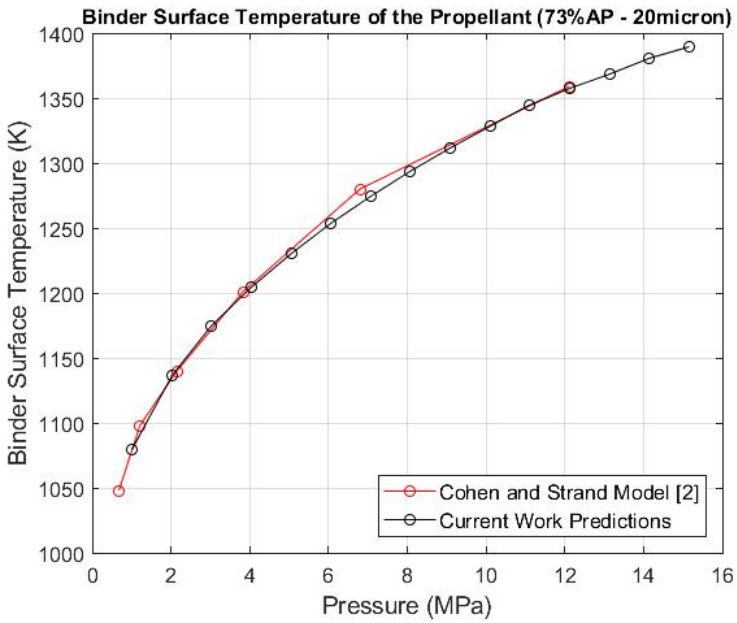

Figure 3.6: Binder Surface Temperature Comparison of Cohen et al [2] with the Current Work Predictions for 73 AP% - 20μ Propellants.

Talking for both surface temperatures, the ones Cohen and Strand provided [2] and what is found with the parametric study of this work are in very good agreement as can be seen from Figure 3.5 and Figure 3.6.

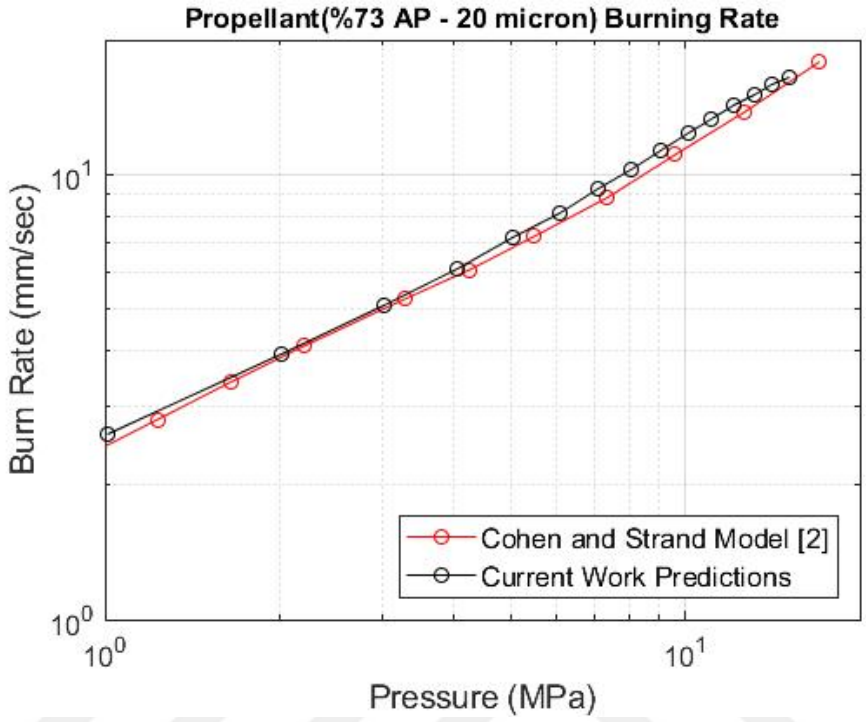

Figure 3.7: Burning Rate Comparison of Cohen and Strand Model [2] with the Current Work Predictions for 73 AP% - 20μ Propellants.

After evaluating some parameters given in the model, numerical scheme predictions in terms of burning rate data are compared with the Cohen and Strand data [2]. From Figure 3.7, it can be seen that own parametric study gives almost the same results with what Cohen and Strand [2] got with their model. Alongside 73%AP-20μ propellant data, Cohen and Strand [2] provided data for other propellants.

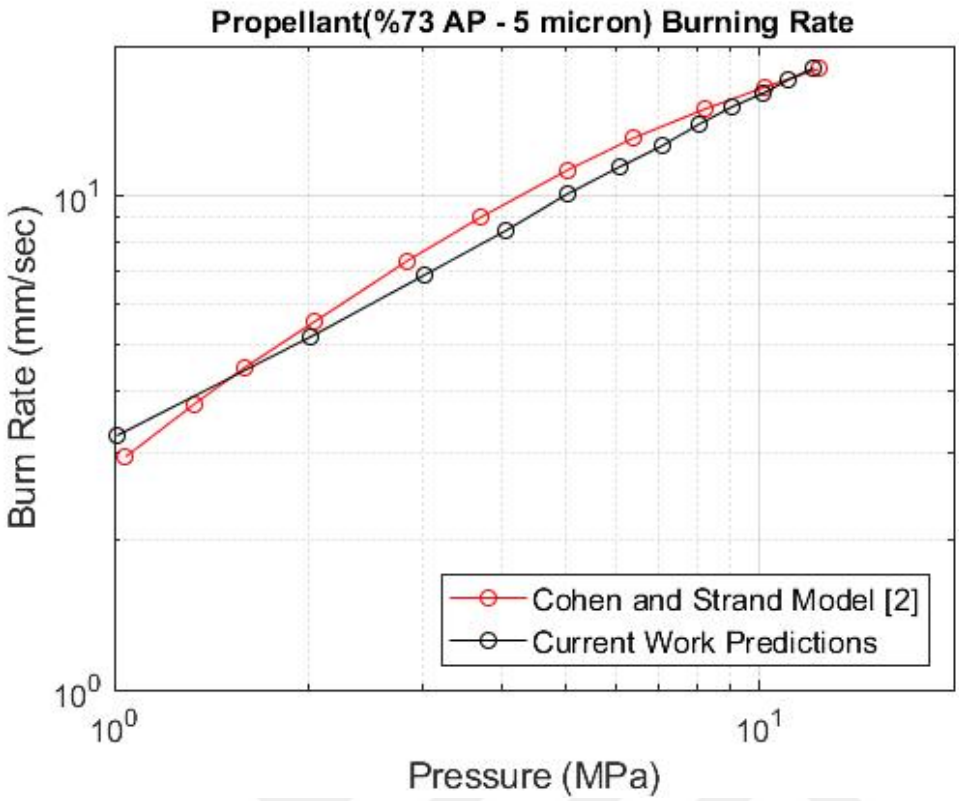

Figure 3.8: Burning Rate Comparison of Cohen and Strand Model [2] with the Current Work Predictions for 73 AP% - 5μ Propellants.

Considering the propellant that has 73% AP which is 5μ of size, although the models give close results, compared to the 20μ data there seems less agreement between them as can be seen from Figure 3.8. Having obtained parameters from different sources may be the reason for having these differences for this propellant type.

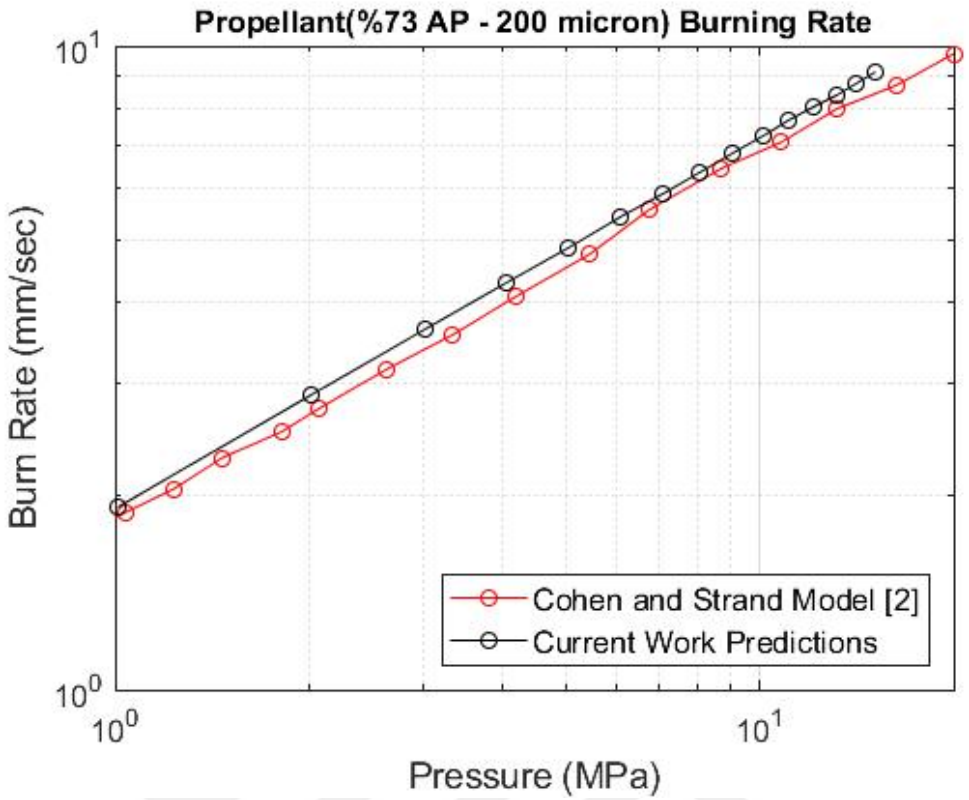

Figure 3.9: Burning Rate Comparison of Cohen and Strand Model [2] with the Current Work Predictions for 73 AP% - 200μ Propellants.

For the 200μ propellant that has the same AP percent as before (73%), the two predictions seem to agree at almost all pressure values as provided in Figure 3.9. In this chapter, only the comparison of Cohen and Strand model [2] with the current work is mentioned. Comparison of them with the experimental results is provided in Chapter 4 for all propellants. In the next subsection, flow chart of the catalyzed AP/HTPB propellant is provided.

3.1.3 Catalyzed AP/HTPB Model

About the catalyzed composite propellants, there are several models developed in the literature. Extensions to the basic BDP model [3] are used to account for the catalytic effect. Although Cohen [46] and Beckstead [47] developed some models, what Krishnan and Jeenu [4] proposed is used as a reference which includes a surface and subsurface heat release assumption. They also have the BDP model [3] as a

reference for the other surface area and conservation equations.

For the AP/binder interface, Cohen et al [48] and Jones and Strahle [49] observed that incorporating catalysts doesn't promote reaction of gases with the binder, or make any changes in pyrolysis, but it triggers the gas phase reactions at the AP/binder interface. So it is believed that catalysts do not directly involved in the reactions between oxidizer and binder, but they speed up the process.

Coming to the modeling part, adding catalyst to composite propellants is believed to affect mostly the pre-exponential factor [46] [47]. Therefore, that pre-exponential factor is modeled as the sum of uncatalyzed and catalyzed Arrhenius form.

$$m_{ox,s,catalyzed} = A_{ox,s}[1 + A_{fc} * K_{ox,s} * \Omega/(\Omega + \Gamma)]exp(-E_{ox}/(R * T_s)) \quad (3.62)$$

where A_{fc} is the oxidizer particle area fraction, Ω is catalyst mass concentration in binder multiplied by catalyst surface area and Γ is catalyst specific surface dependent constant. Here in the equation, subscript "s"" stands for surface while "ss"" will be used for subsurface in below equations. Similarly subscript "cped" used to show associated condensed phase exothermic decomposition whereas subscript "subl" is associated with oxidizer sublimation beyond this part.

Giving the pre-exponential factor in Arrhenius form, heat release of the oxidizer flame is given as follows:

$$\begin{aligned} Q_{ox} = (1 - A_{fc}) * (\epsilon * Q_{ox,cped} + (1 - \epsilon) * Q_{ox,subl}) + \\ A_{fc} * (\epsilon_{catalyzed} * Q_{ox,cped} + (1 - \epsilon_{catalyzed}) * Q_{ox,subl}) \end{aligned} \quad (3.63)$$

As it stands, heat release is modeled in two parts as condensed phase reactions and sublimation. For the mass conservation, the model includes following changes to the BDP [3] model for catalytic additives.

$$\dot{m}''_t S_0 = (\dot{m}''_{ox,s} S_{ox,s} + \dot{m}''_{ox,ss} S_p)/\alpha \quad (3.64)$$

$$\dot{m}''_t S_0 = ((\dot{m}''_{f,s} S_{f,s} + \dot{m}''_{ox,ss} S_p)/\Phi)/(1-\alpha) \tag{3.65}$$

Again, conservation equation is separated into surface and subsurface parts. For the energy balance, the model has only the following variation:

$$\begin{aligned}
&[(\dot{m}''_{ox,s} S_{ox,s} + \dot{m}''_{f,s} S_{f,s})\beta_f + \dot{m}''_{ox,ss}(1+1/\Phi)S_P]Q_{PDF} \\
&= [(\dot{m}''_{ox,s} S_{ox,s} + \dot{m}''_{f,s} S_{f,s})\beta_f + \dot{m}''_{ox,ss}(1+1/\Phi)S_P]C_P(T_{PDF} - T_0) + \dot{m}''_{ox,s} S_{ox,s}\beta_f Q_{ox} \\
&\qquad + \dot{m}''_{f,s} S_{f,s}\beta_f Q_f + \dot{m}_{ox,ss}(1+1/\Phi)S_P Q_{ss}
\end{aligned} \tag{3.66}$$

Other heat release equations are taken as the same as before. And finally, surface temperature equation is used to finish the model.

$$\begin{aligned}
\dot{m}''_T C_P(T_s - T_0) = &-\dot{m}''_{ox,ss}(1+1/\Phi)(S_P/S_0)Q_{ss} - \dot{m}''_{ox,s}(S_{ox}/S_0)Q_{ox} \\
&- \dot{m}''_{f,s}(S_f/S_0)Q_f + [\beta_F[\dot{m}''_{ox,s}(S_{ox}/S_0) + \dot{m}''_{f,s}(S_f/S_0)] \\
&+ \dot{m}''_{ox,ss}(1+1/\Phi)(S_P/S_0)]Q_{PDF}exp(-\epsilon^*_{PDF}) + \\
&(1-\beta_F)\dot{m}''_{ox,s}(S_{ox}/S_0)(Q_{AP}exp(-\epsilon^*_{AP}) + Q_{FF}exp(-\epsilon^*_{FF}))
\end{aligned} \tag{3.67}$$

For the parameters used in the model, following values are provided [4].

$$E_{ox,ss} = 32.5 kcal/mole \tag{3.68}$$

$$A_{ox,ss} = 10^8 g/cm^2 \tag{3.69}$$

$$T_r = 550K \tag{3.70}$$

Using the model, following comparison of burning rate is obtained by Krishnan et al [4] for catalyzed composite propellants.

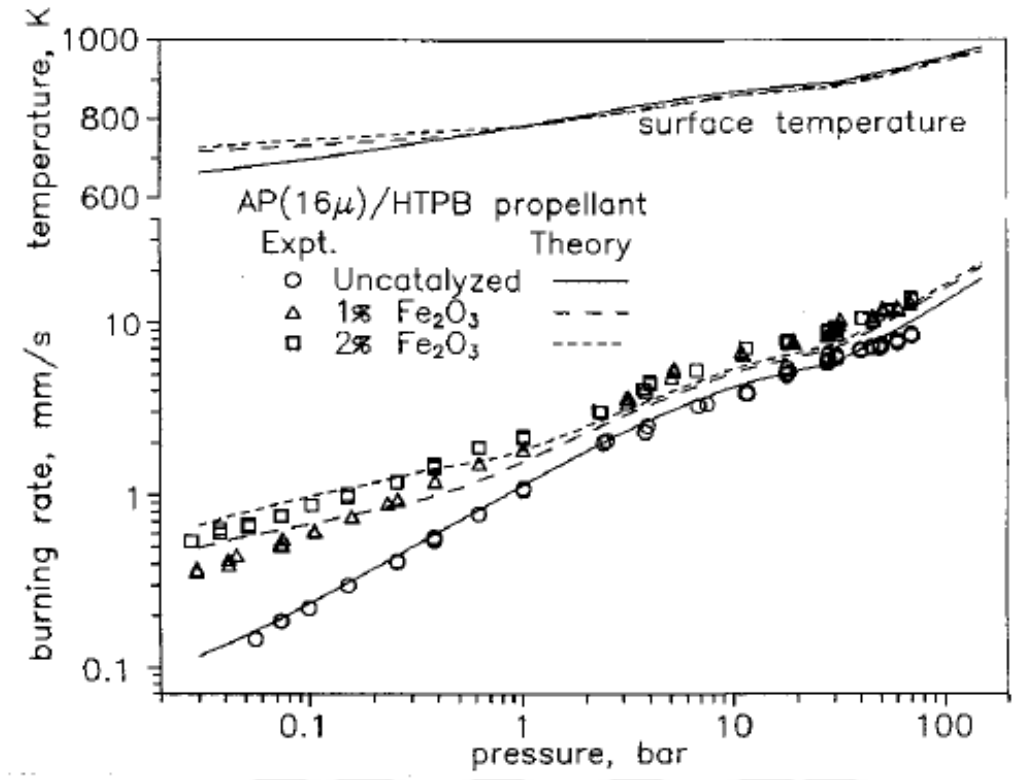

Figure 3.10: Comparison of Experimental Work with Theoretical Studies by Krishnan and Jeenu [4] for Catalyzed Composite Propellants.

As seen from Figure 3.10, the model was able to predict well especially at smallest pressures for 73%AP based composite propellants with having 1% and 2% percent of iron oxide [4] [50].At higher pressures, the model has deviations up to 20% which is acceptable. Comparison of the numeric predictions with the own experimental results is provided in Chapter 4 of the thesis.

3.2 Experimental Methodology

The main objective of this study is to compare burning rates of numerical scheme predictions with the experimental results for composite propellants. For this reason, experimental work has been done using in-house developed composite propellants in a strand burner test setup in this study.

General information about the experimental setup is provided in this chapter. Brief

description of components in the setup is given including their features. After introducing the setup, information related with the tests itself is mentioned. Test matrix is the first thing to be evaluated regarding the tests. The reasons behind choosing the matrices are presented. Test plan is the final part in which details of experiments such as at which pressures tests are conducted, how many data are collected is supplied.

3.2.1 Test Setup

Schematic of the experimental setup is given in Figure 3.11 and description of each component is presented below.

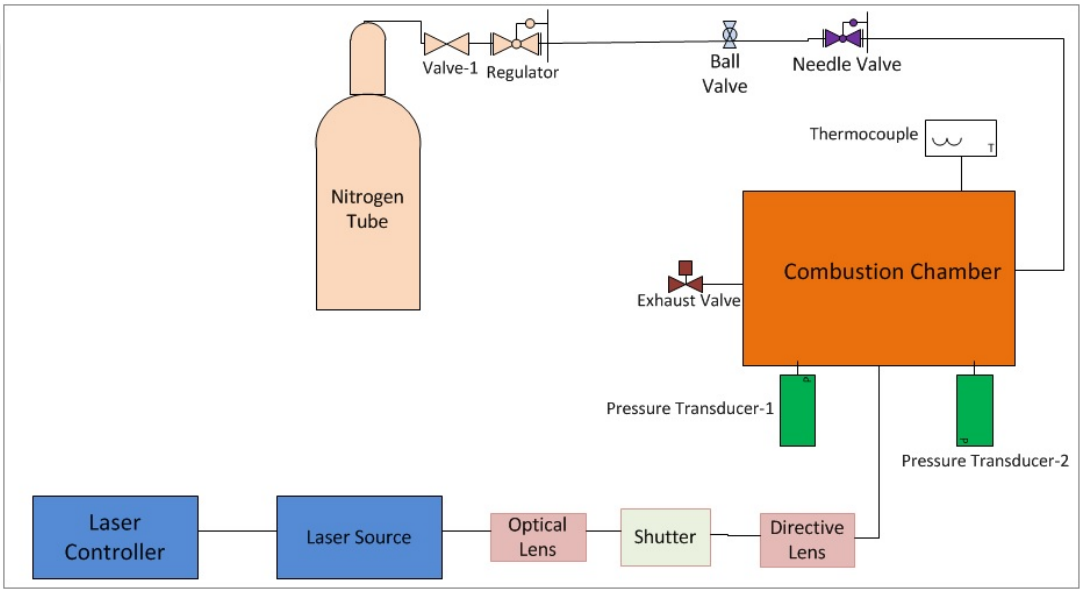

Figure 3.11: Schematic of the Test Setup.

The components of the setup provided in Figure 3.11 are basically a CO_2 laser source, optical lenses, a shutter, a strand burner, a nitrogen tube, some valves, pressure sensor and data acquisition system. General photograph of the setup is given below, and major components of the system are shown. Detailed component explanations are given later in this section.

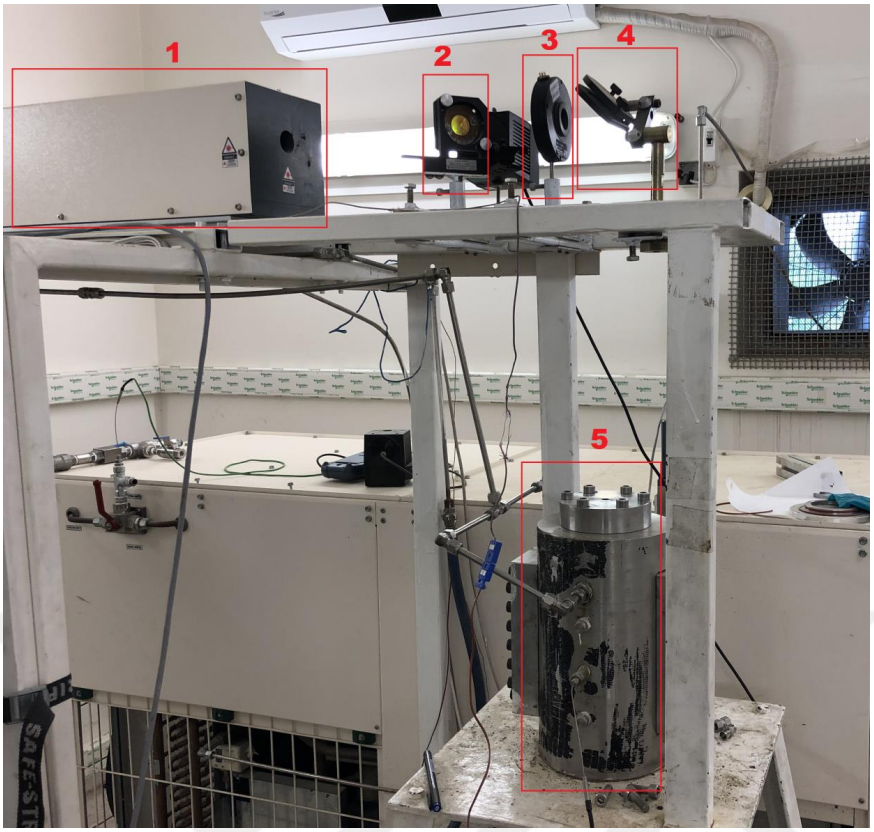

Figure 3.12: General View of the Test Setup.

Briefly explaining the Figure 3.12, the laser coming out from the laser source (Label "1") passes through lenses (Label "2" and Label "4") and a shutter (Label "3"). Then it enters the combustion chamber (Label "5") to start the ignition. Nitrogen tube is used to pressurize the chamber; pressure sensor is used to gather the pressure data. Data acquisition system is utilized to obtain burning rate. Finally some valves are used in the setup for nitrogen gas to flow into the chamber and to discharge it after the experiment is completed. All components of the setup are explained in details below.

3.2.1.1 Control Panel

There is the control panel exists in the setup, given in Figure 3.13, to control the valves in the system, and to visualize the pressure and temperature values within the viewpoint.

Figure 3.13: Strand Burner Control Panel.

The valve labeled with "1" in the above picture is referred as the ball valve. It is used for coarse tuning while pressurizing the chamber. "2" labeled valve is the needle valve, and it is used for fine tuning to obtain intended pressure. The valve located in upper left of the control panel, "3", is the exhaust valve and it is opened to discharge the gas inside the chamber after the combustion process is completed.

3.2.1.2 CO_2 Laser Source

To ignite the propellant, there is the CO_2 laser source used in the setup. A power source shown in Figure 3.14 is used to actuate the laser.

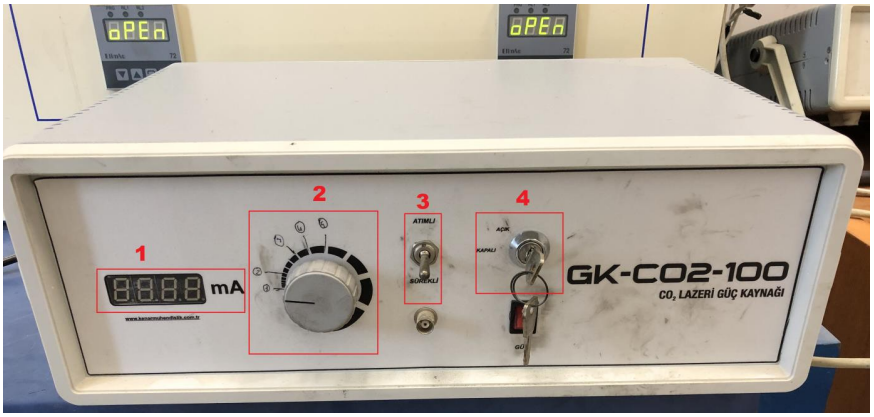

Figure 3.14: CO_2 Laser Source Controller.

In Figure 3.14:

- Label "1": Digital indicator of the laser output in terms of mA
- Label "2": Laser power regulator switch (On the left output is minimum, on the right laser output is maximum)
- Label "3": Switch button (At the up position laser is provided continuously, at the down position laser is provided on a frequency basis)
- Label "4": Key of the laser source (When it is up laser is open, when it is turned left laser is closed)

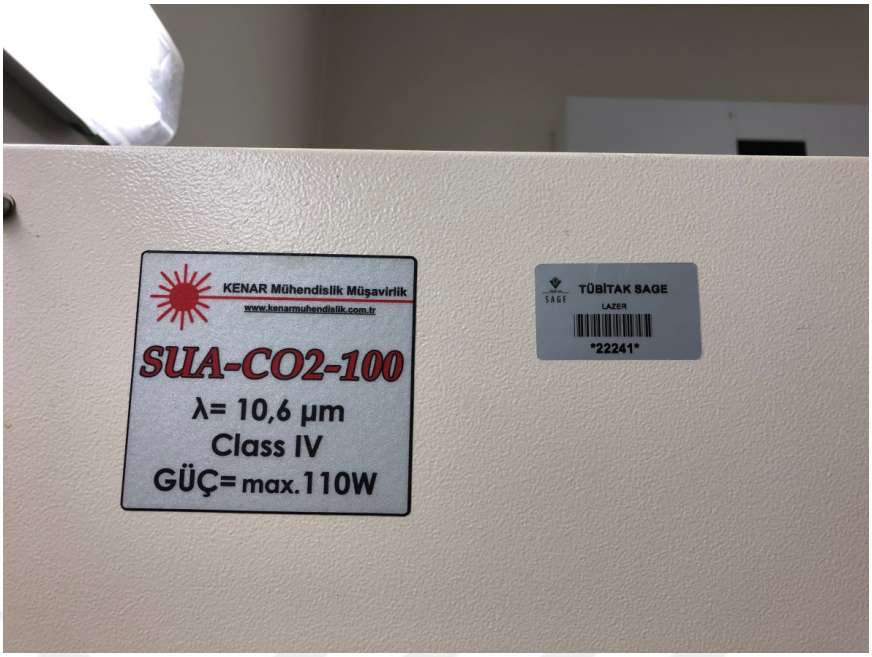

Figure 3.15: CO_2 Laser Details.

Laser source itself is class IV and has a wavelength of 10.6 μm as given in Figure 3.15. It produces a profile of having 3.5 mm diameter at the surface it is projected on. Maximum power of the laser is 110W and it can be arranged optional in between 0-110W.

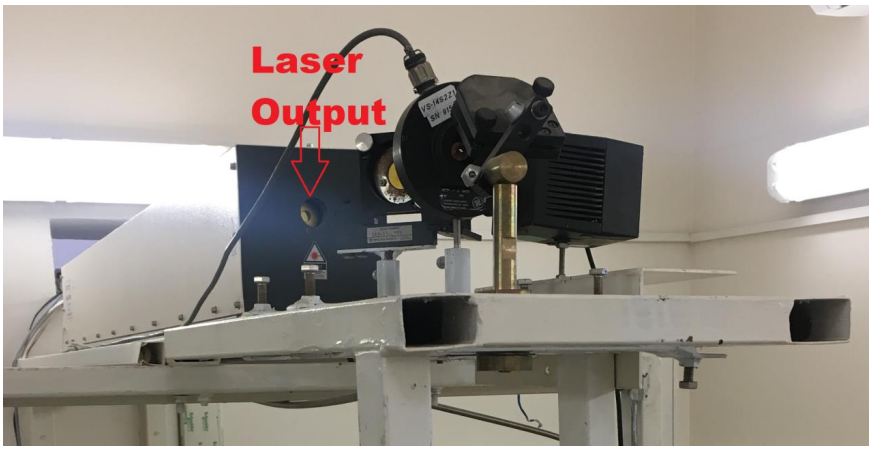

Figure 3.16: Exit Port of the Laser.

The laser beam leaving from the exit port is directed (from the red arrow shown in Figure 3.16) to the optical lens which is explained later.

3.2.1.3 Nitrogen Tube and Regulator

For the Nitrogen tube, there is the set as seen in Figure 3.17 that consists of 15 single tubes which is used in the setup. Each tube has a maximum pressure supply of 230 bars and has a high-purity level of 99.999 % as shown in Figure 3.18.

Figure 3.17: Nitrogen Tube and Regulator.

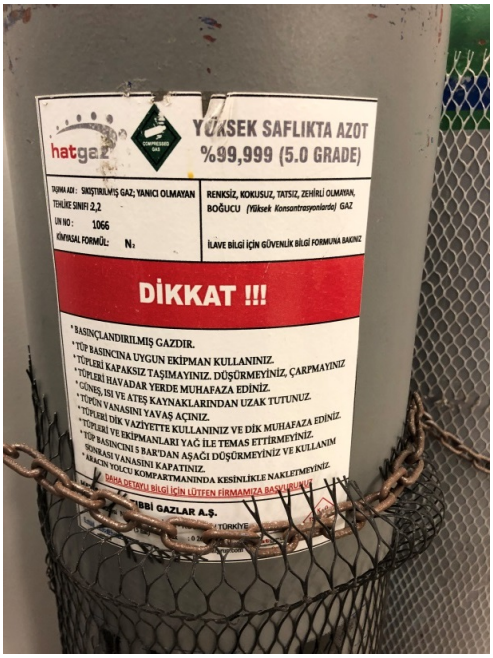

Figure 3.18: Nitrogen Tube Details.

Additionally there is the regulator placed in front of the tubes (as shown in Figure 3.17) to regulate the pressure sent into the chamber. The input side of the regulator has a range of 0-230 bar, whereas the output is 0-200 bar. Therefore, the pressure can be arranged up to 200 bar pressure values. Detailed regulator picture is provided in Figure 3.19.

Figure 3.19: Regulator on the Nitrogen Tube.

3.2.1.4 Optical Lens

Laser, coming from the exit port of the source, passes through the optical lens. This lens is used to reflect the 15% of the laser input and allows the remainder to pass [1]. The place of the optical lens in the setup is given in Figure 3.20.

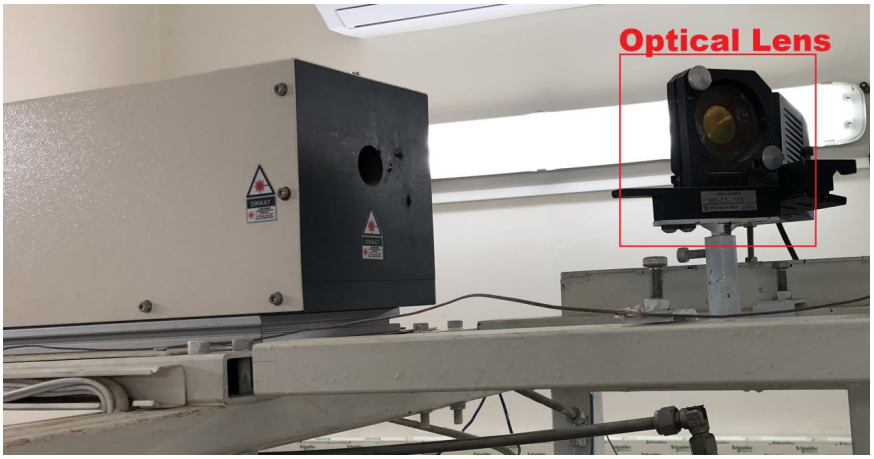

Figure 3.20: Optical Lens.

A power-meter absorbs the projected part from the optical lens, and this way the power level of the laser can be known [1].

Figure 3.21: Power-meter that Reads Data from Reflected Part.

For instance, in Figure 3.21, supplying approximately 30W from the laser controller, the power-meter reads 4.75W from the reflections of optical lens.

3.2.1.5 Shutter

A shutter is placed after the optical lens, as can be seen in Figure 3.22. This component provides user to check the time span of laser source onto the propellant sample.

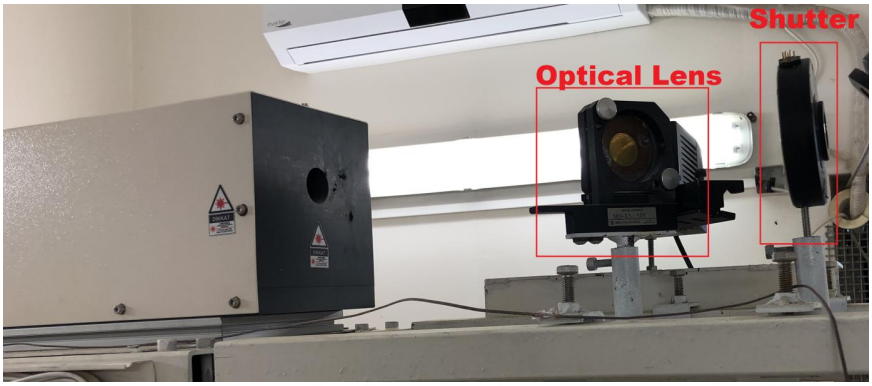

Figure 3.22: Optical Lens and Shutter.

The shutter is provided from Uniblitz Electronic Company with a product serial code "VS14S2Z1".

Figure 3.23: Shutter Blades Closed on the Left and Opened on the Right.

Blades of the shutter can either be closed or opened as desired which is given in Figure 3.23. The details of the shutter working principle is explained below.

Figure 3.24: Uniblitz Shutter Actuator.

Controlling the time interval of laser is provided by the shutter as follows: From Figure 3.24, using the switch button "4" the unit of delay time is chosen. With the buttons that are boxed in "3", the time is selected. Multiplying the time with the unit that was selected before, the delay time till the opening of blades is calculated. Similarly, using the switch button "2" the unit of exposure time is selected. With the buttons that are boxed in "1", the time of exposure is selected. Multiplying exposure time with its unit, the time that blades are in open position is calculated.

3.2.1.6 Directive Lens

The laser passing from the shutter is steered with a directive lens into the combustion chamber as given in Figure 3.25.

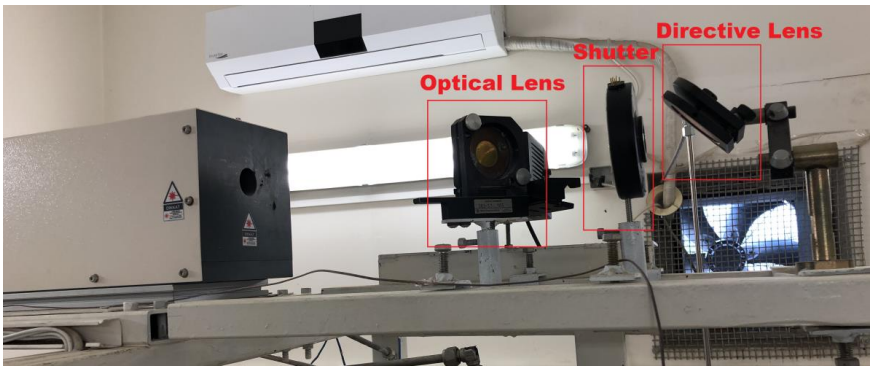

Figure 3.25: Optical Lens, Shutter and Directive Lens.

3.2.1.7 Combustion Chamber

The laser beam that passes through the directive lens is led to the combustion chamber to start the ignition process. Position of the chamber in the setup is provided in Figure 3.26.

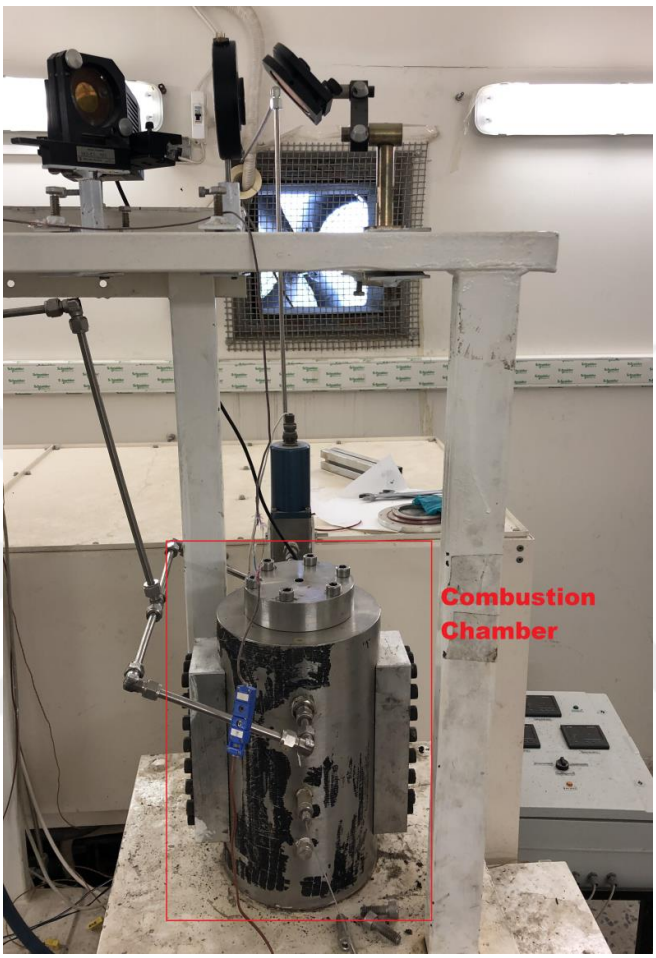

Figure 3.26: Combustion Chamber.

The chamber is famously known as strand burner, has an internal volume of approximately 1 dm^3 and it is designed to withstand more than 500 bar pressure values. But from the nitrogen tube, that much pressure cannot be supplied and mostly 230 bar values can be seen inside the chamber.

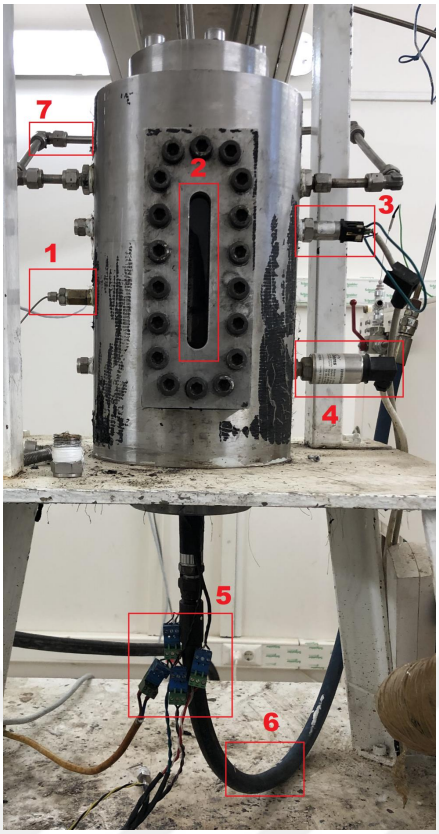

Figure 3.27: General Test Setup from Side View.

From Figure3.27:

- 1 : Thermocouple to measure the temperature inside the chamber
- 2 : Plexiglas window which is used to record the combustion process
- 3 : Pressure Transducer 1 - Keller/PAA-21Y model with a 222155.025/01 serial number that has a pressure measurement range up to 250 bar
- 4 : Pressure Transducer 2 - GEMS 2200BGC2501A3UA model with a supply range 7 - 35 Vdc, output range 4 - 20 mA, pressure range 0 – 250 BarG and operating temperature -40°C to 125°C
- 5 : Break Wire Connections
- 6 : The hose from the nitrogen gas tube that goes inside the chamber
- 7 : Discharge pipes

3.2.1.8 Voltage Supplier

To supply voltage for the break wires, HAMEG HM8040-2 voltage supplier is used which is shown in Figure 3.28.

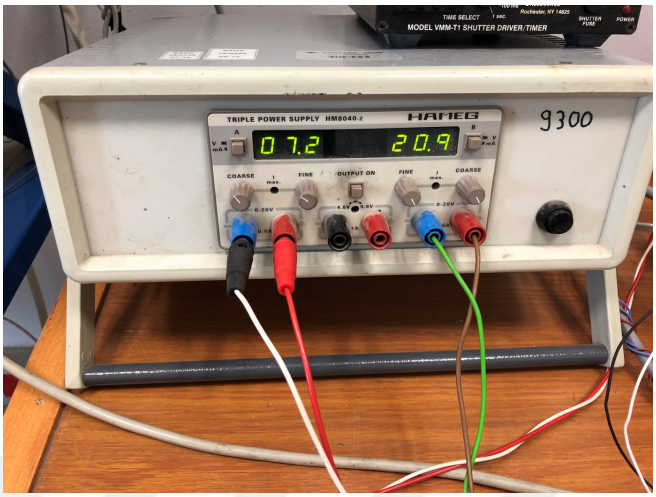

Figure 3.28: Voltage Supplier.

3.2.1.9 Data Acquisition System

Output of the pressure transducer is connected to NI 9239 voltage module and the module is connected to NI cDAQ-9134 data acquisition system. The picture of the NI module is given in Figure 3.29.

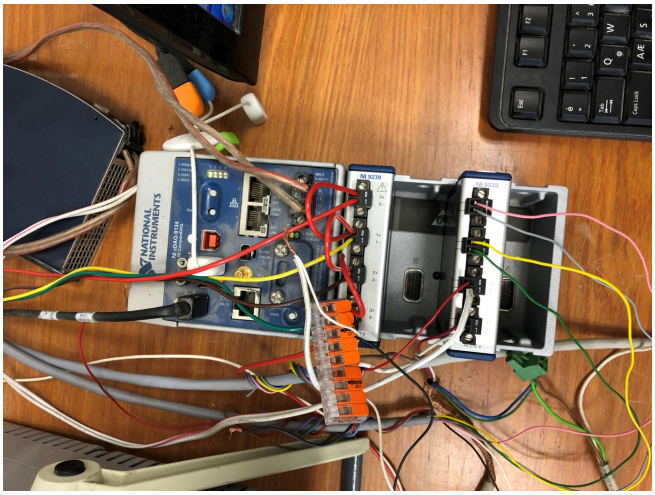

Figure 3.29: Data Acquisition System.

3.2.1.10 Heating and Cooling System

To condition the temperature inside the chamber, there is a heating and cooling system used in the setup. Tests are conducted at 25±1°C, and to make sure the temperature inside the chamber is as determined, the system given in Figure 3.30 is used.

Figure 3.30: Temperature Adjustment System.

From the bottom box, there is the switch key and when it is turned to "1", the system is in heating condition. On the other hand, when the switch is turned to "2", the system

is in cooling condition. From the upper boxes, the left one shows the digital section of heating and the right one shows the digital section of cooling part.

3.2.2 Test Matrix and Test Plan

After providing the details of the experimental setup, particular features about the tests are given in this section. The test matrix and the reason behind the selection of that matrix are presented first. Details of the test plan such as how many data are collected, which pressure values are chosen are given to conclude this chapter.

3.2.2.1 Test Matrix

Although the more tests, the larger database would be obtained, it is not possible to make experiments for all kind of composite propellants due to economical and time constraints. The test matrix must be accomplished in such a way that it covers most of the work studied. In order to do that, the test matrix was constituted by narrowing down the data from literature and the models studied. To be more clear, it would make more sense to make experiments which were already been covered in the past to have a chance to compare own results with the past studies. On the other hand, from the industrial perspective, it would be wiser choice to work on the propellant ingredients that are already in stores instead of the ones that will be supplied later. Combining these factors, following test matrices are obtained for AP/HTPB composite propellants and catalyst added AP/HTPB propellants in Table 3.4 and 3.5 respectively.

Table 3.4: Test Matrix for only AP/HTPB based Composite Propellants.

AP diameter (μm)	**AP% in AP/HTPB**
10	70 73 77 80
40	70 73 77 80
90	70 73 77 80
200	70 73 77 80

For the first matrix, diameters of AP's are selected as 10, 40, 90 and 200μm to cover the most range desired. For all the sizes of AP, loading percentage of it is chosen as 70%, 73%, 77% and 80% to complete the AP/HTPB composite propellant matrix. Normally for a composite propellant that consists of AP and HTPB, ingredients would have a percentage of x% and (100-x)% for the oxidizer and binder respectively. But to procure the bonding and curing of the propellant ingredients, there must be some materials used in the propellant formulation as given in Table1.2. For that reason, all the propellants manufactured within the scope of this matrix include between 1% - 2% percent of IPDI and tepanol from HTPB percent.

For the second part of this work which includes catalysts for composite propellants, another test matrix is constituted. Having same reasons behind generating the matrix as above, following matrix given in Table 3.5 is obtained.

Table 3.5: Test Matrix for AP/HTPB based Composite Propellants with Fe_2O_3 Additives.

AP (%)	**AP diameter (μm)**	**Iron Oxide (%)**
73	10 40 90 200	1
73	10 40 90 200	2
80	40 90	1

This time, 73% and 80% percent of AP loaded composite propellants are selected to work on. For the 73% there is more data provided in the literature, therefore the same sizes of AP are chosen as before with the Fe_2O_3 percent of 1% and 2%. For the 80% AP loaded composite propellants, only 40 μm and 90 μm sizes of AP are thought to be studied with the additional 1% percent of Fe_2O_3.

3.2.2.2 Test Plan

As can be seen from Table 3.4 and Table 3.5, 16 AP/HTPB propellant batch and 10 AP/HTPB + Fe_2O_3 propellant batch is manufactured to serve the purpose of this study. For each propellant, pressure values to be selected to conduct experiments on are 25, 50, 75, 100 and 125 bars. These pressure values are determined but since the gas inside the nitrogen tube decreases, pressure values couldn't be the given numbers exactly for all experiments and they may vary from a test to another. If, for instance, the gas inside the tube decreases below 20 bars, the following tests are conducted at 10-15 bars not to waste the remainder of it. Similarly, if max pressure of one tube decreases below 125 bars, max pressure of the following test values are shifted from 125 to 100 bars. But all in all, five different sets of pressure values are set to conduct

experiments for each propellant. At each pressure value, three tests are conducted for each propellant to have reliable data. And for one test, there is four break wires used in the sample holder as given below in Figure 3.31.

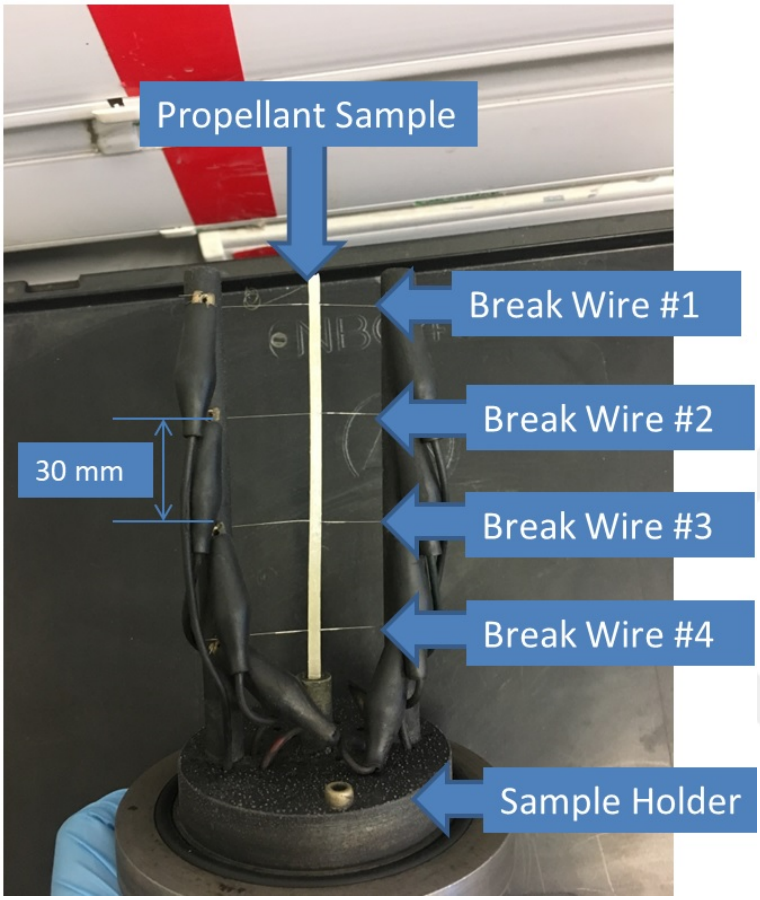

Figure 3.31: Propellant Sample Holder Details.

As the propellant burns, wires break out one by one and the distance between two wires is 30 mm. By knowing the time that each wires are broken out, the burning rate of the propellant can be calculated. Having four break wires, three burning rates can be obtained for a propellant at a given pressure point. As a result, having combined all the data, 26 propellant batch*5 pressure points*3 tests at each pressure point = 390 tests are conducted within the scope of this work. Obtaining three burning rate data for each test, 1170 data for burning rate of AP/HTPB composite propellants plus AP/HTPB + Fe_2O_3 propellants are obtained.

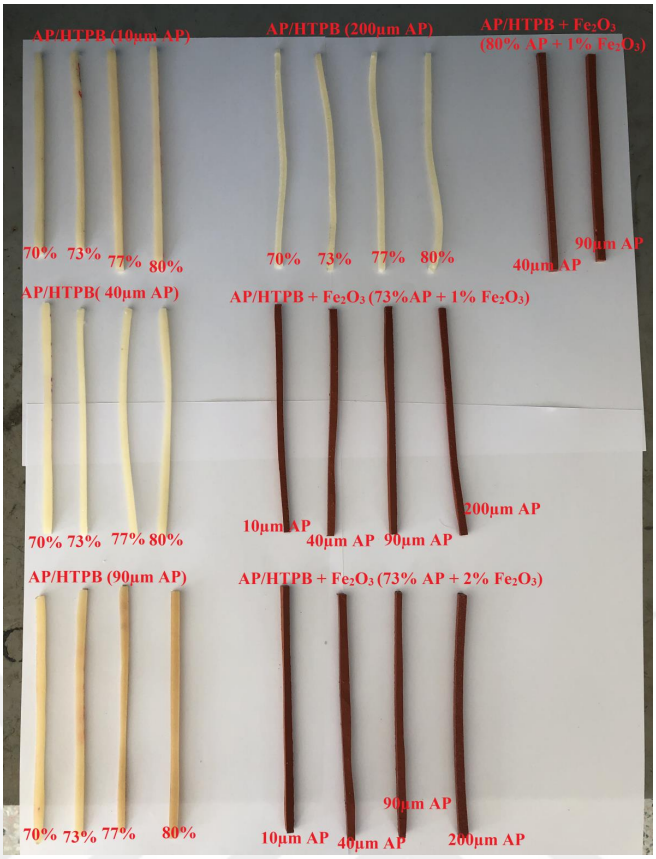

Figure 3.32: A Sample for all Propellants Experimented.

Figure 3.32 captures all the propellant types studied within the scope of this work. As it is seen, adding Fe_2O_3 to the AP/HTPB based propellants makes them darker and while the color of AP/HTPB based propellants are almost light yellow, catalyst added propellants seem to be brick red.

Starting from the next chapter, results of the experimental work are presented and then comparison of the numerical scheme predictions with the experimental results is followed for each propellant experimented.

CHAPTER 4

RESULTS AND DISCUSSION

In this part of the study, results of the experimental work for the propellant batches given in the previous section are presented. Sample of an experimentally obtained data is presented first and then burning rate results of the experiments are provided. Error bars are also incorporated in the results. As it is mentioned in the previous chapter, nine data points are obtained for a propellant at a determined pressure. To include error bars, average of the nine data is calculated and given in the corresponding plots. For the second part of this chapter, which presents comparison of the numerical scheme predictions with the experimental results, all of nine obtained data for a propellant at each pressure are provided. After presenting each comparison, discussion of the results are presented in this section.

4.1 Experimental Results

In the first section of this chapter, experimental results are provided in logarithmic plots. Before presenting the results, a sample from data acquisition system is given in Figure 4.1.

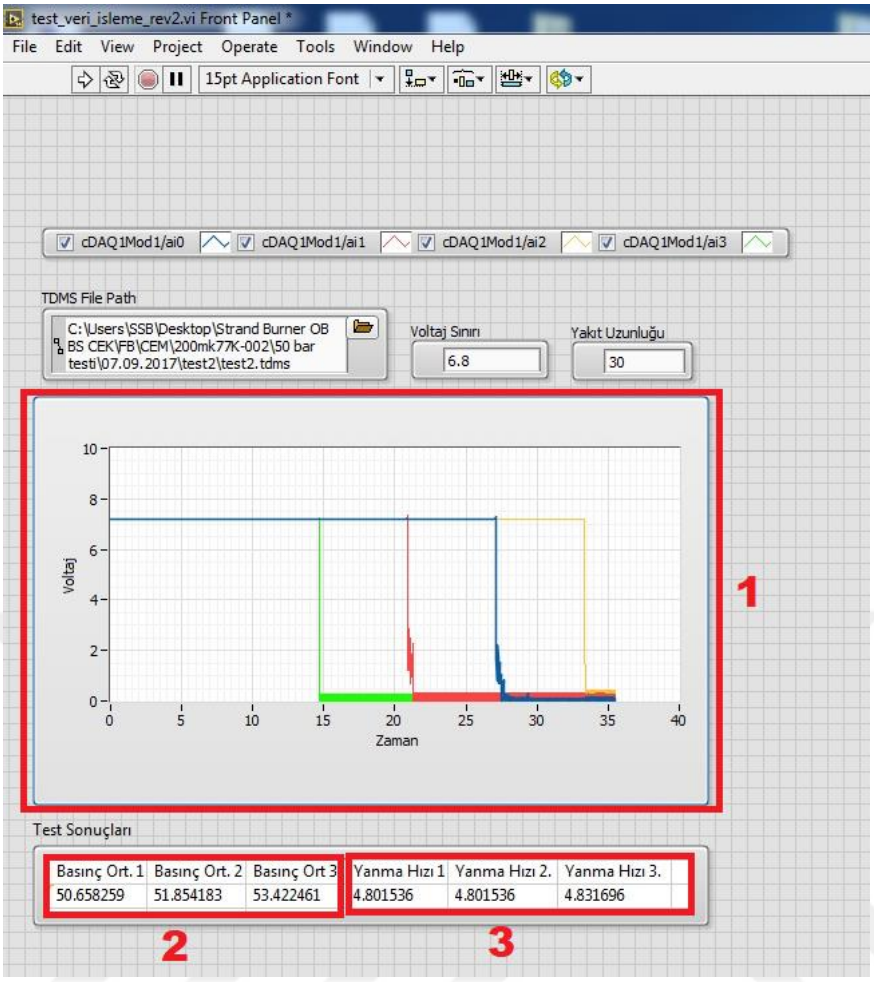

Figure 4.1: An Example of Experimental Data Obtained - 77% AP 200 μm data of 50 bars pressure.

The sample is from 77% AP loaded composite propellant with having AP diameter of 200 μm and the pressure is 50 bars. From the tagged box "1" in Figure 4.1, the voltage value of each wire is given with respect to time. For four different wires, four different colors are chosen so that it is clear to see the time of break for each wire. As it is seen, each voltage drops to "0" (zero) value when corresponding wire breaks away. Additionally, it is seen that there is some noise in this data and that may be explained as after wires break away, the flame of the propellant causes wires to move up and down unpredictably. That unpredictable movement may end up in some connection points between two broken wires and at these circumstances voltage may be read from the data acquisition system. From the pointed box "2" in Figure 4.1, average pressure values during the test are taken. And lastly, for the box "3", burning

rate at each section is gathered.

An example of an own propellant burning in the strand burner is given in Figure 4.2.

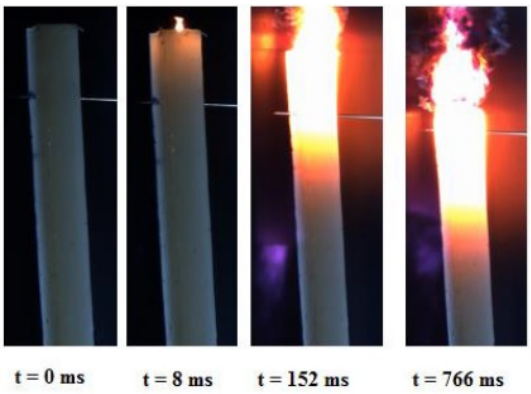

Figure 4.2: An Example of a Strand Burner Test (77% AP - 40μm Composite Propellant, 50 bar).

Figure 4.3 shows the burning rate data obtained from experiments for propellants having 10 μm AP. The graphs are plotted on log-log scale to see if Saint Robert's Law is satisfied.

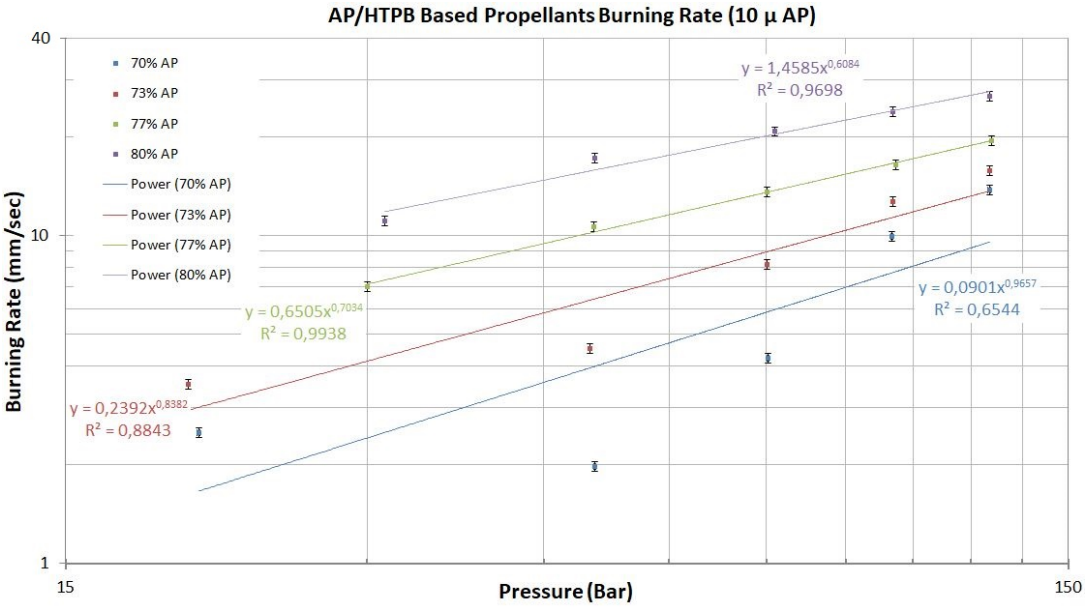

Figure 4.3: Experimental Results for Propellants Having 10 μm AP.

From Figure 4.3, it is seen that data for 77% and 80% solid loaded propellants agree well with the Saint Robert Law. For the 73% AP loaded propellant, data seems acceptable with the R^2 value being equal to 0.88. But for the 70% loaded propellant, it is seen that too much variations are observed on burning rate. There seems to be an almost decreasing burning rate up to 50 bars of pressure. From that point, the increase in burning rate with increasing pressure can be seen. Having such unstable behavior of burning rate is believed to be coming from manufacturing caused problems. Manufacturing the propellants, the batch is put under vacuum conditions not to have any discontinuities. But sometimes, the gaps comprised in the propellants even the batch is vacuumed properly. This situation is occurred when the bonding between ingredients are not satisfactory enough. Those gaps in the propellants yield in unstable burning rate behavior due to corrupted propellant surface area. These circumstances are believed to be reasons for having too much variations on the burning rate of 70% AP loaded propellants.

Figure 4.3 also includes experimental data with error bars. In the strand burner method, there could be three different experimental errors obtained. Two of them is related with burning rate and the other is related with measured pressure values. For the burning rate errors, which are shown by vertical bars in Figure 4.3, they are

either obtained from the data logging system or caused by the ruler sensitivity. To be more clear, it is previously mentioned that the distance between two wires is 30 mm, this distance is measured by using a ruler and first error regarding the burning rate is coming from that process. Since rulers have a sensitivity of 1 mm, 30 ± 1 mm is used to calculate the error. For the second type, an error can be obtained from the data logging system. It is obtained from the NI module data sheet [51] that own NI-9239 module has an accuracy level of 0.03%. Therefore, if the time to pass the distance between two wires is read for instance 11.94162 seconds for 70% AP loaded propellants with having 10μm APs, then the real time becomes $11.94162 \pm 0.03\%$ seconds. As a result, following error calculations are obtained for the vertical bars.

$$\dot{r}_{max} = L_{max}/t_{min} = 31mm/(11.94162 * (1 - 0.03\%))seconds = 2.5967mm/sec \tag{4.1}$$

$$\dot{r}_{min} = L_{min}/t_{max} = 29mm/(11.94162 * (1 + 0.03\%))seconds = 2.4277mm/sec \tag{4.2}$$

Therefore, obtained burning rate of 2.51222 mm/sec has an experimental sensitivity of 3.36%. These error bars are plotted on all figures for the experimental work in this study. Additionally, as it is mentioned before, nine data points are obtained for one propellant at one pressure. In order to incorporate error bars, average of nine data is provided here, but for the comparison part which is given after providing experimental results, all nine data are incorporated in the plots. Up to this point, vertical error bars are mentioned and for the horizontal bars which shows the error of pressure values read from the pressure transducers, they are not included in the plots. It is obtained from the transducer data sheet [52] that the transducer used in the experiments has an accuracy level of 0.25%, incorporating such tiny bar on the plots is not visual, therefore they are not included but only mentioned.

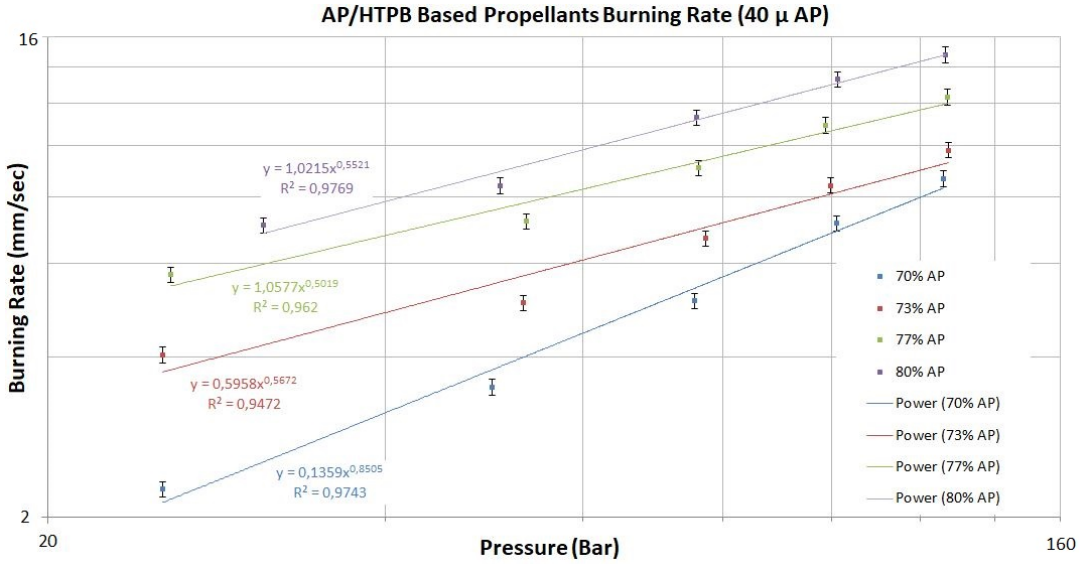

Figure 4.4: Experimental Results for Propellants Having 40 μm AP.

For the propellants that have 40 micron of AP sizes, all data from Figure 4.4 seem to fit well to power law with minimum R^2 value being equal to 0.947. Providing the data for 40μm AP based propellants, again average of the nine obtained burning rate values for each pressure is given in the plot to include error bars. For the burning rate discussion, it is observed that increasing oxidizer percent in the propellants increases the burning rate.

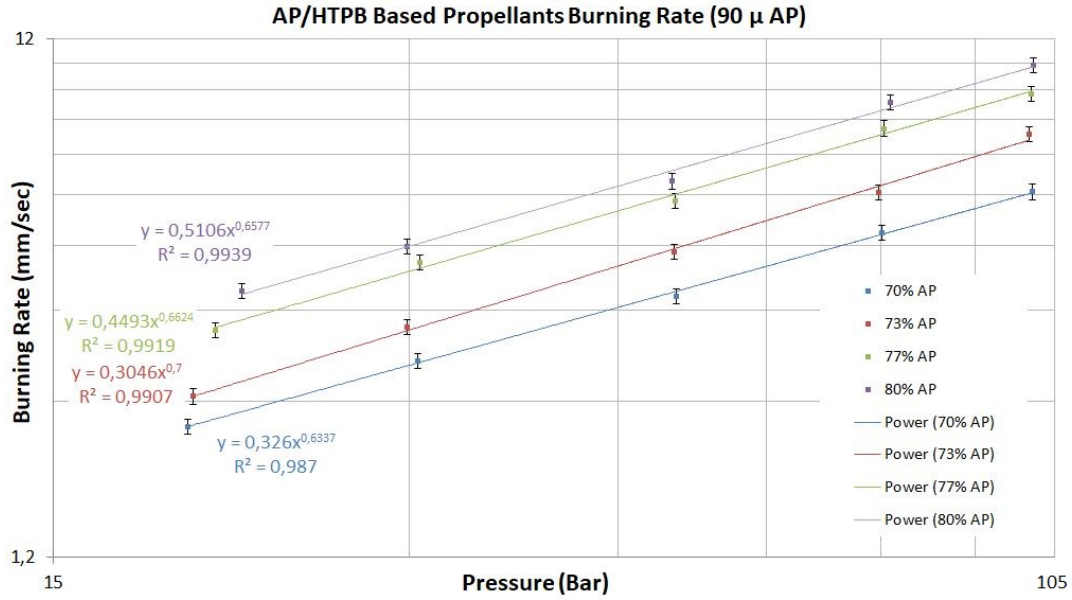

Figure 4.5: Experimental Results for Propellants Having 90 μm AP.

Evaluating propellants with 90 micron AP's, again the data from Figure 4.5 seem perfectly good in terms of power law with minimum R^2 value being equal to 0.987. Similar affect of oxidizer percent on burning rate is also obtained here and burning rate increases with increasing oxidizer percent in the propellants.

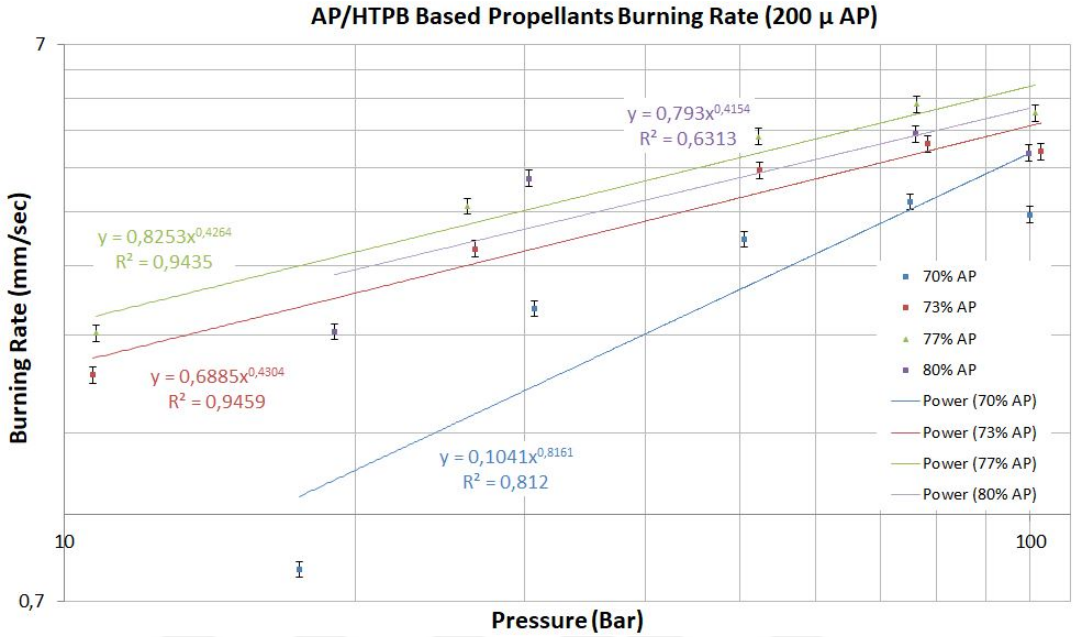

Figure 4.6: Experimental Results for Propellants Having 200 μm AP.

Last propellant based on only AP and HTPB is the one that has AP diameter of 200 μm. Experimental results are given in Figure 4.6. Although having obtained acceptable data for 73% and 77% loaded of these propellants, there seems unstable data for 70% and 80% AP loaded propellants. To be more clear, experimental results reveal that at lowest pressures, 70% AP loaded propellants have burning rates that are significantly smaller than what is expected to satisfy the Saint Robert's law. Additionally, at higher pressures, a plateau burning seems to occur for the same propellant. Another propellant, which consists of 80% AP, has burning rate that increases up to 50 bars and then decreases unexpectedly. The R^2 values based on power law also seem to be 0.812 and 0.63 for 70% and 80% AP loaded propellants respectively, which demonstrates that there must be a problem related with those data. The reason may be the manufacturing problems such as not being able to mix the ingredients well because of higher particle diameter sizes. Not mixing the propellant properly may also pave the way to have discontinuities in the propellant which results in having unstable

burning rate data. Another reason could be the AP itself which are obtained from different suppliers and using different AP's from different sources might be the reason for the unstable results. Additionally, observing all data for 200 μm AP propellants, there seems that burning rate won't increase after some pressure values. As a result, plateau burning can be seen for all of them. Up to 70-80 bars of pressure, burning rate increase can be seen , but after that point almost all data stay constant or decreases.

After providing data for AP/HTPB based propellants, experimental data for catalyzed propellants is presented next.

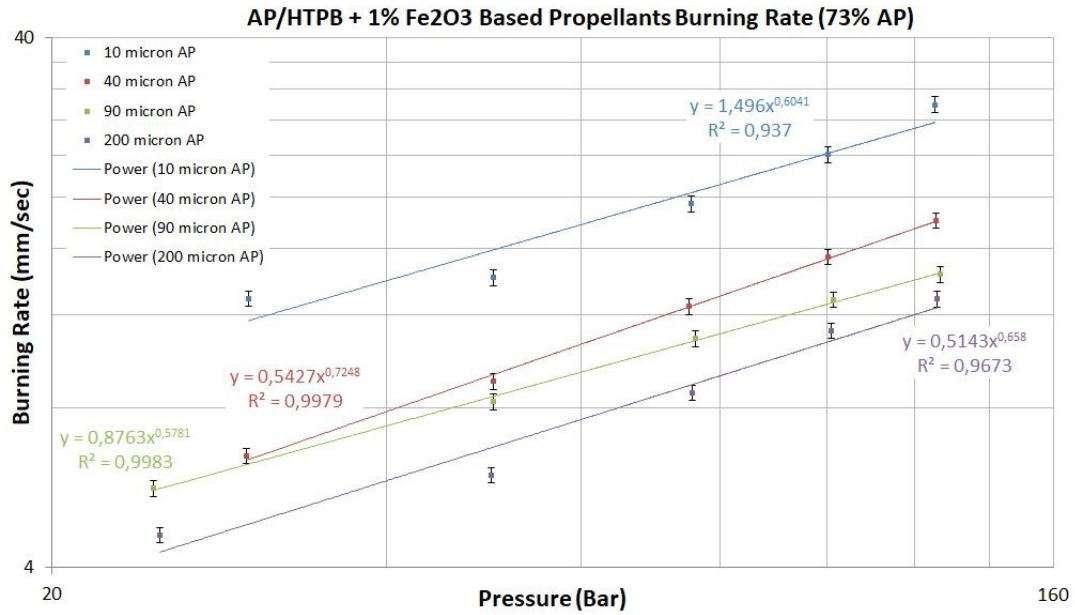

Figure 4.7: Experimental Results for 73% AP Based Propellants with Having %1 Fe_2O_3.

First of all, data for propellant that has 73% AP loading with 1% Fe_2O_3 additive is presented in Figure 4.7. Obtained results seem acceptable with regard to Saint Robert's Law. It seems that effect of oxidizer particle size on burning rate is obtained here and decreasing the diameter of oxidizer increases the burning rate. Effect of catalyst, Fe_2O_3, is presented later in this chapter after providing all experimental results.

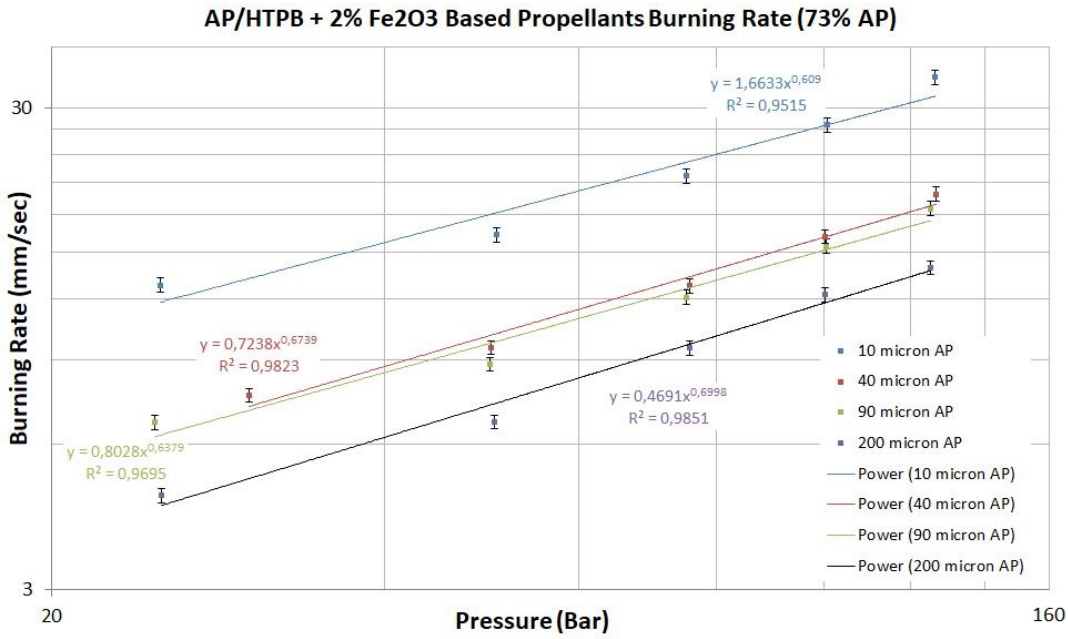

Figure 4.8: Experimental Results for 73% AP Based Propellants with Having %2 Fe_2O_3.

In addition to the AP/HTPB propellants having 1% Fe_2O_3, AP/HTPB propellants with having 2% Fe_2O_3 is investigated. From Figure 4.8, it is seen that all data fit well to power law, and increasing catalyst percent by 1% has increased the burning rate as can be obtained from Figure 4.7 and Figure 4.8. Additionally, how particle size affects the burning rate is also obtained for these propellants. Burning rate increases as the particle size of the oxidizer decreases. To see the effect of catalyst addition, plots for the comparison of them with uncatalyzed propellants are provided below in this chapter from Figure 4.10 to Figure 4.13.

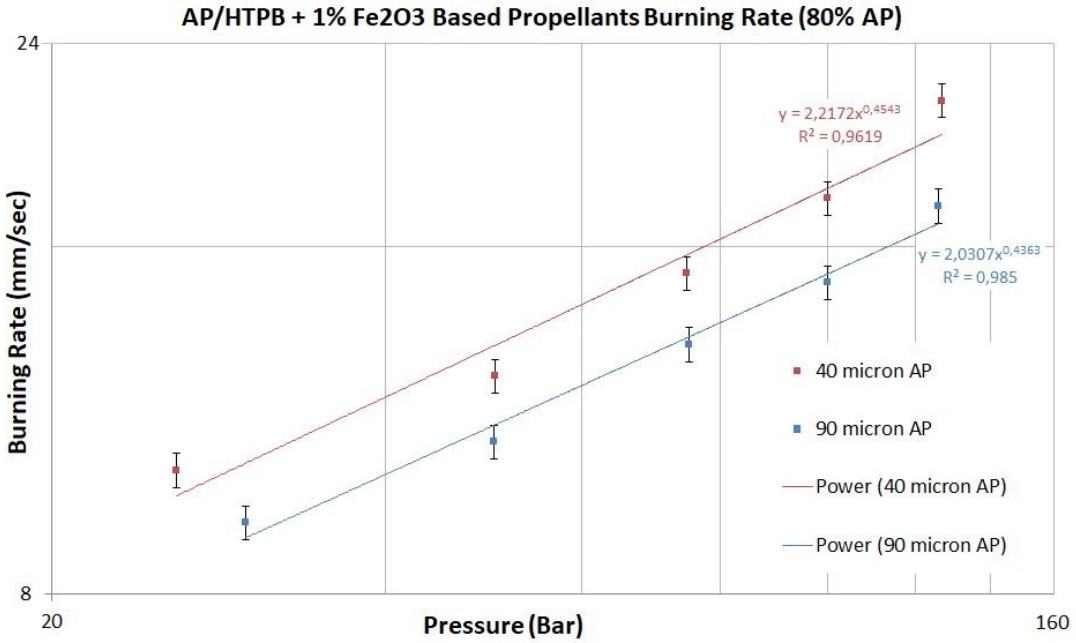

Figure 4.9: Experimental Results for 80% AP Based Propellants with Having %1 Fe_2O_3.

Finally, last two propellant batch that consists of 80% AP + 1% Fe_2O_3 with having AP diameters of 40 and 90 μm are evaluated. Experimental results are provided in Figure 4.9 and they reveal that decreasing diameter of the oxidizer increases the burning rate as expected. How catalyst affects burning rate of AP/HTPB based composite propellants is investigated below.

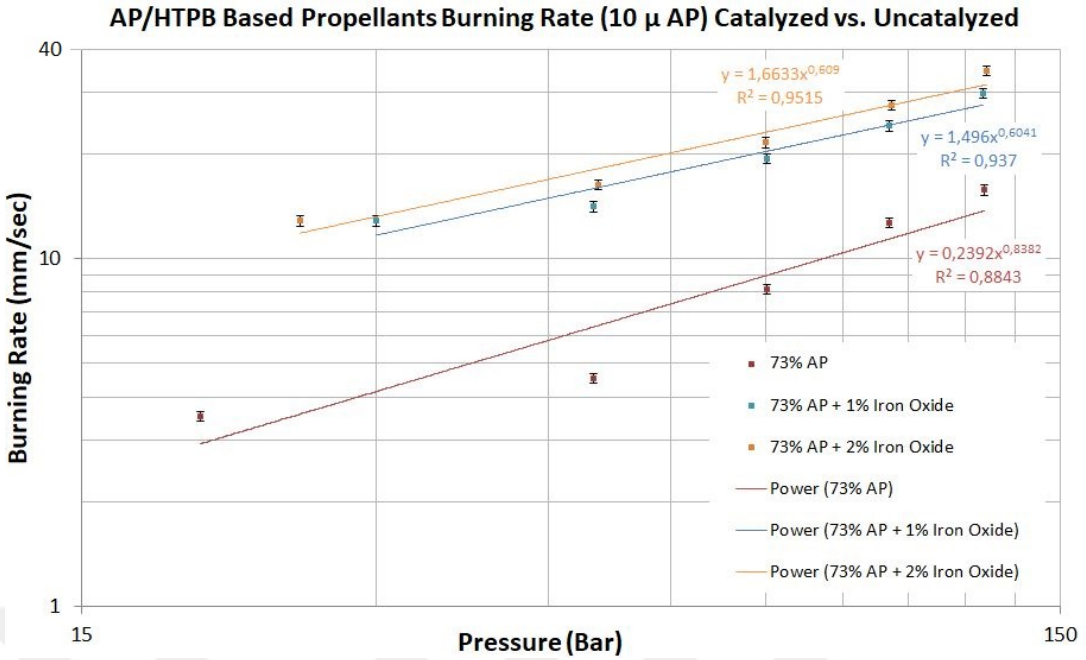

Figure 4.10: Comparison of Catalyzed vs. Uncatalyzed 10μm AP Based Propellants Burning Rate.

Comparison to see catalyst effect starts with propellants having 10μm AP's. As can be seen from Figure 4.10, adding 1% of Fe_2O_3 to the corresponding uncatalyzed propellants significantly increases the burning rate. On the other hand, adding one more percent of Fe_2O_3 to the 1% catalyzed propellants doesn't make drastic changes. Other than that, in terms of satisfying Saint Robert's Law, acceptable data are obtained for these propellants with having minimum R^2 value of 0.88.

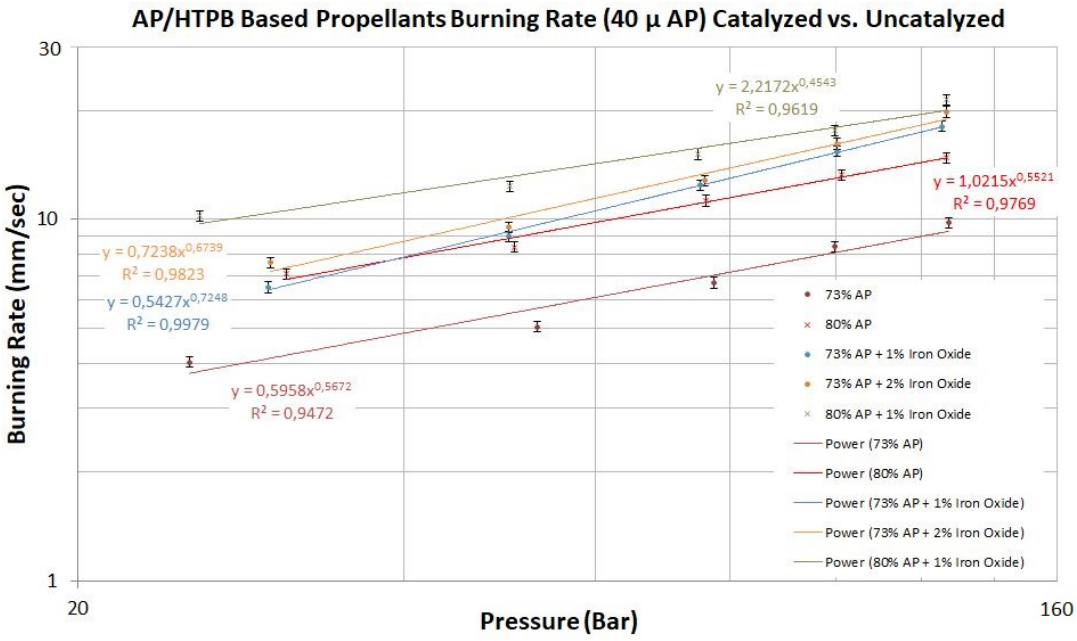

Figure 4.11: Comparison of Catalyzed vs. Uncatalyzed 40μm AP Based Propellants Burning Rate.

Investigating 40μm AP based propellants, burning rate data of 73% and 80% percent solid loaded propellants are given in Figure 4.11. Similarly, catalyst addition increases the burning rate and it is observed that 80% loaded propellants with 1% Fe_2O_3 added have higher burning rates compared to 73% loaded propellants with 2% Fe_2O_3 added. Additionally, 1% of catalyzer addition to the uncatalyzed propellants makes huge impact on the burning rate, while adding one more percent to the catalyzed propellants provides a smaller increase.

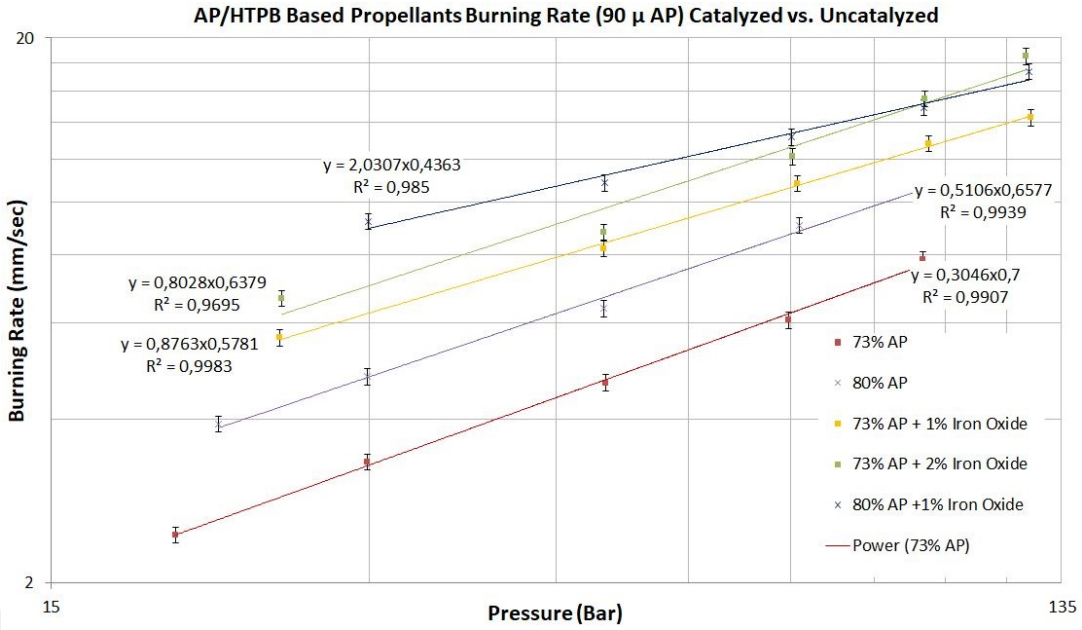

Figure 4.12: Comparison of Catalyzed vs. Uncatalyzed 90μm AP Based Propellants Burning Rate.

Comparison of catalyst effect for 90μm AP based propellants is given in Figure 4.12. How the addition of catalyst to the uncatalyzed and catalyzed propellants have different effects can also be seen here for 73% AP loaded propellants with having 90 μm AP. While 1% catalyzed propellants have inevitably larger burning rates compared to the uncatalyzed of the same propellants, the gap in the burning rate is smaller in between 1% and 2% catalyzed propellants. 80% solid loaded with 1% catalyst added propellants have also higher burning rates compared to the 73% solid loaded with 2% catalyst added propellants as obtained previously for 40 μm AP data.

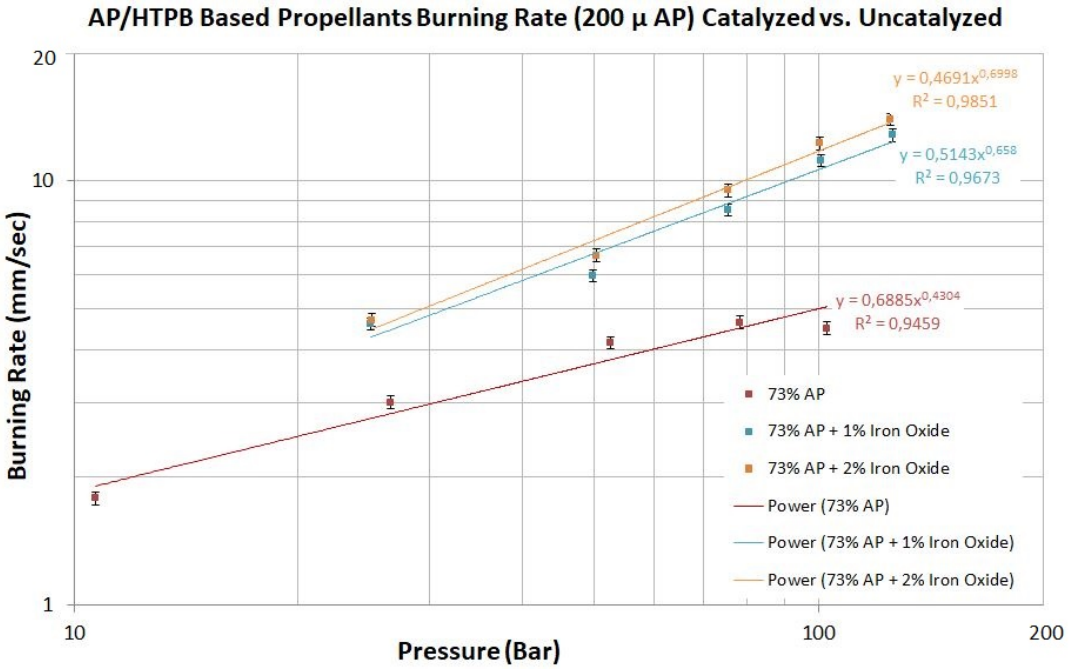

Figure 4.13: Comparison of Catalyzed vs. Uncatalyzed 200μm AP Based Propellants Burning Rate.

Lastly for this section of the chapter, burning rate of the 200μm AP based propellants is provided in Figure 4.13. Similarly as before, 1% of catalyst addition makes a huge impact on burning rate, while adding one more percent doesn't make significant changes. Therefore, it is a general conclusion coming from this feature that for uncatalyzed AP/HTPB based propellants, to increase burning rate, Fe_2O_3 addition contributes a lot. But, on the other hand, that contribution becomes smaller going from 1% catalyzed propellants to 2% catalyzed of the same propellants.

4.2 Numerical Scheme Predictions and Comparison with the Experimental Results

In this part of the study, experimental results given in the previous section are compared with the numerical scheme predictions. By doing this, again the graphs are separated in order not to confuse the large data. AP/HTPB based composite propellants, having AP sizes of 10μm, 40μm, 90μm and 200μm are evaluated first. Then Fe_2O_3 added AP/HTPB propellants are compared. The literature has also been sur-

veyed and if data for exact type of propellant in terms of propellant ingredients and weight percent of each ingredient is found in the literature, then it is used in the comparison, if not, propellants with closer ingredients are used. After each comparison, discussion of results and reasons for having differences are provided to conclude this chapter.

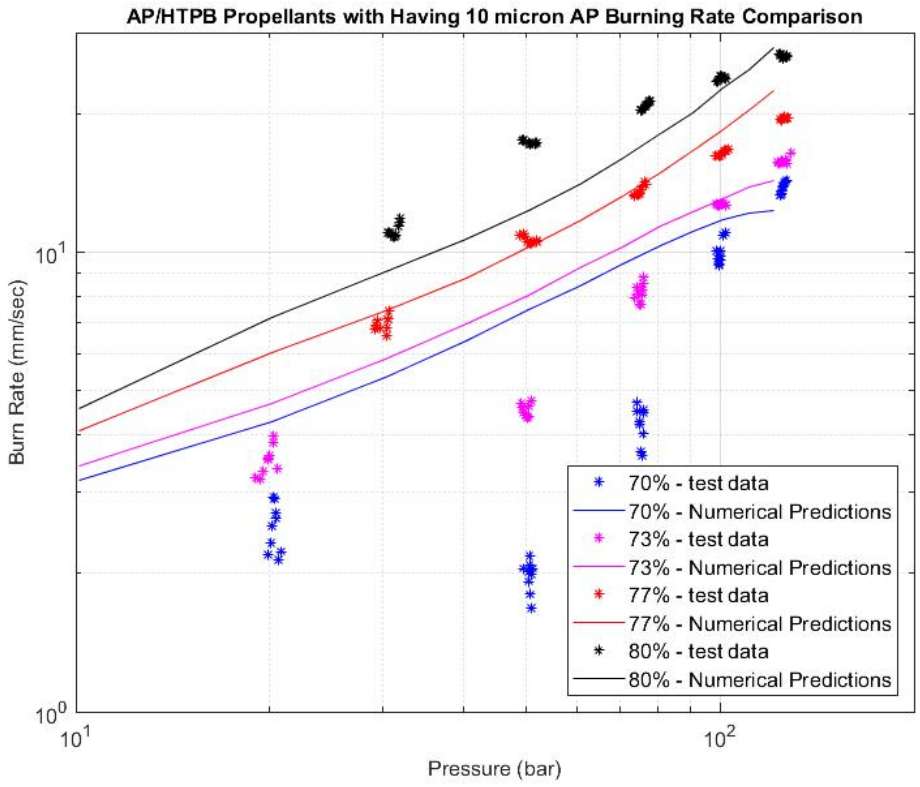

Figure 4.14: Burning Rate Comparison of AP/HTPB based Propellants with AP size of 10 μm.

Beginning with the propellants that have 10 μm AP of size, comparison of the numerical scheme with the experimental results is provided in Figure 4.14. It is observed that for 70% and 73% solid loaded propellants, predictions only agree with experiments at pressures of 100 bars or higher. Below of that pressure, significant deviations observed between the model and results. For 77% solid loaded propellant, the predictions seem to fit perfectly with the experimental results. Only 10% difference can be seen at most between the model and experimental results at pressures higher than 100 bar values. Other than that, predictions seem to have almost the same outcome

with the experiments for 77% solid loaded propellant. For the propellants having 80% solid loading, the predictions give acceptable results for most of the pressure values worked on. Also, it is observed that approaching towards lower pressure values, unstable behavior of these propellants increases. The reasons behind having differences could be the manufacturing caused problems or uncertainties in the thermophysical properties. To see the effect of unknown thermophysical properties, sensitivity analysis is made below in this chapter. Other than that, there could be another reason coming from the propellants ingredients. They are provided from different suppliers around the world and they come with not having the exact diameter of size but instead, Gaussian distribution in terms of AP sizes is obtained. Having experimented any other size of AP in this experiment could be another reason for having differences. Since 10 μm is a very small size, it is very sensitive to changes of size of even 1-2 microns.

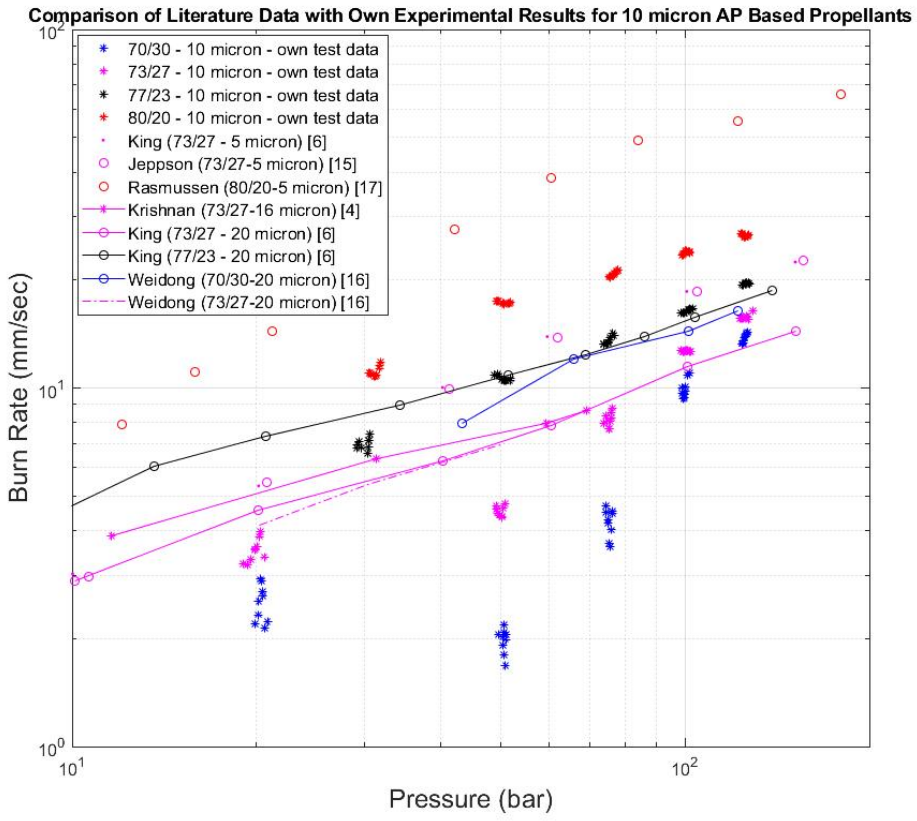

Figure 4.15: Literature Data for AP/HTPB based Propellants with 10 μm or close AP sizes.

To compare own experimental results with the data from the literature, Figure 4.15 is presented. Experimental data from the literature is obtained from King [6], Jeppson [16], Rasmussen [18], Krishnan [4] and Weidong [17]. For the 70% solid loaded propellants comparison, it is seen that data from Weidong [17] has higher burning rates compared to own experimental work. Not too much data is provided for his work but for the provided ones, the differences may come from the bonding agent percentage used in the propellants. What percent of his propellants include those bonding agents isn't given, therefore this could be a reason for having different burning rates. For the 73% solid loaded propellants, data for 5μm, 16μm and 20μm are found in the literature and they are compared with the own 10μm data. It is observed that King [6] and Jeppson's [16] 5μm data have higher burning rates as expected because of the smaller particle sizes. King's [6] and Weidong's [17] 20μm and Krishnan's [4] 16μm propellants have very close and even higher burning rates compared with own 10μm data. Observing higher burning rates for them is not expected since they used larger particle sizes but as it is mentioned before, any propellant ingredients are obtained from suppliers with having Gaussian distribution of them. Since 10μm is very small size for propellants, having experimented propellants that have larger size of AP from Gaussian distribution may lead to get smaller burning rates. For the 77% solid loaded propellants, it is seen that there is an agreement between King's [6] data and own experimental work. Lastly for the 80% solid loaded propellants, Rasmussen's [18] 5μm data has higher burning rates compared to own experimental study with 10μm as expected.

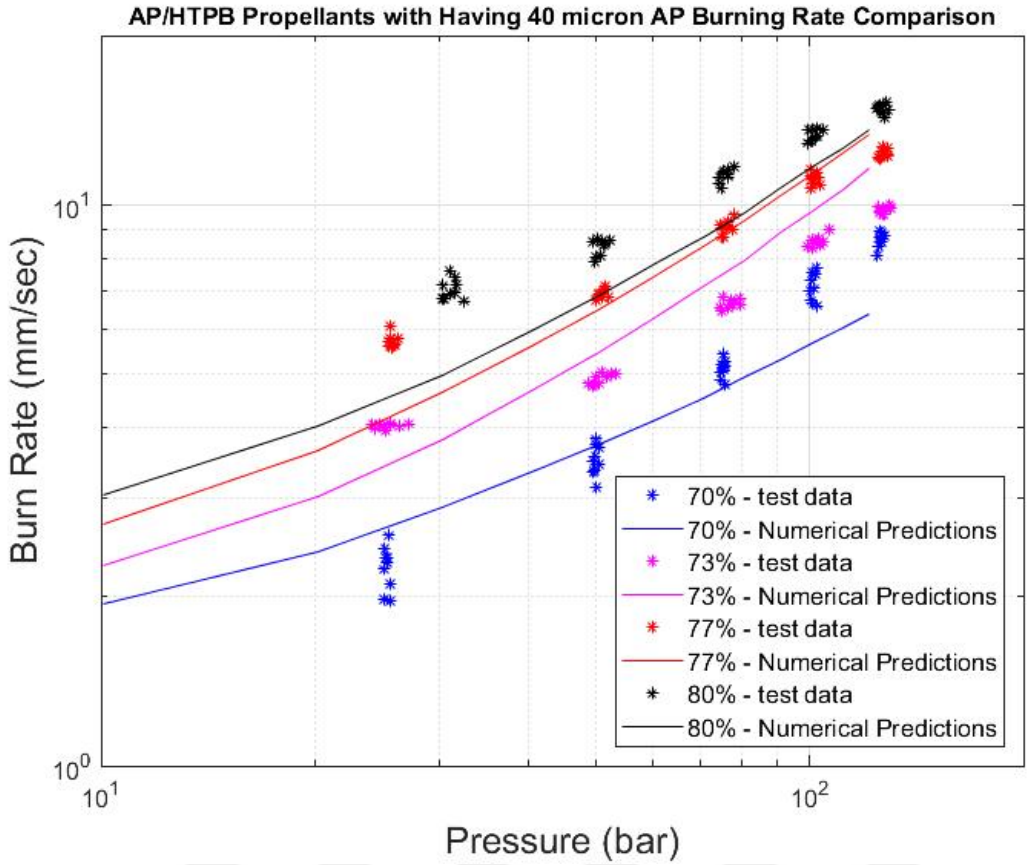

Figure 4.16: Burning Rate Comparison of AP/HTPB based Propellants with AP size of 40 μm.

After providing 10 μm AP based propellants, comparison data for 40 μm AP based propellants is given in Figure 4.16. Considering all propellants with different solid loadings, despite not having the exact outcome with experiments, the predictions and the experimental results are close to each other and the trend of all propellants seem to be matched. Considering all these facts, it can be said that promising results are obtained for propellants that have 40 μm AP. The uncertainties in the thermophysical properties may be the reason for having differences and uncertain parameters are investigated in this chapter to see their effect on burning rate.

For the burning rate discussion, it is observed that deviations occur at lower pressure values. Since this phenomenon is also observed for previously presented propellants, it is deduced that those AP/HTPB based propellants have unstable behavior in common at low pressure values. To examine the situation, the term Pressure Deflagration

Limit(PDL) is addressed. This is the threshold value for solid propellants that must be passed for self-sustained combustion to occur [29]. Value of that limit changes with the chemical composition of the propellants, therefore each propellant has its own minimum pressure limit to burn properly. Not only self-sustained combustion doesn't occur below the limit, but also approaching towards the limit from higher pressure values, unstable behavior of propellants increases. For this reason, in own experiments it is seen that variation of burning rate increases at smallest pressure values.

Starting from below, sensitivity analysis of uncertain parameters are provided. For those analysis, heat of binder decomposition and heat release in the primary flame are investigated.

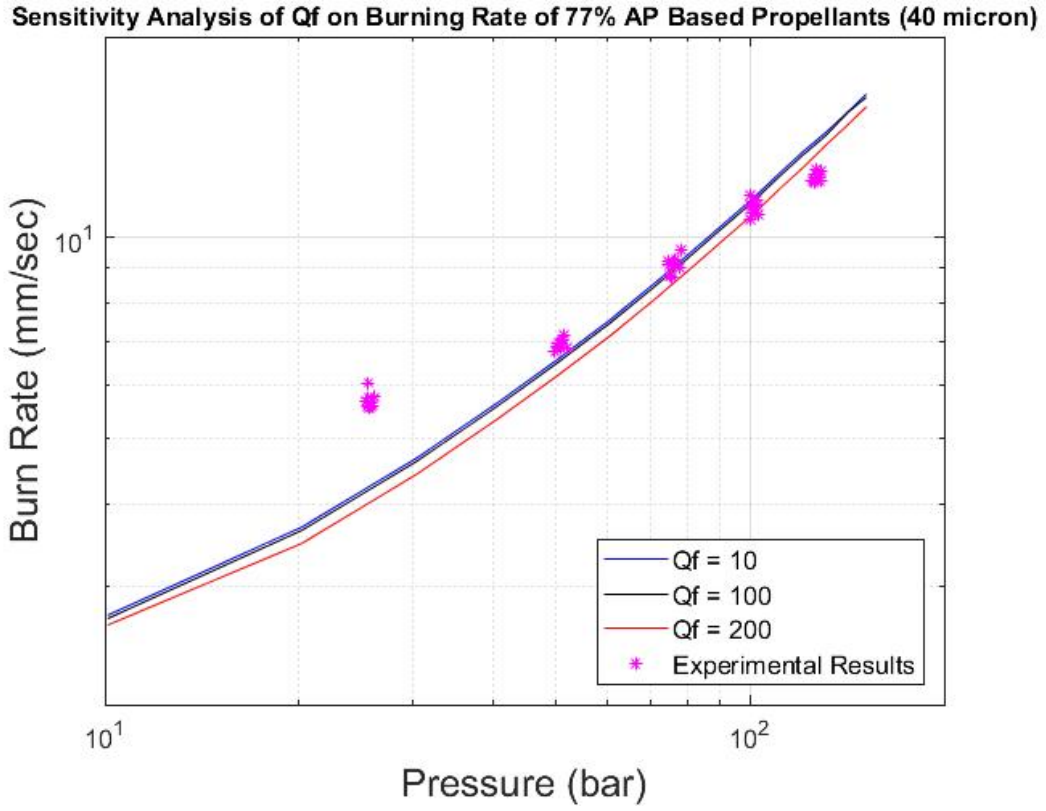

Figure 4.17: Sensitivity Analysis of Q_f on Burning Rate of 77% AP Based Propellants (40 micron AP).

First of all, Q_f of uncertain parameters mentioned in Chapter 3 is investigated. Change of burning rate for different Q_f values is provided in Figure 4.17. It is seen that, al-

though values of 10 and 100 for Q_f give closer burning rate outcome, visible alteration is obtained when Q_f equals to 200 cal/g. As a result of this, it is interpreted as on the order of 0-100 cal/g assumption for Q_f is reasonable for this numerical method. Higher than these values makes impact at burning rate with at most 5% decrease.

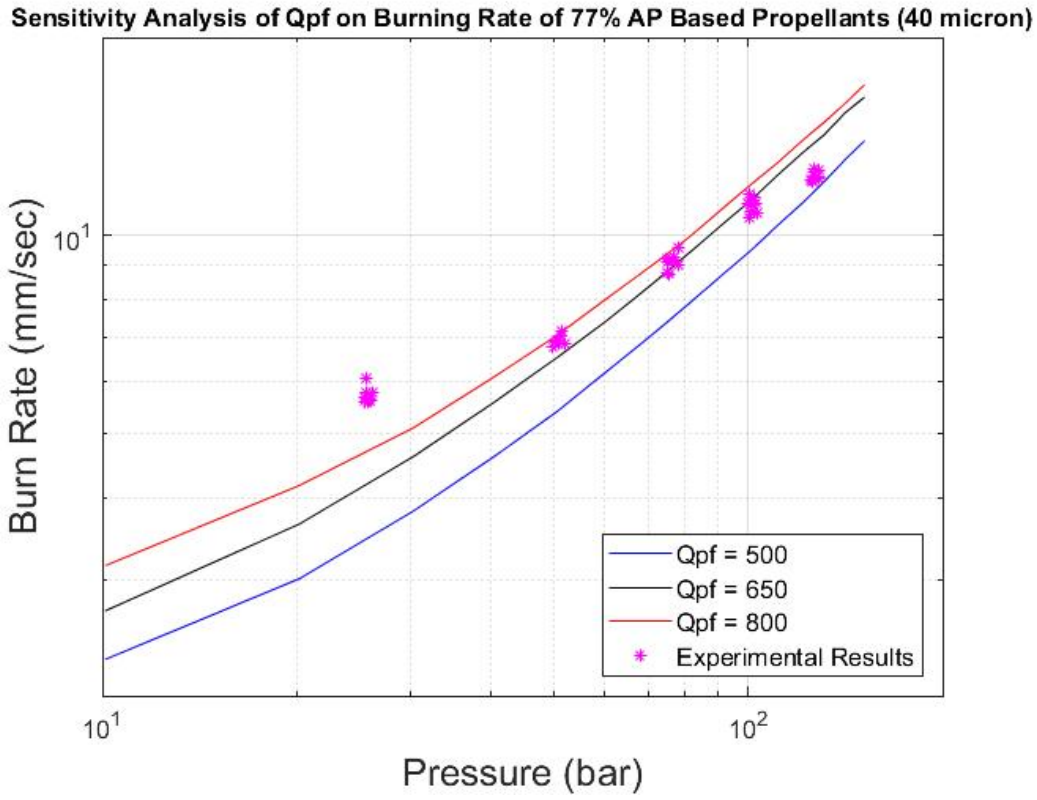

Figure 4.18: Sensitivity Analysis of Q_{PF} on Burning Rate of 77% AP Based Propellants (40 micron AP).

Another parameter which is neither not found exactly in the literature nor not obtained through measurement techniques is the primary flame heat release, Q_{PF}. Effect of it can be seen in Figure 4.18 and in between the boundaries, it seems that changing Q_{PF} affects the burning rate inevitably. Higher burning rates are obtained with increasing Q_{PF} and it is observed that especially up to 100 bar pressure values, predictions give better results when Q_{PF} is increased. By looking at this graph, it is demonstrated that uncertainty of Q_{PF} is one of the reasons for having differences between numerical predictions and experimental results. Results of the sensitivity analysis are only given for 77% AP based propellants with having 40μm AP, but similar results are obtained for all propellants in this study.

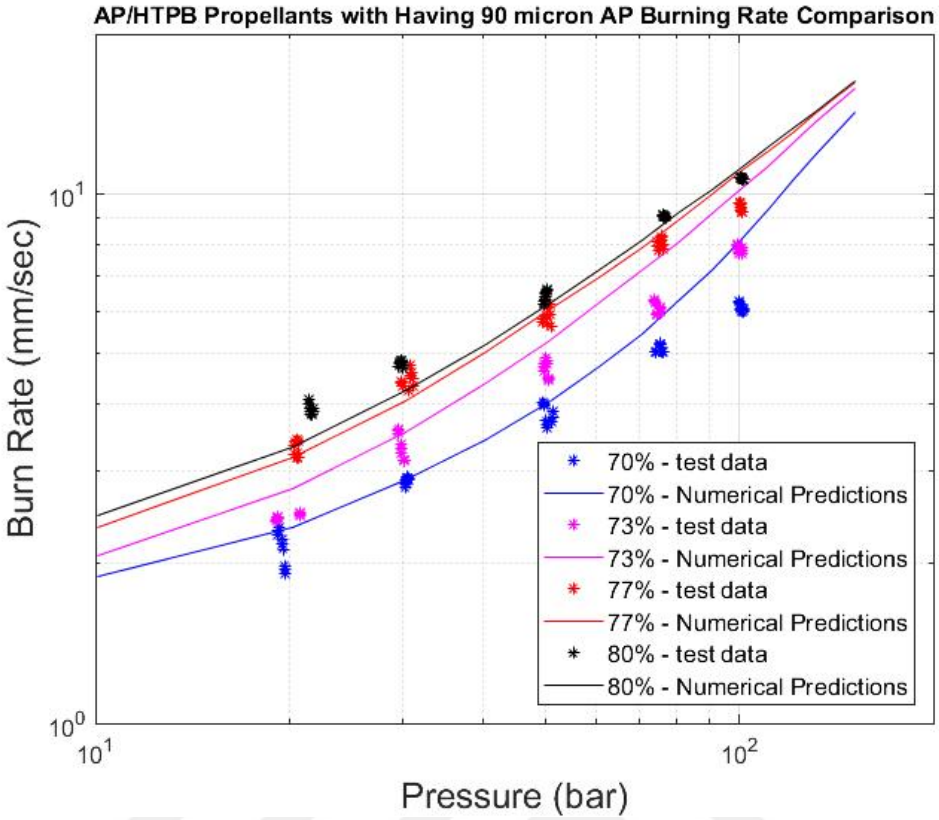

Figure 4.19: Burning Rate Comparison of AP/HTPB based Propellants with AP size of 90 μm.

Coming through larger AP particles, propellants with having 90 μm AP are investigated next. Data of comparison is presented in Figure 4.19. As a general observation, all experimental data seem to agree well with the numerical predictions. After pressure values of 80 bar, there can be counted some variations for 70% and 73% loaded propellants. Additionally, differences of at most 14% can be seen for 80% loaded propellants at smallest pressures. The main reason for having differences is thought to be uncertainties in the thermophysical properties.

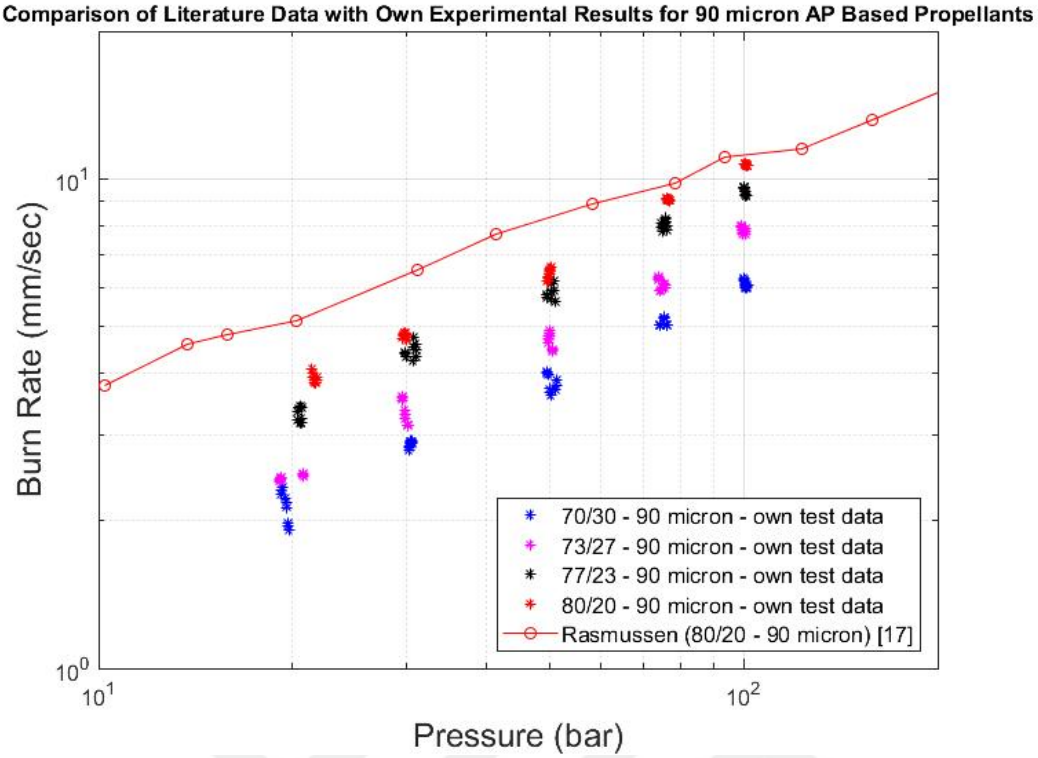

Figure 4.20: Literature Data for AP/HTPB based Propellants with 90 μm AP sizes.

Comparison of 90μm AP based composite propellants is given in Figure 4.20 which includes Rasmussen's [18] data. It is seen that own 80% percent solid loaded data has closer results to his data with having differences of at most 20% at smallest pressures. Different bonding percent for different studies could be a reason for obtaining discrepancies.

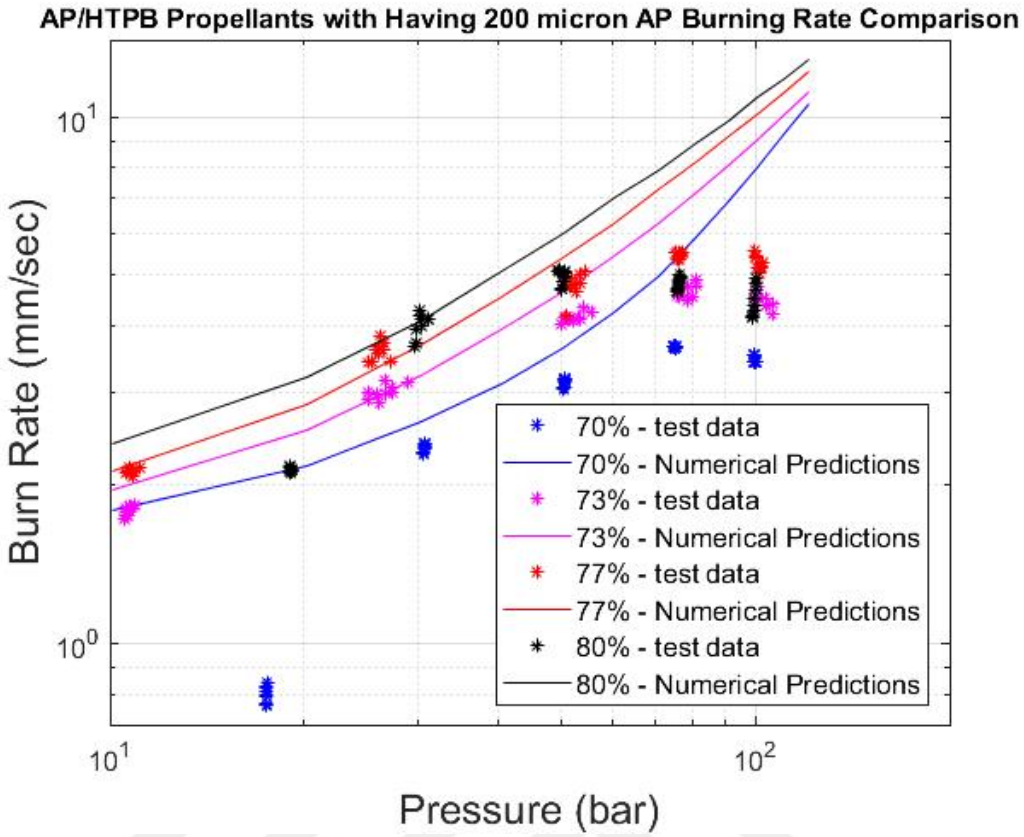

Figure 4.21: Burning Rate Comparison of AP/HTPB based Propellants with AP size of 200 μm.

Last propellant that consists of AP/HTPB is the one that has 200 μm of AP size. Predictions and experimental results for corresponding propellants are given in Figure 4.21. It is seen that, for all solid loading types, numerical predictions have satisfying outcome at mid-range pressures up to 50 bar. On the other hand, all experimental results reveal to have a plateau burning after that pressure. At those plateau burning regime, there can be differences up to 50% between predictions and results. The reasons behind having these differences could be not having properly mixed such large sizes of AP with other ingredients. That way, no matter how pressure is increased, propellants have unstable behavior and even minor decreases in burning rate can be seen with increasing pressure. Also, not using enough bonding elements may result in having unstable data for these largest AP particles. Some part of the differences are also believed to be coming from the uncertainties of the propellants.

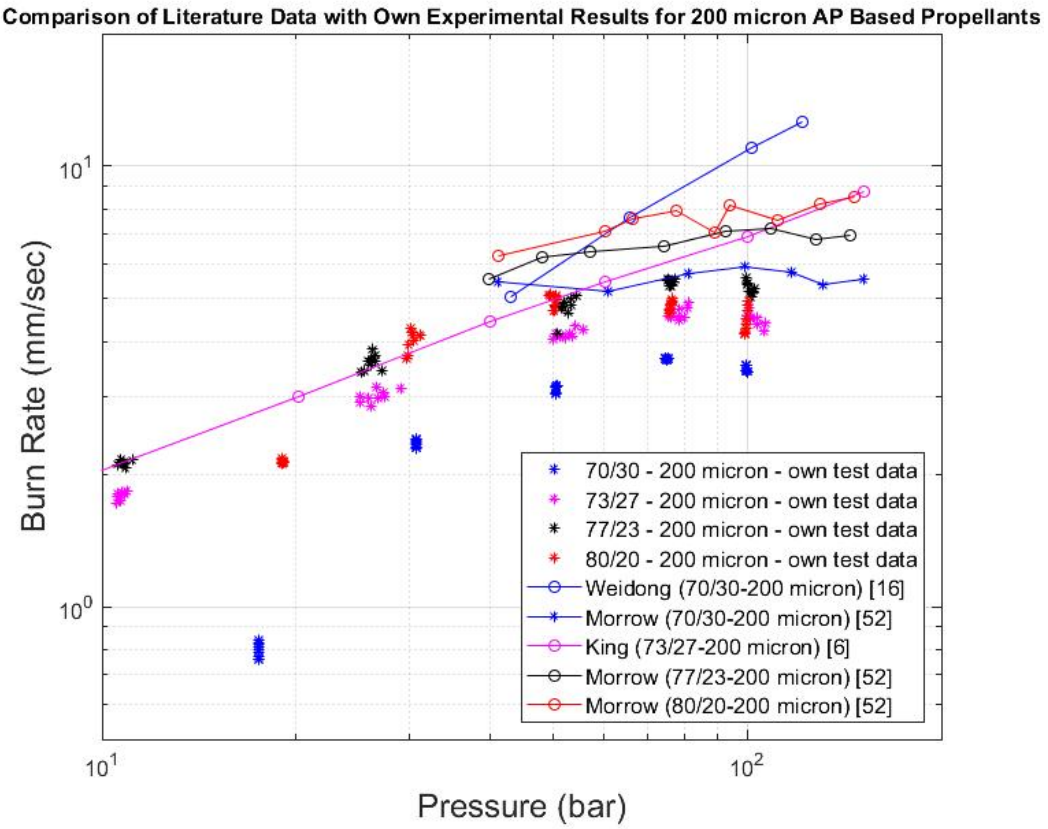

Figure 4.22: Literature Data for AP/HTPB based Propellants with 200 μm AP sizes.

Comparison of propellants that consist of 200μm AP's is provided in Figure 4.22. It is seen that for 70% AP loaded propellants, deviations occur for all experimental work of Weidong's [17], Morrow's [53] and own. Supplementary ingredients may differ from one work to another, which may be a reason for obtaining different burning rates. For the 73% AP loaded propellants, King's [6] and own experimental work agree well up to 50 bar pressure values but then own study has a plateau burning which is not seen King's [6] data. For the 77% AP based propellants, acceptable closer results are obtained with the Morrow's [53] data with having 16% differences. His data also behave in a way that leads to plateau burning as can be seen from Figure 4.22. Similar observation can be seen for 80% AP based propellants. The trend of the own experimental work is similar to the Morrow's [53] data and plateau burning also seem to be obtained by him. The differences may come from the plasticizer percent in the propellants.

After presenting AP/HTPB based composite propellants without catalyst, comparison of the predictions with the experimental results for catalyst added APCP's is provided next.

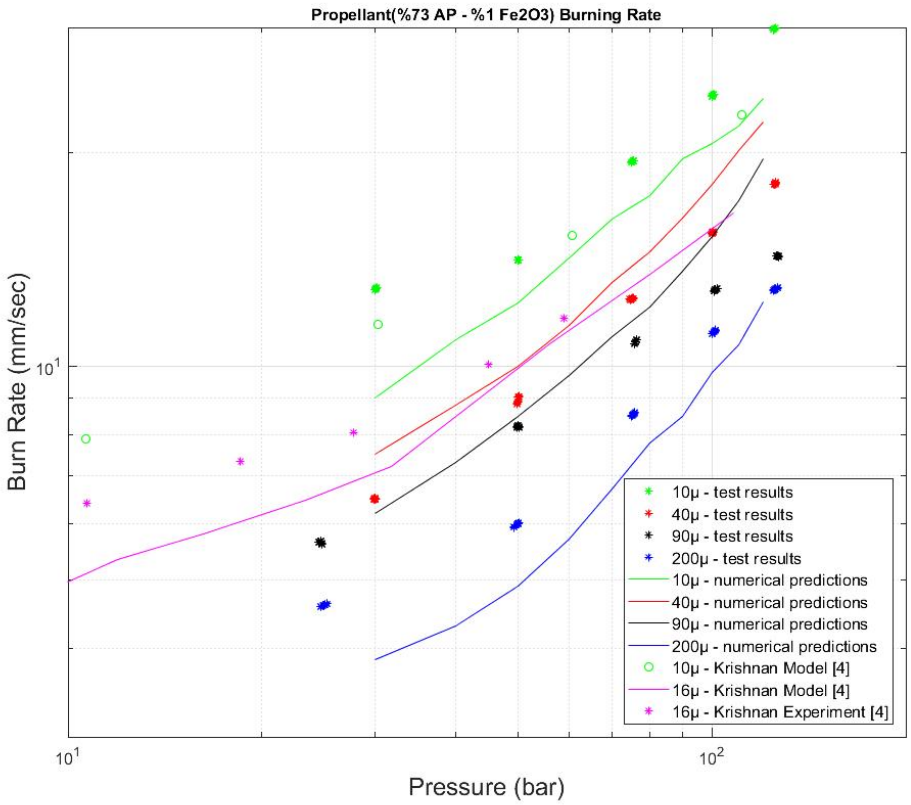

Figure 4.23: Burning Rate Comparison of 73% AP + 1% Fe_20_3 based Propellants (Experimental Data from Krishnan [4]).

Starting with the 1% Fe_20_3 added 73% AP based propellants, the comparison of the experimental results and corresponding numerical predictions is given in Figure 4.23. In that figure, propellants that have 10μm, 40μm, 90μm and 200μm AP sizes are compared and additionally, work done by Krishnan [4] which includes comparison of 16μm AP based propellants burning rate is incorporated. To evaluate the data, acceptable agreement can be said between numerical predictions and the experimental results. For the 10μm AP based propellants, it seems that there is at most 40% difference between test results and numerical predictions which is only observed at smallest pressures. Other than that, the difference is up to 20% between them. Also for that data, Krishnan [4] model has close outcomes to both own numerical scheme

and experimental work. For the 40μm and 90μm AP based propellants, closer results can be seen and an agreement is obtained between predictions and test results. However, it is also observed that Krishnan's [4] 16μm data has closer results to the own 40μm data which, for those propellants, can be counted as an unexpected outcome. It should have been more close to the own 10μm data and the reason for having obtained this property is believed to be coming from bonding elements percentage used in the propellants. For another propellant batch which consists of 200μm AP and 1% Fe_20_3, it is deducted from Figure 4.23 that at higher pressure values, the outcome of predictions and experimental work are very close to each other, but at smaller pressures there can be differences up to 30%. The reason for having differences is believed to be the uncertain properties of the propellants.

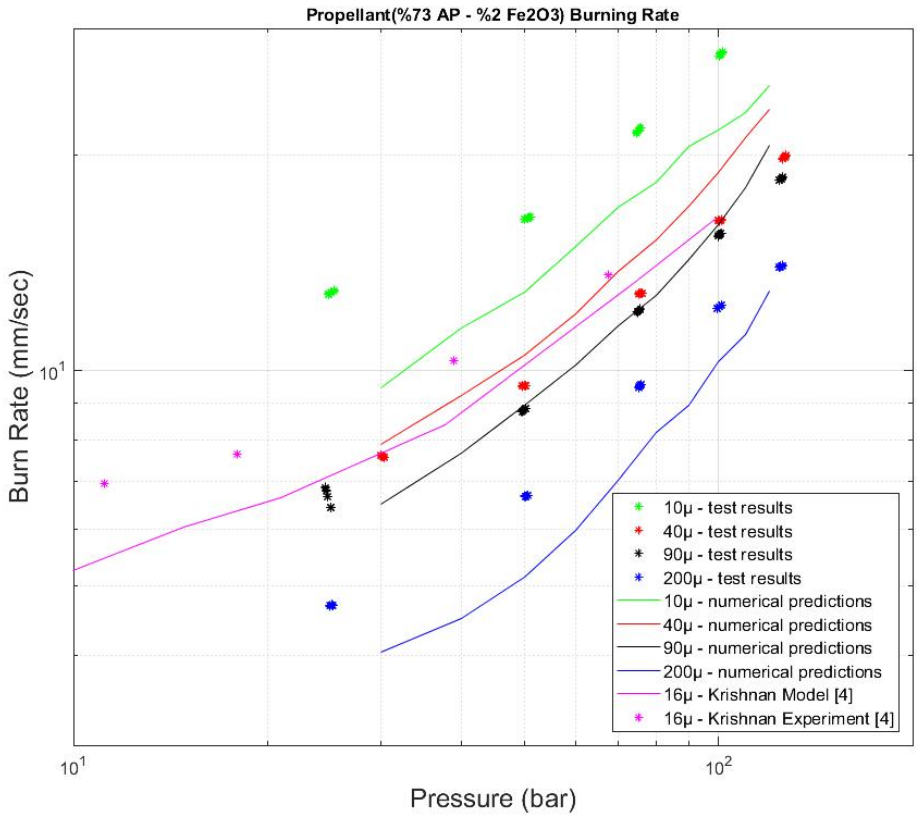

Figure 4.24: Burning Rate Comparison of 73% AP + 2% Fe_20_3 based Propellants (Experimental Data from Krishnan [4]).

Evaluating 1% Fe_20_3 added 73% AP loaded propellants, 2% Fe_20_3 catalyst additive of the same solid loaded propellant data is given in Figure 4.24. Again in this figure,

both AP sizes are included to compare and the work done by Krishnan [4] is also included to see where the 16μm AP based propellants stand in between own experimental work. It is observed that for 10μm based propellants, there is a clear shift which almost causes 30% difference between the experimental work and test results. The reason of having those differences could be coming from the uncertain parameters or the manufacturing process. Producing these propellants, there is the vacuum process that must be applied and not enough putting the batch under vacuum may result in having gaps comprised in the propellants. Those gaps lead to higher burning rates than the reality which can be counted as a reason. For the 40μm and 90μm AP based propellants, again there is an agreement between predictions and experimental results. 16μm AP based data is also observed to be in between own 10 and 40 μm data which is as expected due to sizes of AP. For the 200μm AP based propellants, the difference of at most 25% can be seen between predictions and results at smallest pressures. While uncertain parameters of the propellants may lead to have that difference, it can also be coming from the manufacturing process in which not mixing the larger AP sizes with other ingredients properly may lead to obtain higher burning rates.

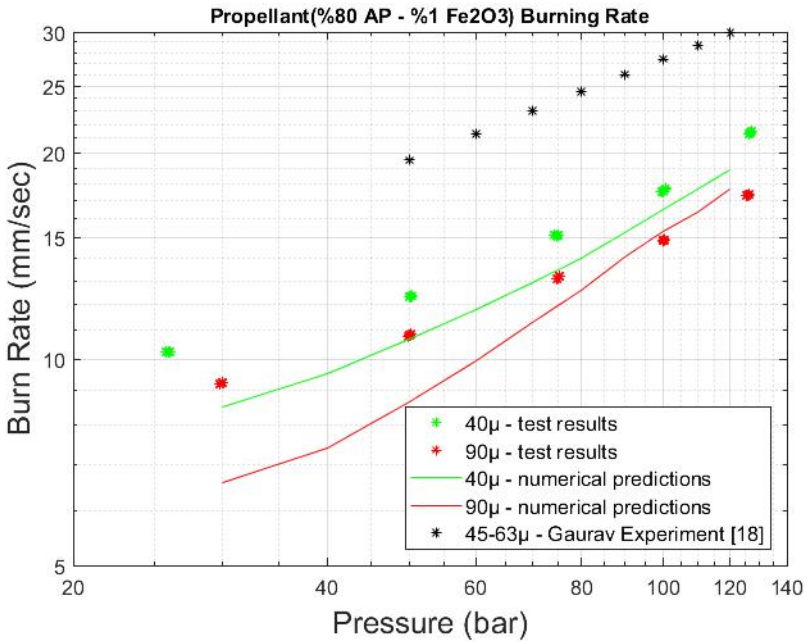

Figure 4.25: Burning Rate Comparison of 80% AP + 1% Fe_20_3 based Propellants (Experimental Data from Gaurav [19]).

Last propellants, which include 80% AP and 1% Fe_20_3 are investigated next. It is seen from Figure 4.25 that, although they are acceptable, there are differences observed between numerical predictions and experimental results for both 40 and 90 μm AP based propellants. Up to 25% difference is seen for 40μm data and up to 20% difference is obtained for 90μm data. The differences might be due to uncertain parameters of the propellants or the manufacturing process. Another observation is that Gaurav [19] used between 45-63 μm APs and he obtained larger burning rates than own propellants. It is not expected results since his AP sizes are larger but there might be plasticizer percentage differences in those batches or the manufacturing methods are different which can cause visible effects on burning rates.

To conclude this chapter, comparison is made for the current work which combines several mathematical models from the literature and the experimental work for determined composite propellants. Promising results were obtained for many types of them, but discrepancies are also observed for some of them which are believed to be caused by manufacturing problems, having Gaussian distribution of AP's or the unknown parameters of the propellants. In the next chapter, general conclusion from this study and discussion for the future is provided.

CHAPTER 5

CONCLUSION

The purpose of this study was to compare real time data of composite propellants burning rate with theoretical models. It would be useful to have such methods for obtaining burning rates instead of strand burner experiments, test firings etc in terms of time and money facts.

Theoretical studies have begun from 1960's to model the burning rates, but the formulations of the propellants is too broad to finish the job that already began. Within the time span of this work and for the sake of Tübitak SAGE's needs, test matrices have been constructed. From 10 to 200 micron AP diameters with having solid percent of 70 to 80 propellants were investigated within the scope of this work. Moreover for the catalysts, Fe_2O_3 was chosen to be studied since it is the most preferable one around.

Numerical methods based on BDP [3], Cohen and Strand [2] were studied to combine them in a numerical code with the parametric work mentioned. For the catalytic part, the method developed by Krishnan et al [4] was taken as a basis.

Experimental work has been conducted using high pressurized Strand-Burner setup located at Tübitak SAGE's Combustion Technologies Research Facility. Having 3 tests conducted at each pressure and repeating each tests 3 times for all propellants, 9 data points are obtained to observe repeatable burning rate data of each propellant. Total of 390 tests are conducted in this work to compare numerical scheme predictions of AP/HTPB and AP/HPTB plus Fe_2O_3 based propellants with experimental results. Having obtained 1170 burning rate data with those number of tests, comparison of the results with predictions is provided for each propellant batch manufactured.

At the end of the experiments, effects of AP particle size, AP percent and catalyst ad-

ditive on burning rate are obtained. As expected, it is seen that burning rates increase with lowering AP particle size, increasing AP percent in the propellant and Fe_2O_3 addition to the propellants.

As a general result to this study, comparison of the numerical method predictions with the experimental work has been obtained. It can be said that promising burning rate predictions are observed for many types of propellant batch manufactured. Besides having some discrepancies for some propellants, almost all results reveal that the work could be open to be developed more for other ingredients of the propellants. Interpreting the results, it is observed that for mid-size AP particles(40μm and 90μm) numerical predictions give promising results but approaching towards either 10μm or 200μm AP based propellants, least accurate predictions are obtained. It is also observed that plateau burning is seen for propellants having 200μm AP particles at all AP loadings (70%, 73%, 77%,80%) after some critical pressure values for AP/HTPB based propellants. This is believed to be coming from not properly mixing those larger AP's with the other ingredients which results in unstable burning behavior. Continuing the discussion, approaching towards lower pressure values, again unstability of the propellants burning rate is also increased. Solid propellants' burning rate strongly depends on the pressure and there is the term, pressure deflagration limit, which determines the minimum boundary of pressure for them to burn stably. Below or closer to that limit, burning rate may become unpredictable. For each propellant that has different ingredients, that limit may change and as a result, unstable behavior approaching lower pressure values is observed.

Another discussion is observed for catalyzed propellants at the end of this study. Even 1% of catalyzer contributes a lot to burning rate compared to uncatalyzed propellants for all AP sizes and AP percent of this study. But 1% more of catalyzer addition to the catalyzed propellants doesn't affect that much.

For the discrepancies, there are two types of them obtained in this study. First discrepancy is between numerical predictions and experimental work, second discrepancy is between data from the literature and own test results. There can be many things to be counted for having those discrepancies but beginning with the part that is between predictions and experimental results, manufacturing problems is believed to occupy

the major fraction. For AP particles with larger sizes such as 200μm, there could be mixing or bonding problems related with manufacturing. To be more clear, not being able to mix larger AP's with other ingredients could be the first reason for having discrepancy between predictions and experimental results. Additionally, bonding may not be satisfactory enough for those larger AP's which creates another reason. There is also a vacuum process used during the manufacturing of the propellants and unproper period during that process may result in gaps comprised in propellants which causes unstable burning. Moreover, the propellant ingredients are supplied from different suppliers around the world. From them, APs are obtained with not having exact sizes but instead, Gaussian distribution of the sizes are provided. Having experimented any sizes rather than the determined ones may also result in burning rate variations with numerical predictions. Another reason for having discrepancies between predictions and results is the uncertain properties of the propellants. As it is given in the thesis, heat of binder decomposition and heat in the primary flame parameters are open to debate and they couldn't be defined in exact numerical values. Sensitivity analysis of them demonstrates that changing the heat of binder decomposition from 10 to 200 cal/g affects the burning rate as much as 5%, on the other hand changing primary flame heat release from 500 to 800 cal/g affects the burning rate almost 50%. Therefore, uncertain parameters of the propellants are believed to be one of the major reasons for having discrepancies.

For the discrepancies obtained between data from the literature and own experimental work, there can be again many things to be counted. Manufacturing method differences are believed to be the first reason for obtaining different burning rates for the same propellants comparing own batch results and the data from literature. Manufacturing is a combined process of conditioning the ingredients, mixing them, putting them under vacuum conditions and curing them together. Any different methods applied by the authors in the literature may result in obtaining different burning rate data for the same propellants at the same pressure. Therefore, any difference in manufacturing methods is believed to be a major reason for the discrepancies observed between own experimental results and data from literature. There is also a reason that is about propellant ingredients. For own propellants for instance, there is between 1% and 2% curing agent and plasticizer used from HTPB percent for propellants to

procure the bonding. For the data provided in literature, these bonding agents percent is not given in most of the works and since differences in bonding percent yields in differences in major ingredients such as HTPB in the propellants, this could be a reason for obtaining discrepancies in burning rate for different studies. Another reason could be the mean AP diameter as stated in above paragraph. Any researcher may have worked on different Gaussian distribution of AP sizes, therefore having obtained different burning rates is reasonable because of not having experimented the same size.

For the future, this work can be extended to investigate other propellant ingredients such as metal fuel additives. Aluminum is the major preferred ingredient for metal additives and extending the code to predict burning rates of composite propellants with metal additives could be an exciting one. Also, there are propellants used in rocketry that consist of different sizes of AP. Predicting burning rates of bimodal propellants could be a good examination for the future studies.

REFERENCES

[1] S. C. Özcan, S. Cürdaneli, and A. Ulaş, "Burning Rate Comparison of a Mathematical Model with Experimental Results for AP/HTPB Based Composite Propellants," *54th AIAA/ASME/SAE/ASEE Joint Propulsion Conference*, no. 2018-4578, Cincinnati, Ohio, USA, July 9-11, 2018.

[2] N. S. Cohen and L. D. Strand, "An Improved Model for the Combustion of AP Composite Propellants," *17th Joint Propulsion Conference*, no. 1981-1553, Colorado Springs, CO, USA, July 27-29, 1981.

[3] M. W. Beckstead, R. L. Derr, and C. F. Price, "A model of Composite Solid Propellant Combustion Based on Multiple Flames," *AIAA Journal*, vol. 8, no. 12, pp. 2200–2207, Dec. 1970.

[4] S. Krishnan and R. Jeenu, "Surface Reaction Model for Catalyzed Composite Solid Propellants," *AIAA Journal*, vol. 30, no. 11, pp. 2788–2791, Nov. 1992.

[5] K. K. Kuo and M. Summerfield, *Fundamentals of Solid-Propellant Combustion*, vol. 90. American Institute of Aeronautics and Astronautics, 1984.

[6] M. K. King, "Model for Steady-State Combustion of Unimodal Composite Solid Propellants," *16th Aerospace Sciences Meeting*, no. 1978-216, Huntsville, AL, USA, Jan. 16-18, 1978.

[7] "Types of Chemical Rocket Engines." `https://www.sciencelearn.org.nz/resources/393-types-of-chemical-rocket-engines`. [Online; accessed 14-March-2019].

[8] "The engine types: solid, liquid and hybrid and a fourth." `https://www.narom.no/undervisningsressurser/sarepta/rocket-theory/rocket-engines/`

the-engine-types-solid-liquid-and-hybrid-and-a-fourth/. [Online; accessed 1-September-2019].

[9] "Nozzle Design." https://www.grc.nasa.gov/WWW/K-12/airplane/nozzled.html. [Online; accessed 10-June-2019].

[10] "Propellants for rockets and guns." https://www.ict.fraunhofer.de/en/comp/em/treib.html. [Online; accessed 02-September-2019].

[11] "Solid Propellant Burn Rate." https://www.nakka-rocketry.net/burnrate.html. [Online; accessed 11-June-2019].

[12] "Successful Firing of Large Hybrid Rocket Motor." https://www.nammo.com/news-and-events/news/nammo-successfully-fires-large-hybrid-rocket-motor/. [Online; accessed 11-June-2019].

[13] L. Galfetti, D. L. L. T, F. Severini, L. Meda, G. Marra, M. Marchetti, M. Regi, and S. Bellucci, "Nanoparticles for Solid Rocket Propulsion," *Journal of Physics: Condensed Matter*, vol. 18, no. 33, 2006.

[14] C. E. Hermance, "A Model of Composite Propellant Combustion Including Surface Heterogeneity and Heat Generation," *3rd and 4th Aerospace Sciences Meeting*, vol. 4, no. 1966-112, New York, NY, USA, Jan. 24-26, 1966.

[15] M. K. King, "A Model of the Effects of Pressure and Crossflow Velocity on Composite Propellant Burning Rate," *15th Joint Propulsion Conference*, no. 1979-1171, Las Vegas, NV, USA, June 18-20, 1979.

[16] M. B. Jeppson, M. W. Beckstead, and Q. Jing, "A Kinetic Model for the Premtxed Combustion of a Fine AP/HTPB Composite Propellant," *36th AIAA Aerospace Sciences Meeting and Exhibit*, no. 1998-447, Reno, NV, USA, Jan. 12-15, 1998.

[17] V. Yang and W. Cai, "A model of AP/HTPB Composite Propellant Combustion," *38th Aerospace Sciences Meeting and Exhibit*, no. 2000-311, Reno, NV, USA, Jan, 10-13, 2000.

[18] B. Rasmussen and J. R. A. Frederick, "A Nonlinear Heterogeneous Model of Composite Solid Propellant Combustion," *35th Joint Propulsion Conference and Exhibit*, no. 1999-2228, Los Angeles, CA, USA, June 20-24, 1999.

[19] G. Marothiya, C. Vijay, K. Ishitha, and P. A. Ramakrishna, "Effects on Burn Rates of Pellets and Propellants with Catalyst-Embedded AP," *Journal of Propulsion and Power*, vol. 34, pp. 969–974, July 2018.

[20] B. Mumcu, "Application of Ultrasonic Burning Rate Measurement Method on Closed Bombs." Middle East Technical University, 2013.

[21] S. Açık, "Internal Ballistic Design Optimization of a Solid Rocket Motor." Middle East Technical University, 2010.

[22] F. M. Teodor-Viorel Chelaru, "Hybrid Rocket Engine, Theoretical Model and Experiment," *Acta Astronautica*, vol. 68, no. 11-12, pp. 1891–1902, 2011.

[23] E. W. Price, "History of Solid Rocket Motors," *34th AIAA/ASME/SAE/ASEE Joint Propulsion Conference and Exhibit*, no. 1998-3978, Cleveland, OH, USA, July 13-15, 1998.

[24] P. Kuentzmann, "Introduction to Solid Rocket Propulsion," *Internal Aerodynamics in Solid Rocket Propulsion*, May. 2002.

[25] D. J. Moser and E. L. Keith, "Liquid Propellants as a Replacement for Solid Rocket Motor Strap-On Boosters," *31st Joint Propulsion Conference and Exhibit*, no. 1995-2457, San Diego, CA, USA, July 10-12, 1995.

[26] "Introduction to Liquid-Propellant Rocket Engines," AIAA paper, Modern Engineering for Design of Liquid-Propellant Rocket Engines, 1/22., 1992.

[27] P. M. Sforza, *Solid Propellant Rocket Motors. Theory of Aerospace Propulsion, 617/668.* 2017.

[28] R. Lucas, *Propulsion Elements for Solid Rocket Motors. Solid Rocket Propulsion Technology, 1/33.* 1193.

[29] S. Cürdaneli, "Experimental on the Measurement of Ballistic Properties of Solid Propellants." Middle East Technical University, 2007.

[30] "Solid Rocket Motor Nozzles." https://ntrs.nasa.gov/archive/nasa/casi.ntrs.nasa.gov/19760013126.pdf. [Online; accessed 11-March-2019].

[31] M. Johannsson, "Optimization of Solid Rocket Grain Geometries." Royal Institute of Technology (KTH), 2012.

[32] H. Austruy, *Double Base Propellants*. Solid Rocket Propulsion Technology, 1993.

[33] M. C. Yıldırım, "Grain Burnback Analysis in the Design of a Solid Propellant Rocket Motor." Middle East Technical University, 1998.

[34] M. F. Gomes, "Internal Ballistics Simulation of a Solid Propellant Rocket Motor." Universidade Da Beira Interior, 2013.

[35] N. Kubota, "Survey of Rocket Propellants and Their Combustion Characteristics," *Fundamentals of Solid Propellant Combustion*, pp. 1–52, 1984.

[36] A. Ulaş, "Literatür Araştırma Raporu," tech. rep., Mechanical Engineering Department, Middle East Technical University, Jan. 2016.

[37] H. Yaman, V. Çelik, and E. Değirmenci, "Experimental Investigation of the Factors Affecting the Burning Rate of Solid Rocket Propellants," *Fuel*, vol. 115, pp. 794–803, 2014.

[38] G. P. Sutton, *Rocket Propulsion Elements*. Sixth Edition, John Wiley Sons Inc, 1992.

[39] B. L. Crawford, C. Huggett, F. Daniels, and R. E. Wilfong, "Direct Determination of Burning Rates of Propellant Powders," *Analytical Chemistry*, vol. 19, no. 9, pp. 630–633, 1947.

[40] L. T. Deluca, "Evaluation of Methods for Solid Propellant Burning Rate Measurements," tech. rep., NATO RTO Advisory Report, August 2001.

[41] Özen Atak, "Ultrasonic Measurement of Solid Propellant Burning Rates in Closed Bombs and Subscale Motors." Middle East Technical University, 2016.

[42] L. Strand, K. Magiawala, and R. Mcnamara, "Microwave Measurement of Solid Propellant Pressure Coupled Response Function," *Journal of Spacecraft and Rockets*, vol. 17, pp. 483–488, Nov. 1980.

[43] L. C. Yang, E. L. Miner, and T. C. Romanos, "Application of Plasma Capacitance Gage for Real Time Measurements of Solid Rocket Motor Internal Insulation Erosion," *26th Joint Propulsion Conference*, no. 1990-2327, Orlando, FL, USA, July 16-18, 1990.

[44] C. F. Price, T. L. Boggs, and R. L. Derr, "The Steady State Combustion Behavior of Ammonium Perchlorate and HMX," *17th Aerospace Sciences Meeting*, no. 1979-164, New Orleans, LA, USA, Jan. 15-17, 1979.

[45] W. Cai, P. Thakre, and V. Yang, "A Model of AP/HTPB Composite Propellant Combustion in Rocket-Motor Environments," *Combustion Science and Technology*, vol. 180, pp. 2143–2169, Oct. 2008.

[46] N. S. Cohen, "Review of Composite Propellant Burn Rate Modeling," *AIAA Journal*, vol. 18, pp. 277–293, Mar. 1980.

[47] M. W. Beckstead, "A Model for Solid Propellant Combustion," *Symposium(International) on Combustion*, vol. 18, pp. 175–185, Dec. 1981.

[48] N. S. Cohen, R. W. Fleming, and R. L. Derr, "Role of Binders in Solid Propellant Combustion," *AIAA Journal*, vol. 12, pp. 212–218, Feb. 1974.

[49] H. E. Jones and W. C. Strahle, "Effects of Copper Chromite and Iron Oxide Catalysts on AP/CTPB Sandwiches," *Symposium(International) on Combustion*, vol. 14, pp. 1287–1295, 1973.

[50] S. Krishnan and R. Jeenu, "Combustion Characteristics of AP/HTPB Propellants with Burning Rate Modifiers," *Journal of Propulsion and Power*, vol. 8, no. 4, pp. 748–755, July 1992.

[51] "Datasheet NI 9239." `http://www.ni.com/pdf/manuals/375939b_02.pdf`. [Online; accessed 05-September-2019].

[52] "2200 Series / 2600 Series - General Purpose Industrial Pressure Transducers." `https://cdn.kempstoncontrols.com/files/`

703d895b12803d7cf655dd0d65ab0a7d/2200BGC2501A3UA.pdf. [Online; accessed 05-September-2019].

[53] G. R. Morrow and E. L. Petersen, "The Effects of AP Particle Size and Concentration on AP/HTPB Composite Propellant Burning Rates," *55th AIAA Aerospace Sciences Meeting*, no. 2017-0831, Grapevine, Texas, USA, Jan. 9-13, 2017.